

AUTOMATIC DETECTION AND IDENTIFICATION OF CELLS IN DIGITAL IMAGES OF DAY 2 IVF EMBRYOS

Marwa Ali Elshenawy

Ph.D. Thesis

2012

AUTOMATIC DETECTION AND IDENTIFICATION OF CELLS IN DIGITAL IMAGES OF DAY 2 IVF EMBRYOS

Marwa Ali Elshenawy

**School of Computing, Science and Engineering
University of Salford, Salford, UK**

**Submitted in Partial Fulfilment of the Requirements of the
Degree of Doctor of Philosophy, 2012**

Table of Contents

Contents	i
Glossary	vi
List of Tables	vii
List of Figures	ix
Acknowledgements	xiv
Declaration	xv
Abstract	xvi
<i>Chapter 1 Introduction</i>	<i>1</i>
1.1 Introduction to infertility	2
1.1.1 Oocyte retrieval.....	2
1.1.2 Sperm collection	3
1.1.3 Fertilization	3
1.1.4 Embryo cleavage.....	4
1.1.5 Embryo grading	5
1.1.6 Transferring problem	10
1.2 The image dataset used in this study	11
1.3 Aims and objectives	14
1.4 Thesis structure.....	15
<i>Chapter 2 Literature survey</i>	<i>18</i>
2.1 Previous work on cell detection	18
2.2 Previous work on embryo detection	20
2.3 Conclusion.....	27

Chapter 3 Digital Image Processing 29

3.1 Image representation	29
3.2 Image pre-processing	30
3.2.1 Image brightness and contrast enhancement.....	30
3.2.2 Histogram equalization	33
3.2.3 Image smoothing.....	35
3.2.4 Image segmentation	40
3.2.4.1 Edge detection.....	40
3.2.4.2 Thresholding	44
3.3 Object detection.....	45
3.3.1 Hough Transform.....	45
3.3.2 Template matching.....	47
3.4 Implementing the Image processing algorithms	49
3.5 Conclusion.....	49

Chapter 4 Pre-processing of the embryo images..... 50

4.1 Introduction	50
4.2 Magnification compensation	51
4.2.1 Detection of the ZP	51
4.2.2 The size of ZP	54
4.3 Edge detection	55
4.3.1 Edge selection using basic techniques	55
4.3.2 Edge detection using a new approach.....	56
4.3.3 Edge detection using convolution mask	59
4.4 Conclusion.....	60

Chapter 5 Embryo Detection using the Hough Transform 61

5.1 Introduction	61
5.2 Proposed technique.....	62
5.3 Results of applying Hough Transform	67
5.4 Results using the Hough Transform.....	78
5.5 Conclusions	79

Chapter 6 Embryo detection using template matching 81

6.1 Introduction	81
6.2 The proposed algorithm.....	82
6.2.1 Templates generation	82
6.2.2 Correlation process	85
6.3 Results using the SAD and NCC correlation techniques	89
6.3.1 Considering one peak value	89
6.3.2 Considering peak values	93
6.4 Summary of template matching results	97
6.4 Conclusion.....	98

Chapter 7 Embryo detection using Binary Template Matching 99

7.1 Introduction	99
7.2 The binary template matching technique	100
7.3 Results for the binary templates matching technique	102
7.4 Summary of the binary template matching results	110
7.5 Conclusion.....	111

Chapter 8 Refining the Binary Template Matching..... 112

8.1 Introduction	112
8.2 Refining the binary template matching results	113
8.2.1 Applying filters	113
8.2.2 Applying two templates	122
8.3 Conclusion.....	128

Chapter 9 Results and Discussion..... 129

9.1 Introduction	129
9.2 Summary of Results	130
9.3 Results for the testing dataset	134
9.3.1 Applying the algorithm	134
9.3.2 Results.....	140
9.4 Classification results.....	141
9.5 Conclusion.....	143

Chapter 10 Conclusions..... 144

10.1 Summary of the aims and objective and work done	144
10.2 Summary of the results and findings	145
10.3 Future work	147

<i>Bibliography</i>	145
<i>Appendix A</i>	152
<i>Appendix B</i>	154
<i>Appendix C</i>	173
<i>Appendix D</i>	179
<i>Appendix E</i>	187
<i>Appendix F</i>	202
<i>Appendix G</i>	225
<i>Appendix H</i>	226
<i>Appendix I</i>	232
<i>Appendix J</i>	238

Glossary

ART	Assisted Reproductive Technologies
BPS	Border Percentage Sensitivity
ICM	Inner Cell Mass
ICSI	Intra Cytoplasmic Sperm Injection
IPS	Interior Percentage Sensitivity
IVF	In Vitro Fertilization
NCC	Normalized Cross Correlation
SAD	Sum of Absolute Difference
TE	Trophectoderm
ZP	Zona Pellucida

List of Tables

Table 1.1 Parameters of embryo quality	13
Table 2.1 Mean blastomere sizes of embryos at different cleavage stages (Hnida et al. (2004)).....	21
Table 2.2 Mean blastomere volume as function of degree of fragmentation (Hnida et al. (2004)).....	22
Table 2.3 Detection method of the features	23
Table 2.4 Summary of the survey	27
Table 5.1 The value of the array	65
Table 5.2 Values after elimination	67
Table 5.3 Hough-based technique results	79
Table 6.1 One peak template matching results	97
Table 6.2 Multi-peak template matching results	97
Table 7.1 Binary template matching technique results	110
Table 8.1 Results when applying median filter	121
Table 8.2 Results when using Hough Transform on filtered images	122
Table 8.3 Enhanced "AND" technique results	127
Table 9.1 Hough-based technique results	130
Table 9.2 One peak template matching results	131
Table 9.3 Multi-peak template matching results	131
Table 9.4 Enhanced template matching technique results	132
Table 9.5 Results when using Hough Transform on filtered imaged.....	132
Table 9.6 Results when applying median filter	133
Table 9.7 Enhanced "AND" technique results	134

Table 9.8 Summary of the results.....	140
Table 9.9 Classification results	141
Table 9.10 Results used for classification.....	142

List of Figures

Figure 1.1 Oocyte retrieval	3
Figure 1.2 ICSI.....	4
Figure 1.3 Embryo development stages	4
Figure 1.4 Zygote scoring features	5
Figure 1.5 Scott's zygote scoring grades	6
Figure 1.6 Cleaved embryo grading features	7
Figure 1.7 Blastocyst grading features.....	9
Figure 1.8 Gardner's system (top) embryo development grading (bottom) ICM and TE grading.....	10
Figure 1.9 Embryos transfer.....	10
Figure 2.1 Subjective features of human zygote.....	23
Figure 3.1 Image representation.....	29
Figure 3.2 Image histogram	31
Figure 3.3 Image brightness enhancement (top) original image (middle) image after increasing the brightness (bottom) image after decreasing the brightness	31
Figure 3.4 Contrast enhancement (a) original image (b) image after contrast enhancement	33
Figure 3.5 Example of histogram equalisation	35
Figure 3.6 Neighbourhood (a) 4 neighbours (b) 8 neighbours	36
Figure 3.7 3x3 masking process.....	37
Figure 3.8 3x3 mean smoothing mask	38
Figure 3.9 Effect of mean smoothing mask	38

Figure 3.10 Effect of median smoothing	39
Figure 3.11 Different types of edges (a) ideal image (b) digital image (c) abrupt change in grey level (d) ramp change in the grey level (e) first derivative of the ramp.	41
Figure 3.12 Roberts 2x2 masks.....	42
Figure 3.13 Sobel 3x3 masks	43
Figure 3.14 Prewitt 3x3 mask	43
Figure 3.15 Thresholding using histogram	44
Figure 3.16 The xy plane and the parametric plane.....	45
Figure 3.17 Hough transform of a circle with fixed radius.....	46
Figure 3.18 Template Matching.....	48
Figure 3.19 Results of NCC	48
Figure 4.1 Result of detecting the ZP using Hough Transform	52
Figure 4.2 Mid-points of the ZP.....	53
Figure 4.3 The result after ZP detection	54
Figure 4.4 Image after applying Sobel and Prewitt	56
Figure 4.5 Using different thresholds on Sobel	56
Figure 4.6 Intensity of the border.....	57
Figure 4.7 Difference between the intensity	58
Figure 4.8 Merging the two results	58
Figure 4.9 Edge detected using Elshenawy method	59
Figure 4.10 Convolution kernel	59
Figure 4.11 Image after applying the convolution kernel.....	60
Figure 5.1 Algorithm used for applying Hough Transform.....	62
Figure 5.2 The accumulator values	64

Figure 5.3 Plot of X and Y coordinates	66
Figure 5.4 Plotted results on the image.....	67
Figure 5.5 Image samples after applying Sobel.....	68
Figure 5.6 Sample of result on image 3	69
Figure 5.7 Sample of result on image 26	69
Figure 5.8 Sample of result on image 10	70
Figure 5.9 Result of image 14.....	71
Figure 5.10 Sample of images after applying Elshenawy algorithm	72
Figure 5.11 Image 3 result after using Elshenawy algorithm	73
Figure 5.12 Result of image 26	73
Figure 5.13 More results using Elshenawy algorithm on image 10.....	74
Figure 5.14 Results of image 14	75
Figure 5.15 Results of convolution mask on image 3.....	76
Figure 5.16 Results of the image 26 using convolution mask	77
Figure 5.17 More results using the convolution mask	77
Figure 5.18 Result of image 14.....	78
Figure 6.1 Template contents.....	83
Figure 6.2 Histogram analysis. (a) Original image (b) histogram of the image	84
Figure 6.3 Peak values	85
Figure 6.4 Sample of the template	85
Figure 6.5 Correlation procedure	86
Figure 6.6 SAD technique (a) image (b) template (c) the differences (d) the value of the SAD.....	87
Figure 6.7 NCC technique (a) image (b) template (c) the value after applying NCC	88
Figure 6.8 Results of image 3	89

Figure 6.9 Results of a sample image 13	91
Figure 6.10 Results of image 7	92
Figure 6.11 Result of image 16.....	93
Figure 6.12 Sample of results with more than one peak of image 3	94
Figure 6.13 Sample of image 24	95
Figure 6.14 Another misleading result of image 12.....	95
Figure 7.1 Binary ring template	100
Figure 7.2 Binary representation of the images after applying different edge detection algorithms (a) Sobel (b) Elshenawy algorithm (c) convolution mask	100
Figure 7.3 Output from convolution mask technique (a) original (b) inverted.....	101
Figure 7.4 Summary of the algorithm.....	102
Figure 7.5 Results obtained from an example image.....	103
Figure 7.6 Corresponding cells colour-coded	104
Figure 7.7 Results image 10.....	106
Figure 7.8 results of image 15.....	107
Figure 7.9 Result of noisy image.....	109
Figure 8.1 Example images after edge detection, with and without the different filters.....	114
Figure 8.2 Summary of the algorithm when applying the median filter.....	114
Figure 8.3 Results when using Sobel (a) with median filter (b) without median filter on image 3	115
Figure 8.4 Results when using Elshenawy algorithm (a) with median filter (b) without median filter on image 3	116
Figure 8.5 Results when using convolution mask (a) with median filter (b) without	

median filter on image 3.....	117
Figure 8.6 More results when using Sobel (a) with median filter (b) without median filter on image 15	118
Figure 8.7 More results when using Elshenawy (a) with median filter (b) without median filter on image 15.....	119
Figure 8.8 More results when using convolution mask (a) with median filter (b) without median filter on image 15	120
Figure 8.9 Ring (a) and disk (b) binary templates	122
Figure 8.10 Surface of the desired equation	123
Figure 8.11 Summary of the algorithm.....	124
Figure 8.12 Sample of results using Elshenawy detector algorithm on image 3	125
Figure 8.13 Result using convolution mask on image 16.....	126
Figure 9.1 ZP detection of a testing image	135
Figure 9.2 Results of the enhanced "AND" technique.....	137
Figure 9.3 Sample of another image	138
Figure 9.4 Results of the image	139

Acknowledgements

To my father's soul, my beloved husband for his support and love, the two jewels of my life Yasmeen and Omar, my dearest mother, my sweetest sisters, my nephew (Ahmed) and niece and (Nourhan) and the smallest and cutest one of all Laila. Not to forget my in-laws.

I would like to thank my supervisor Prof. Tim Ritchings for his great effort, support and opinion.

I would also like to thank Dr. Hesham Salem the head of the Al-Ajyal clinic in Alexandria, which supported my work with the required data.

Finally, I would like to extend my thanks to all the faculty members of the Arab Academy for Science and Technology.

Declaration

No portion of the work referred to in this thesis has been submitted in support of an application for another degree or qualification of this or any other university, or institute of learning.

Abstract

Medical image processing has experienced dramatic expansion, and has been an interesting research field that attracted expertise from applied mathematics, computer sciences, engineering, biology and even medicine. This work is concerned with developing image processing techniques to automate the detection and classification of cells in digital images of day 2 embryos for suitability for In Vitro Fertilization (IVF) treatment. In IVF treatment eggs are removed from the ovaries of the woman and injected with sperms of the man in a dish in the laboratory so that fertilization can take place and yield embryos. The embryos are then graded and examined to decide which embryos are the best to be re-implanted into the woman's womb again. The grading system used in this work involved day 2 embryos, and a dataset of 40 images was provided by Al Agyal clinic in Alexandria. At this stage of development the embryos should have 4 approximately circular cells with similar sizes in order to be considered as suitable for re-implantation.

The work develops an automated image processing system which firstly locates the embryo in a microscope image, and then detects the cells in the embryo and matches their properties against the criteria for re-implantation. Although the main problem was the overlapping of the cells in the images, it was also found that the size (magnification) and the brightness also varied from one image to another and these factors had to be taken into consideration during the development of the detection algorithms. Once the perimeter of the embryo had been located, several edge detection techniques including the Sobel, Prewitt and Canny operators were examined as pre-processing for the circular Hough Transform. From 94 cells, only 62 cells (65%) were detected, but at the same time 226 of false cells were also detected. As an alternative approach, template matching was investigated, using templates with a range of sizes which were selected to match the acceptable size criteria for re-

implantation and at the same time take into consideration the different magnification scales of the images used. The Sum of Added Differences (SAD) and the Normalized Cross Correlation (NCC) were used as a measure of the match. The NCC technique gave better results than SAD, which failed to detect any true cells. NCC technique only detected 50% of true cells, and further refinement to this approach was made. This involved binarisation of the images and templates, and the creation of two new edge-detection algorithms, one of which was based on the convolution technique while the other was based on the difference of the grey level between the border of the cell and its background. These changes have increased the cell detection accuracy to 80%, and reduced the detection of false cells from 118 to 39.

Of the 40 images available, 30 images were used to develop the automated system while 10 images were left to test the performance of the system. In the case of the 10 images, 5 had larger embryos and 5 smaller ones than the 30 images, where the embryos had similar sizes. It was found that 85% of the cells in the 10 images were properly detected with only 6 false cells found. As the missed cells and false cells were distributed among the 40 images, only 8 were analysed correctly (all true cells detected and no false cells found) but these were all correctly identified as suitable or not suitable for re-implantation. Further work is required to improve the cell detection algorithm, and to decrease further the number of false cells detected and hence improve the classification of the embryo.

Chapter 1 Introduction

Overview

A brief introduction to the study described in this Thesis is given. It includes a brief introduction to the clinical background to infertility and IVF treatment, which leads to the importance of the grading process in selecting suitable embryos for implantation. The dataset of microscope images of embryos that is used is then described, followed by the aims and objectives of the study. Finally the contents of each Chapter will be described.

Medical image processing has experienced dramatic expansion, and has been an interesting research field that attracted expertise from applied mathematics, computer sciences, engineering, biology and even medicine. Many of these applications involve the analysis of cells seen through microscopes for disease detection, classification and monitoring. Typical of these has been the segmentation and classification of blood cells. This included the segmentation of red blood cells that was proposed by many such as Vromen et al (2009) and also the segmentation and classification of different white blood cells that was proposed by many such as Bikheth et al. (2000). The classification of blood diseases such as malaria using medical image processing has been also a relevant point that has been proposed (Ross et al. 2006).

This study is concerned with developing and implementing a system that automatically classifies human embryo cells as seen through a microscope as suitable for

implantation. These cells are the product of a lab fertilization of a woman's egg with the man's sperm, the fertilization in a lab with the human aid being a solution to a specific infertility problem. These fertilized eggs are classified as suitable for implantation, using grading schemes that are dependent on their age. Accurate classification of these cells will prevent the mother and baby from acquiring many health problems that might occur due to multi-cell implantation. The work described in this Thesis aims to develop and compare image processing techniques that analyse and classify cells for implantation using a grading scheme which is used in clinic for day 2 embryos.

1.1 Introduction to infertility

The term infertility is defined as the inability to conceive despite regular and unprotected intercourse. Infertility in a couple can be due to either the woman or the man, not necessarily both. However, pregnancy may be achieved by using any of the assisted reproductive technologies (ART). There are a number of ART available to infertile couples, in vitro fertilization (IVF) is one of these methods.

In IVF treatment, the eggs are removed from the ovaries of the woman and injected with sperm of the man in a dish in the laboratory so that fertilization can take place. This is accomplished by different IVF procedures (Sallam 2001), including:

1.1.1 Oocyte retrieval

Oocytes (eggs) retrieval is the process whereby a woman's eggs are removed from her ovaries as depicted in Figure 1.1.



Figure 1.1 Oocyte retrieval

In order for this to occur, a woman must first have follicle (potential egg) production stimulated by particular hormones. Once a number of follicles are produced, fertility specialists can then remove these eggs in order to attempt fertilization.

1.1.2 Sperm collection

After the eggs retrieval, the man is asked to bring in his ejaculate in a sterile container. The semen is allowed to liquefy at room temperature and a seminal fluid analysis is performed (Sallam 2001). The semen is prepared for fertilization by removing inactive cells and seminal fluid.

1.1.3 Fertilization

The eggs are then combined with the sperms in a separate dish that contains special culture medium ready for fertilization. In normal IVF, many sperms are placed together with an egg, in the hope that one of the sperms will enter and fertilize the egg. However, in certain cases of severe male infertility, including such as very low sperm count or abnormally shaped sperm or even poor sperm movement, embryologists use intracytoplasmic sperm injection (ICSI), as shown in Figure 1.2, and take a single sperm and inject it directly into an egg. After that the dish is then placed back inside of an incubator. As a result of fertilization, a zygote is formed.

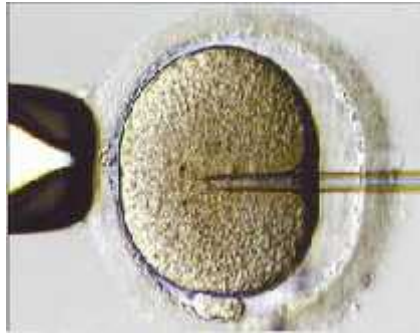


Figure 1.2 ICSI

1.1.4 Embryo cleavage

The zygote now grows to be an embryo by a cell division process and should contain:

2 cells (blastomeres): 24 hours after insemination (Day 1)

4 cells: 48 hours (Day 2)

8 cells: 72 hours (Day 3)

Morula: (Day 4)

Blastocyst: (Day 5-6)

This development of a healthy embryo is depicted below in Figure 1.3.

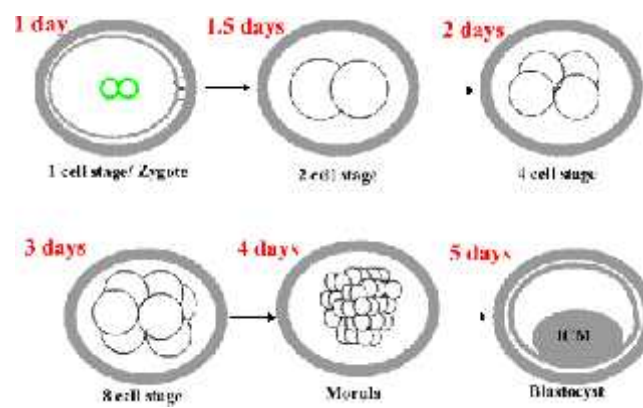


Figure 1.3 Embryo development stages

1.1.5 Embryo grading

Before the implantation process, the embryos should be first examined and graded. This examination improves success rates of pregnancies using IVF and also reduces the number of transferred embryos which causes multifetal pregnancies. Many features have been combined in a variety of different ways to yield different embryo scoring systems. However, all of these scoring systems can be clustered into three main systems: zygote scoring systems, cleaved embryos scoring systems and finally blastocysts scoring systems (Bqczkowski et al. 2004).

Zygote scoring system

In the zygote scoring system, the evaluation is done after 16-18 hours after fertilization and it evaluates the following features, which are shown in Figure 1.4:

- Pronuclear size and symmetry
- Size, number, equality and distribution of nucleoli
- Appearance of cytoplasm

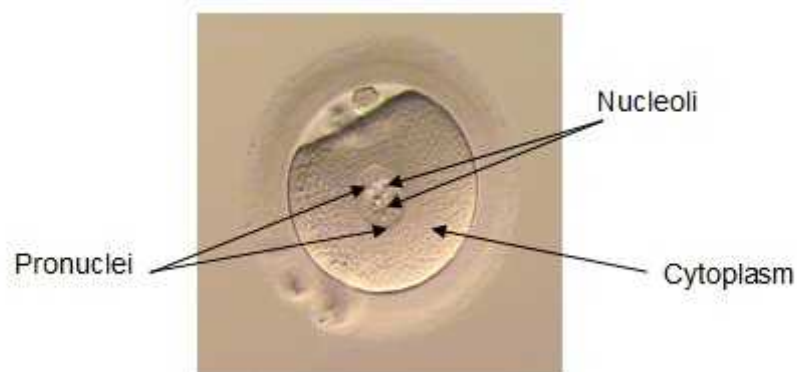


Figure 1.4 Zygote scoring features

The most popular system was that introduced by Scott et al. (2000) and it has been widely accepted and many reports reported its usefulness in the selection of good

embryos and hence better results in implantations. This system uses five grades based on both the number and distribution of nucleoli in the pronuclei, as depicted in Figure 1.5 :

Grade 1: Equal numbers of nucleoli aligned at the pronuclear junction.

The absolute number of nucleoli ranges between three and seven.

Grade 2: Equal numbers of nucleoli of equal size in the same nuclei but one nucleus having alignment at the pronuclear junction and the other with scattered nucleoli.

Grade 3: Equal numbers and sizes of nucleoli which are equally scattered in the two nuclei.

Grade 4: Unequal numbers and/ or sizes of nucleoli.

Grade 5: Pronuclei that are not aligned.

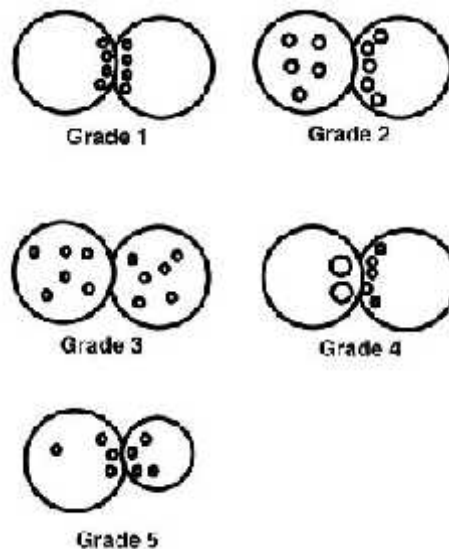


Figure 1.5 Scott's zygote scoring grades

This system was further revised and the new system classified zygotes into four groups according to pronuclear morphology as follows: Grades 2 and 4 zygotes were

combined as Z2 zygote score while the more desirable morphologies grades such as grades 1 and 3 were renamed Z1 and Z3.

Cleaved embryos system

In the cleaved embryos system, the evaluation is done 40-48 hours after fertilization and it evaluates other features than that of the zygote scoring systems, simply because the zygote was now growing to be an embryo and hence its features were changing. These features, which are shown in Figure 1.6 include:

- Number of cells (blastomeres)
- Appearance and size of blastomeres
- Cytoplasm defects (fragments)

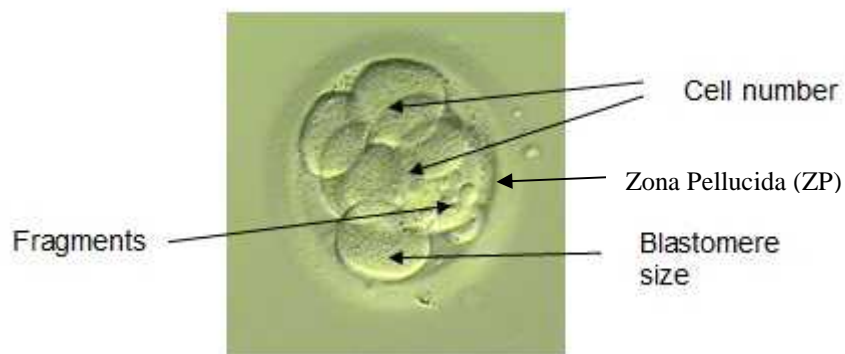


Figure 1.6 Cleaved embryo grading features

The Cleaved Embryo system has been adopted by many researchers including Cummins et al. (1986), Puissant et al. (1987), Staessen et al. (1992), Steer et al. (1992) and Zeibe et al. (1997). However, as a consequence of many research groups, several grading techniques have been introduced, and each clinic uses its preferred grading system. Puissant et al. (1987), for example, used the following scoring technique:

Score 4: embryos with clear, regular blastomeres and either no fragmentation or a maximum of five small fragments;

Score 3: embryos with few or no fragments but with unequal blastomeres ($> 1/3$ difference in size);

Score 2: embryos with more fragments but over $< 1/3$ of the embryonic surface;

Score 1: fragments over $> 1/3$ of embryonic surface.

Two points are added if the embryo has reached the 4-cell stage by 48 h after fertilization. This means that the maximum score of 6 points corresponds to embryos which appear perfect and have reached the 4-cell stage 48 h after fertilization.

On the other hand, Zeibe et al. (1997) used other morphological criteria in which:

Morphology score 1.0: equally-sized symmetrical blastomeres;

Morphology score 2.0: uneven sized blastomeres;

Morphology score 2.1: embryos with 10% fragmentation;

Morphology score 2.2: embryos with 10-20% fragmentation;

Morphology score 3.0: 20–50% blastomeric fragmentation;

Morphology score 4.0: 50% blastomeric fragmentation.

Blastocysts scoring system

Finally, in the blastocysts scoring system, its evaluation is done on day 5 embryo, when the embryo is now said to be in the blastocyst stage. The features in this stage are completely different from the previous ones, as seen in Figure 1.7, as the

formation of a fluid filled cavity in the middle of the embryo (blastocoel) appears, surrounded by a single layer of cells called trophectoderm (TE) and a small protuberance of cells called the inner cell mass (ICM) (Zeibe et al. 1997).

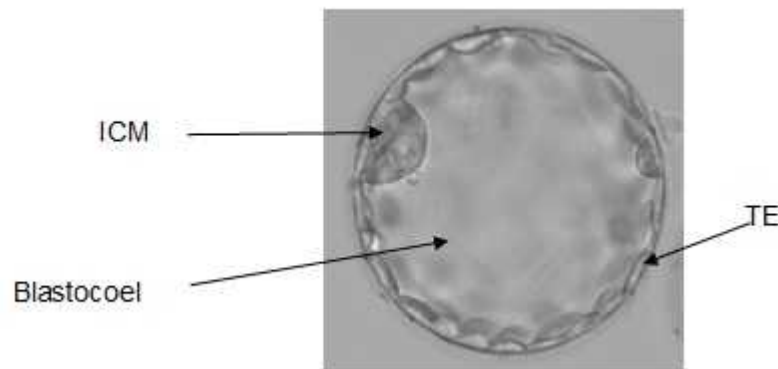


Figure 1.7 Blastocyst grading features

The two most popular blastocyst embryo grading systems are the Dokras et al. (1993) and Gardner et al. (2005) grading systems, both based on morphology. Dokras et al. (1993) grading is based on the blastocoel's rate of development and characteristics of the blastocoel cavity, and blastocysts are graded as BG1, BG2, or BG3. The grading criteria used by Gardner et al. (2005) are given in Figure 1.8, and focus on blastocoel size and developmental characteristics of the inner cell mass and trophectoderm which are initially examined and graded from 1-6. Next, the blastocysts graded 3 through 6 are identified and their inner cell mass and trophectoderm are further graded and given letters A-C.

grade	blastocyst development and stage status		
1	Blastocoel cavity less than half the volume of the embryo		
2	Blastocoel cavity more than half the volume of the embryo		
3	Blastocoel cavity completely filling the embryo		
4	Blastocoel cavity larger than that of the early embryo, with thinning of ZP		
5	Hatching out of ZP		
6	Hatched out of ZP		

ICM	ICM quality	TE	TE quality
A	Many cells, tightly packed	a	Many cells, in a cohesive layer
B	Several cells, loosely grouped	b	Few cells, in a loose epithelium
C	Very few cells	c	Very few large cells

Figure 1.8 Gardner's system (top) embryo development grading (bottom) ICM and TE grading

Despite the large number of published studies, there is no consensus about the most accurate method for grading the embryo. The grading systems used rely mostly on factors such as the embryologists, the IVF clinic or even religious issues. However, the work in this Thesis considers the cleaved embryo system, which was used by the IVF clinic that provided the work with the images.

1.1.6 Transferring problem

The last stage of the IVF process is the transfer of the embryo to the woman's womb using a catheter, as shown in Figure 1.9.

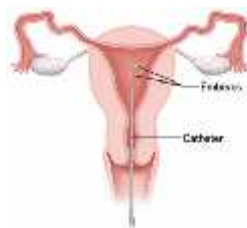


Figure 1.9 Embryos transfer

Generally, two or more embryos are transferred during each IVF cycle. This decision is made upon medical factors such as the number of embryos, the health of the embryos, the patient's age and other factors such as legal issues of the fertility clinic, the country, and sometimes religious matters. The greater the number of embryos that are transferred into the uterus, the higher the risk of having a multiple pregnancy. When multiple pregnancies occur, the health of both the mother and the baby can be seriously affected, so every effort to minimize multiple pregnancies must be taken by the fertility clinics.


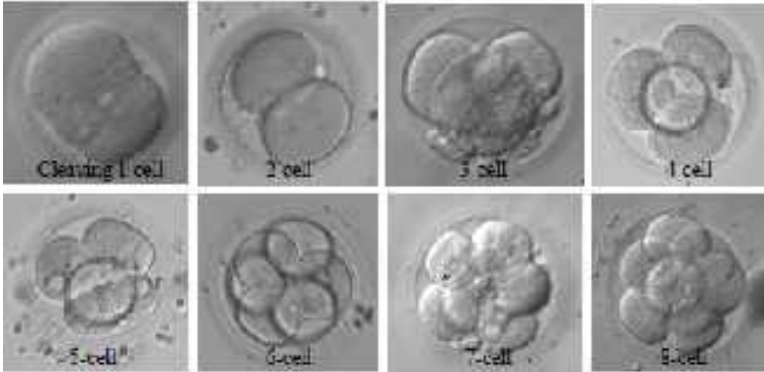
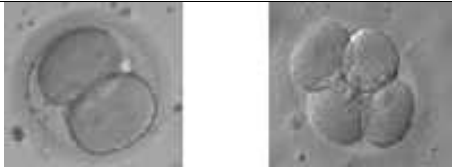
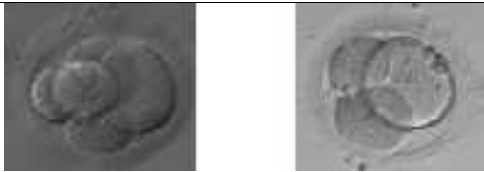
1.2 Problem characteristics

Since implanting more than one embryo caused multiple pregnancies, it is better for both the mother and the baby to try to minimize the number of embryos. This requires choosing the best embryos with the highest grades according to one of the grading techniques mentioned before. An automated system that is able to achieve this would reduce the load on the IVF screeners and provide a consistent and uniform selection of embryos for implantation.

Each clinic chooses a grading system according to many issues, such as the culture media available, the extra cost needed for longer culturing embryos and sometimes the ethical rules of the country or even the religion. The clinic that agreed to support this work was the Ajyal clinic in Alexandria, Egypt. This clinic re-implants the embryos on Day 2, hence uses the Cleaved embryo grading system in particular that of Zeibe et al. (1997), and hence the images used in this study, were Day 2, and their general appearance was the 4 cell embryo seen in Figure 1.3 This technique examines the number of blastomeres, their size and finally the percentage of fragmentation as indicated in Table 1.1. The first row shows the different

fragmentations percentages, the best of which was the first image which had 0% fragmentation. As this percentage increases, the grading level of the embryo decreases. The second parameter shown is the number of blastomeres. This parameter depends on the age of the embryo, a Day 2 embryo should have 4 cells to be considered as a good embryo. As for the last parameter, it is the size of each blastomere, they should be even sized. Therefore, these were the features that will be used and taken into consideration upon creating the system in this thesis.

Table 1.1 Parameters of embryo quality

Parameter	Example				
Fragmentation	 0% fragments 10-30% fragments 20-50% fragments >50% fragments "Totally" fragmented				
Number of blastomeres	 Cleaving 1 cell 2 cell 3 cell 4 cell 5 cell 6 cell 7 cell 8 cell				
Blastomeres size	 even sized blastomeres				
	 uneven sized blastomeres				

The images used in this study were taken using an inverted microscope IX71. This microscope allows the practitioners to see and focus on the embryos. The microscope is connected using an acquisition channel to the computer; this allows the practitioners to see the embryos on the computer monitor using software. This software (CRONUS) is used to capture the images used and save them in a format that allows working upon. The clinic has supported this work with around 40 images. Although the unrest in the country at the time

prevented a larger number of images from being available, the images contained all possible cases of Day 2 embryos that this work can depend upon to develop the required system. The images have different magnification, illumination and also contain overlapping cells. These factors are considered in designing the system. Images were divided into two datasets, one of which contained 30 images. These were chosen to be within the same illumination brightness and magnification and were used to develop the detection and classification algorithms. The other 10 were used at the end to investigate the performance of the algorithms. They had different magnifications and illumination conditions, 5 higher and 5 lower magnifications than the 30 image training dataset. The complete dataset is shown in Appendix A (p.152).

1.3 Aims and objectives

The research question being addressed by this study is whether or not it is possible to develop a prototype automated image analysis system that is able to detect and classify Day 2 human embryo cells as suitable for implantation. A successful system would reduce the load on the IVF screeners and provide a consistent and uniform selection of embryos for implantation. This will also prevent multiple pregnancies.

The specific key aims and objectives were to:

- Map the characteristics and key features of the Day 2 embryo cells that would make them suitable for implantation into features that can be detected by the system.
- Pre-process the image to compensate for magnification and illumination variations in the microscope images.
- Develop and compare different image segmentation and feature extraction

techniques appropriate to these images.

- Identify the most accurate image analysis techniques for classifying the embryo as suitable for implantation.
- Investigate the performance of the approach using images of embryos taken with different microscope magnifications.

1.4 Thesis structure

The chapters of this Thesis are organized as follows:

Chapter 1 gives a brief introduction to the study described in this Thesis. It includes a brief introduction to the clinical background to infertility and IVF treatment, which leads to the importance of the grading process in selecting suitable embryos for implantation. The dataset of microscope images of embryos that was used is then described, followed by the aims and objectives of the study.

Chapter 2 introduces a survey of the previous work done on the detection and grading of embryos. This survey will include the work done on the detection of day 1, day 2 and day 5 embryos. Finally, full analysis of the survey will be judged and the pros and cons of each technique will be stated.

Chapter 3 presents some of these techniques, such as image enhancement techniques, image segmentation methodologies and some object detection methods.

Finally the software that can be used to implement such techniques will be introduced.

Chapter 4 covers the investigation and trials of some of the common segmentation and detection techniques on the embryos' images as a pre-processing stage. It will also include the algorithm used to overcome the different magnifications issue of the images.

Chapter 5 covers the implementation of the circular Hough Transform and application to the embryo images. The technique will use some of the pre-processing stages discussed in the previous chapter, including three different edge-detection algorithms. The results obtained for each of these edge-detection algorithms are compared and discussed in terms of their robustness for cell detection.

Chapter 6 introduces a second technique that will be introduced to detect the blastomere in the embryo. This involves template matching, with templates being designed to match the acceptable sizes of the blastomeres at Day 2. The template design strategy is described first, followed by the implementation of the template matching process. Two measures of the degree of match are investigated, and the results that were obtained with the image dataset are presented and discussed.

Chapter 7 presents an enhanced template matching technique that was developed in this Chapter in an attempt to improve on the poor classifications that

were obtained. The rationale for the enhancements, the implementation of the new techniques and the results that were achieved when applied to the image data set are described.

Chapter 8 gives a refinement on the binary template matching technique. This refinement was essential to decrease the number of false cells detected by the previous binary template matching technique.

Chapter 9 summarises all the results of the previous techniques and provides the measure of performance of each. The technique having the best results will be further used on the rest of the images that were left as a test dataset. Measure will also be provided for these results.

Chapter 10 contains the summary of the work done in this thesis. It summarizes the main aims and objectives and also summarizes the results and the findings obtained. Finally a suggestion for future work will be provided.

Chapter 2 Literature survey

Overview

This chapter introduces a survey on the previous work done on the automated analysis of microscope images of cells in general, followed by more specific work on the detection and grading of embryos, including Day 1, Day 2 and Day 5 embryos. Finally, the advantages and disadvantages of these approaches and techniques are considered in the context of this study.

2.1 Previous work on cell detection

The development of algorithms for biomedical images analysis is not an easy task, but due to the rapid development in the bio-informatics field, much more effort has been focused on automatic analysis of different types of cells seen through microscopes. Such cells are red blood cells, white blood cells, tumour cell and even stem cells.

Bikhet et al. (2000) presented work that recognized and classified different categories of normal white blood cells. The system worked on images captured by a camera attached to the microscope and was in grey level form. Generally in blood analysis three different types of cells are available; white cells, red cells and platelets. These are distinguished by both their

size and colour. In order to distinguish between them in terms of colour, white blood cells appear darker in the grey-scale images than red blood cells and platelets. In the case of size, platelets are the smallest whereas white blood cells were the largest.

The first problem that this work resolved was separating the white blood cells from the rest of the image contents. This was achieved by first applying the median filter to the image and then using thresholding to separate the cells from the background. After this separation, the cells were classified into one of five different types (basophil, eosinophil, lymphocyte, monocyte and neutrophil) according to the information about the size and feature of each of the five types. This approach when tested on the image samples had a percentage of correct classification of the cells of 90%. However, it did not solve the problem of overlapping and touching cells.

Mirosław et al. (2005) used correlation methods to detect mitotic cells automatically. Mitotic cells are cells that have split into two cells with separate nuclei and identical chromosomes. In this work cells were imaged using a camera attached to the microscope. However, when viewed the cells appeared very regular and circular in shape and because of this, the detection method was based on template matching. The templates were created either from a 3D model or from test data. In the latter case, the templates were created by cropping mitotic cells from test images. The 3D models differed depending on the type of the cell. For example, for Kyoto mitotic cells, the template created for this type was a black circle with white boundary, whereas for TDS mitotic cells, a white circle with black boundary was used.

Due to the higher brightness of images the background was grey (intensity 128). The

choice of the radius of the template was estimated and varied from 20 to 32 pixels and the cell membrane was about 2 pixels thick.

The work started the detection process by applying the (3x3) median filter to suppress any fluctuations in the intensities. Then the correlation between the image and the templates was performed. This was followed by a peak detection stage where the highest peaks were detected by using a suitable threshold value, but this caused the generation of many false candidates. These were removed by the validation procedure in the last stage, which was designed to eliminate these.

As a result of this work, it was concluded that a more sophisticated approach was needed to cover all cases when small fluctuations in the image intensity were present. It was also concluded that another optimisation may involve using a local threshold value instead of using a global one, which does not take into consideration the presence of uneven illumination.

2.2 Previous work on embryo detection

Unlike the analysis of microscope images of cells that was discussed in the previous section which tended to be fully automated, the approaches taken by the IVF groups involved with the detection and grading of embryo images include both automated or semi-automated procedures, where some manual control of the process was required.

The work done by Hnida et al. (2004) determined the blastomeres' size at different cleavage stages and defined the deviations in mean blastomere volume as a consequence of embryonic fragmentation. The blastomere size was determined using a sequence of recorded images of the embryos. A total of 232 embryos were used, taken after 48 hours after fertilization, and included 2, 3, and 4 cells. However, the blastomere size of the human embryos was analysed semi-automatically by means of morphology analysis software. This was done using the micrometre slide with the same magnification of the embryo. A line was drawn on the slide and since the outlined distance on the slide was known, the actual physical distance between the two adjacent pixels was calculated. The values describing the blastomere such as the area and the volume were then calculated automatically.

Although the aim of this work was to find a relation between the blastomere size and the volume, rather than detect the blastomere of the embryos, the study gave several important results. The first was that the diameter of the blastomere decreases as the number of blastomeres in an embryo increases, and for example the mean diameter of 2-cell embryos was 80.1 μm whereas that of 4-cell embryos was 64.9 μm , as may be seen in Table 2.1.

Table 2.1 Mean blastomere sizes of embryos at different cleavage stages (Hnida et al. (2004))

	Volume $\pm\text{SE (x10}^6 \text{ m}^3\text{)}$	Diameter $\pm\text{SE (}\mu\text{m)}$
2-cell embryos	0.278 ± 0.09	80.1 ± 9.8
3-cell embryos	0.182 ± 0.09	68.7 ± 12.2
4-cell embryos	0.149 ± 0.06	64.9 ± 8.5

The second significant outcome was that the mean blastomere volume decreased significantly with increasing the degree of fragmentation, indicating that the blastomere size could be used as an indicator of the degree of fragmentation. This is illustrated in Table 2.2.

Table 2.2 Mean blastomere volume as function of degree of fragmentation (Hnida et al. (2004))

Fragmentation (%)	2-cell embryos	3-cell embryos	4-cell embryos
	volume	volume	volume
	\pm SE ($\times 10^6$ m ³)	\pm SE ($\times 10^6$ m ³)	\pm SE ($\times 10^6$ m ³)
0	0.341 \pm 0.09	0.2 \pm 0.04	0.164 \pm 0.05
1-10	0.310 \pm 0.07	0.209 \pm 0.1	0.165 \pm 0.05
11-20	0.260 \pm 0.06	0.175 \pm 0.08	0.136 \pm 0.05
21-50	0.192 \pm 0.09	0.141 \pm 0.08	0.108 \pm 0.05
>50	0.112 \pm 0.06	0.112 \pm 0.04	0.094 \pm 0.08

Although not their main concern these researchers pointed out that computer-assisted tools for the measuring of embryos features would be helpful.

The work described by Beuchat et al. (2008) aimed to provide a software tool that enables the objective measuring of morphological characteristics of embryo, but for only for the Day 1 human zygote. Their work provided measurements of new variables (24 measurements) along with the subjective ones available, as shown in Figure 2.1 on the next page, and then showed the importance of these new measurements to the grading process. In order to calculate these measurements, the subjective features (the pronuclei, oolemma, cytoplasmic halo, polar bodies and finally the nucleolar precursor bodies) needed were detected, and this was the objective of this study. Three groups of images were used, each

from a different clinic. The groups consisted of 188 images, 201 images and 107 images, respectively.

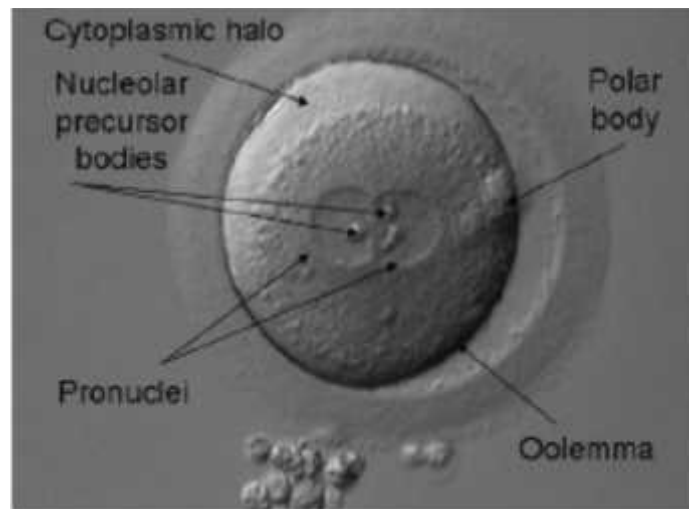


Figure 2.1 Subjective features of human zygote

Some of these features were automatically, semi-automatically or manually detected, as summarised in Table 2.3 .

Table 2.3 Detection method of the features

	Automatic	Semi-automatic	Manual
oolemma	yes		
cytoplasmic halo		yes	
pronuclei		yes	
Nucleolar precursor bodies			yes
polar bodies			yes

As shown in Table 2.3, the only automatic feature detected was the oolemma of the zygote. This was achieved by firstly detecting the foreground and the region with the central oocyte and separating it from the background. The second step was to detect the pixels

belonging to the boundary of the oocyte. For this, Gaussian blur was applied followed by Sobel edge filtering. The formed image was then binarized using Lloyd-Max classification with two classes followed by a thinning process of the available boundary. Finally, an ellipse fitting algorithm was fitted to this oolemma boundary.

The two features that were detected semi-automatically were the cytoplasmic halo and the pronuclei. The detection of the cytoplasmic halo was achieved by selecting few points on the border of the cytoplasmic halo and then applying the ellipse fitting algorithm to these points. As for the pronuclei, a light-correction of the image was followed by histogram equalization, then blurring with a Gaussian kernel and finally Sobel edge detection (Gonzalez et al. 2002). After this, the edge image was correlated to edge templates and the position on the pronuclei determined from the maximum correlated value. Finally, the nucleolar precursor bodies and the polar bodies were manually detected because the automatic approaches were not sufficiently robust.

Morales et al (2008) developed an automatic algorithm that helped embryologists to have more information on the thickness of the Zona Pellucida (ZP). The purpose of this work was to investigate the suggestion that the measurement of the ZP thickness variation was directly related to the implantation rate. Their algorithm was based on an active contour model, but prior to that the image had to be enhanced to increase the contrast of the image and hence that of the ZP. The enhancement involved image thresholding followed by applying a high-pass-Gaussian convolution filter which was optimal in terms of the smoothing. Canny's edge detector algorithm (Canny 1986) was then applied to detect weak edges, and then a derivative of a Gaussian filter was applied to achieve the gradient image of the edge map produced earlier. Finally, the active contour model (snake) (Kass et al. 1988)

was applied on the pre-processed images. When using the snake, the initial position had to be near to the boundary of the object. This was achieved by averaging a pattern from about 60 images to determine a possible location of the centre.

The dataset used consisted of 76 images. They were taken on the second and third days after fertilization. All images were taken using fixed magnification and brightness. Through comparison with images manually segmented it yielded 91.65% accuracy in localisation of the boundaries. However, this approach only detected the ZP and it did not detect the number of blastomeres inside it.

Giusti et al. (2009) presented a practical edge-based technique for segmenting the surrounding of the zygote cell from the rest of the image, although this did not include detecting any of the blastomeres inside the zygote. The segmentation process was divided into two steps. The first step found the approximate location of the cell centre, and this was achieved by getting the image gradient followed by thresholding and then filling in the holes of the largest component found. Hence for each point, the distance to the region boundary was computed and the point with the maximum distance was finally chosen to be the centre. The second step transformed the cell location to polar coordinates and the shortest-path formulation was then used to recover the actual zygote contour. As this approach filled the inside of the contour, it was not being able to detect the blastomeres, and so was limited to images of Day 1 embryos.

Working on the grading of Day 5 embryos Filho et al. (2010) developed a method that required the segmentation of the TE and the ICM, and used the segmentation features for classification. For the outer boundary TE segmentation, the image was thresholded and points

were sampled from the border. These sampled points were then used for an ellipse fitting procedure. For the inner boundary segmentation, an initial circle situated in the centre was used. This circle evolved until it met the inner boundary. However, this segmentation technique did not meet the real TE boundary when manually segmented, and so, the manually segmented approach was used to finish the calculations required for the classification. In the case of the ICM segmentation, the circle was manually initialised at the centre of the cell and then it evolved towards the ICM.

Table 2.4 summarises the relatively little work that has been done on computer-based analysis of images of embryos.

Table 2.4 Summary of the survey

	Outcome of the work
Hnida et al. 2004	used the aid of the computer to semi-automatically measure the dimensions of embryos after different days
Beuchat et al. 2008	detected the features of Day 1 zygotes using automatic, semi-automatic and manual techniques
Morales et al. 2008	automatically detected the thickness of the ZP of the zygote
Giusti et al. 2009	automatically detected the active contour of the zygote
Filho et al. 2010	automatic grading of Day 5 embryos (blastocyst stage)

2.3 Conclusion

After this survey of the relatively limited work that has been done on cell analysis and the embryo detection it can be concluded that:

- The first step in the segmentation and classification process was identifying the required features of the cell and this differed from one cell to another. The features of the red blood cells are different from those of the mitotic cells and from many others.
- The variations in the illumination, magnifications and noise in the images required careful selection and tuning of both the pre-processing and segmentations algorithms, but typical approaches are histogram analysis, thresholding, applying filters and even correlation.
- The analysis and classification of embryos were particularly difficult because of the differing characteristics of embryo at Day 1, 2 and 5 and semi-automated techniques were required in many cases.
- A detected structure was considered a blastomere when the average diameter was $40\mu\text{m}$ and a fragment when the average diameter was $< 40\mu\text{m}$. The mean diameters of 2-, 3-, and 4- cell embryos were $80.1 \pm 9.8\mu\text{m}$, $68.6 \pm 12.2\mu\text{m}$ and $64.9 \pm 8.5\mu\text{m}$, respectively.

The previous work showed the different algorithms and techniques that worked on the segmentation of human embryos, some of which worked on Day 1, 2 or even 5 embryos, and so provided a basis for identifying potentially effective algorithms for this study. Even so, semi-automatic and manual methods were required, so it is likely that algorithms would need

to be developed and tuned for the Day 2 images used in this study. The range of diameters of Day 2 embryos relative to that of the ZP was identified and can be used to compensate for magnification effects.

In the following Chapter, the basic Image Processing techniques for pre-processing and segmentation of the images that were identified in the Literature Review are described.

Chapter 3 Digital Image Processing

Overview

In the previous Chapter the types of image analysis techniques that have been used to analyse microscope images of cells and support the grading of embryos were identified. This chapter describes some of these techniques, such as those for pre-processing images, image segmentation methodologies and object detection methods. Finally the software that can be used to implement such techniques will be introduced.

3.1 Image representation

Digital image processing can be defined as the use of computer algorithms to perform processing tasks on digital images. Digital images are typically represented by a two-dimensional array $M \times N$, where the x coordinates range from 1 to M and the y coordinates from 1 to N as depicted in Figure 3.1.

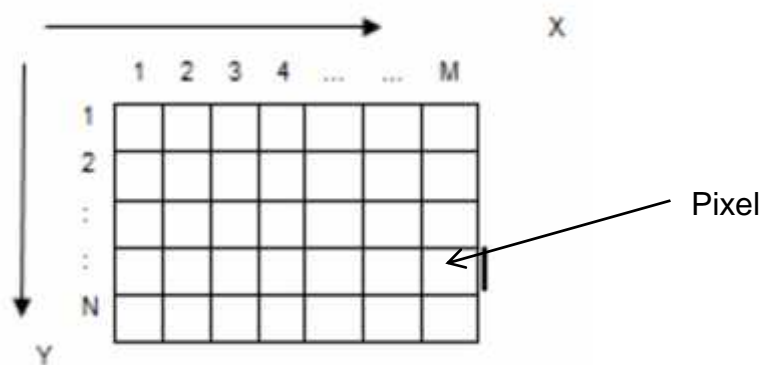


Figure 3.1 Image representation

The small region of the image centred on (x,y) is usually referred to as a picture element, pixel, and has an associated value representing the average brightness in that region. In the case of a monochrome, or grey-scale, image, each pixel value is represented by a numeric value, which is typically in the range from 0 to 255, with 0 representing black, 255 representing white. In binary images the value of each pixel will be either 0 or 1, with 0 representing black and 1 representing white, while each pixel has a triple value in colour images representing the contribution from the three primary colours Red, Green and Blue colours, each value being typically in the range from 0 to 255, where 0 indicates that none of that primary colour is present in the colour of that pixel and 255 indicates a maximum amount of that primary colour. Since the images that we will be working on are captured by the imaging system in grey- scale form, the following algorithms and techniques will concentrate on grey-scale images.

3.2 Image pre-processing

The objective of the image pre-processing algorithms is to change pixel values in the image so that it is more suitable for subsequent analysis than the original image, for a specific application. There is no general theory of image enhancement, and the observer is the judge of how well a particular method has worked (Gonzalez et al. 2002). The pre-processing methods include brightness and contrast enhancement, histogram equalization, image smoothing and filtering and are described in the following sections.

3.2.1 Image brightness and contrast enhancement

In this process the brightness of the whole image is adjusted. This involves the use of a histogram showing the number of occurrences (pixels values) of each frequency level in the

image. An image with L grey levels has the range $r = [0, L-1]$. When r_k is the k^{th} grey level then n_k is the number of pixels in the image having grey level r_k as seen in Figure 3.2 on the next page.

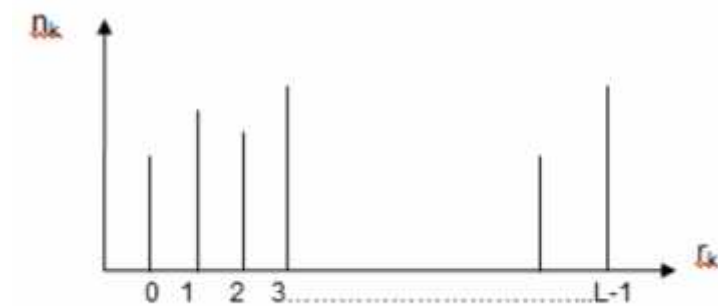


Figure 3.2 Image histogram

Increasing or decreasing the brightness of an image is simply done by the subtraction or addition of a constant from all pixel values. Decreasing the brightness (move the histogram to the left) requires a subtraction operation, while increasing the brightness (move the histogram to the right) requires an addition operation to be performed. An example of this technique is shown in Figure 3.3 for some of the images used in this study.

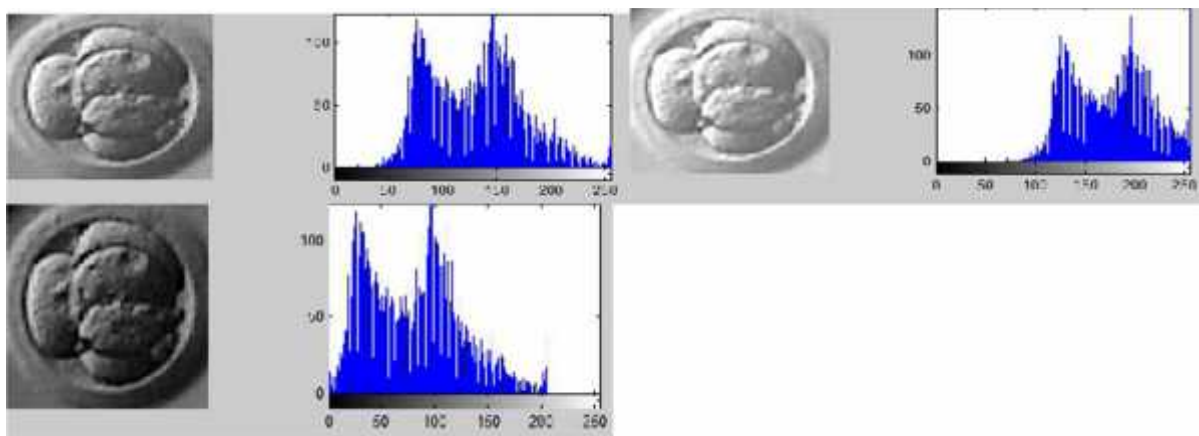


Figure 3.3 Image brightness enhancement (top right) original image (top left) image after increasing the brightness (bottom) image after decreasing the brightness

Unlike, the brightening operations shown in Figure 3.3 which do not change the distribution of the pixel values in the histogram, contrast enhancement is achieved by changing the distribution of pixel values in the original image. The contrast enhancement of the image involves scaling pixel values to stretch the histogram to cover the complete range of grey-level values (Figure 3.4) but it does not change the general shape of the histogram (the peak values are the same) (Awcock et al. 1995). Mathematically, the contrast adjustment operation is defined as:

$$output = \begin{cases} loweroutput & \text{if } input \leq lowerinput \\ loweroutput + (input - lowerinput) \left(\frac{upperoutput - loweroutput}{upperinput - lowerinput} \right), & \text{if } lowerinput < input < upperinput \\ upperoutput & \text{if } input \geq upperinput \end{cases}$$

Where the input value is *input* and its limits are *lower input* and *upper input* and the output value of the image after enhancement is *output* and its limits are *lower output* and *upper output*.

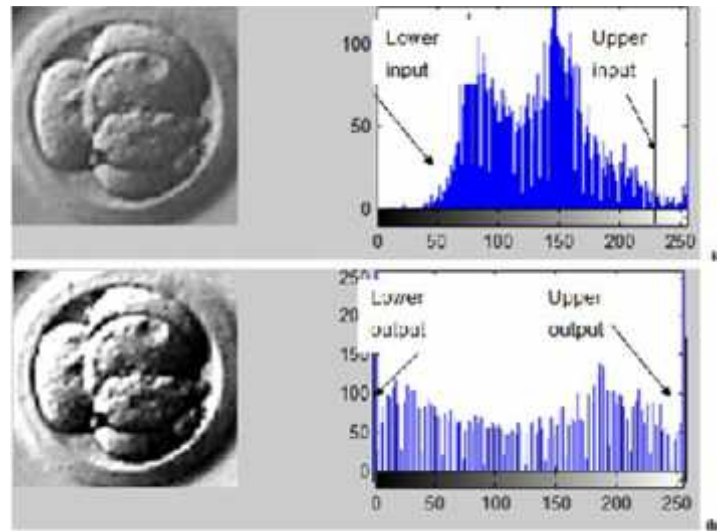


Figure 3.4 Contrast enhancement (a) original image (b) image after contrast enhancement

3.2.2 Histogram equalization

Histogram equalization is used to achieve another form of contrast enhancement. This enhancement is done by adjusting the pixel values to produce a better distribution in the histogram, and ideally all the histograms become equally populated. It usually increases the global contrast of the images, especially when the features of the image are represented by close contrast values. However, it is also useful with the images with backgrounds and foregrounds that are both bright or both dark.

To apply histogram equalization on a grey-scale image it is first necessary to calculate the image's normalised histogram, p from:

$$p(x_i) = \frac{n_i}{n} \quad i \in 0, 1, \dots, L-1$$

Where n_i is the number of occurrences of grey level i , L is the total number of grey levels in the image, n is the total number of pixels in the image. The contents of each histogram bin will range between 0 and 1.

The cumulative distribution function is then derived from:

$$c(i) = \sum_{j=0}^i p(x_j)$$

And finally, the transformation function, $T(i)$ which maps each pixel value i to the new pixel value is given by:

$$T(i) = \text{round}((L - 1) * c(i))$$

This procedure is illustrated in Figure 3.5. Figure 3.5(a) shows the pixels values of a 10x10 image ($n=100$). For simplicity, the grey levels L will be just 16, and this will make the value of i range from 0 to 15. The intermediate values in the histogram equalisation process are shown in Figure 3.5 (b) and the resulting histogram equalised image in Figure 3.5(c).

10	8	15	14	7	11	15	11	15	15
14	13	15	5	6	15	4	11	10	15
13	6	15	13	12	9	12	15	5	15
5	15	15	15	13	15	11	7	14	6
15	9	7	4	8	7	7	11	4	15
4	12	15	11	8	12	5	5	8	5
15	12	9	15	14	6	6	14	11	15
12	5	5	8	11	6	4	5	15	15
10	11	8	15	9	15	14	8	15	10
6	15	7	12	15	8	6	8	5	15

(a) original image

7	6	15	11	4	8	15	8	15	15
11	10	15	2	3	15	1	8	7	15
10	3	15	10	9	6	9	15	2	15
2	15	15	15	10	15	8	4	11	3
15	6	4	1	6	4	4	8	1	15
1	9	15	8	6	9	2	2	6	2
15	9	6	15	11	3	3	11	8	15
9	2	2	6	8	3	1	2	15	15
7	8	6	15	6	15	11	6	15	7
3	15	4	9	15	6	3	6	2	15

(c) image after equalization

i	n_i	$P_i = n_i/n$	$C(i)$	$T_i = 15 * C(i)$
0	0	0	0	0
1	0	0	0	0
2	0	0	0	0
3	0	0	0	0
4	5	0.05	0.05	1
5	10	0.1	0.15	2
6	8	0.08	0.23	3
7	6	0.06	0.29	4
8	9	0.09	0.28	6
9	4	0.04	0.42	6
10	4	0.04	0.46	7
11	9	0.09	0.55	8
12	7	0.07	0.62	9
13	4	0.04	0.66	10
14	6	0.06	0.72	11
15	28	0.28	1	15

(b) Histogram equalization

Figure 3.5 Example of histogram equalisation

3.2.3 Image smoothing

The aim of this process is to smooth the image in order to reduce unwanted noise and so improve the visibility of important structures in the image. Unlike the previous techniques where the modified value of a pixel depended only on the original value of the pixel, this technique uses the values of the surrounding neighbourhood pixels to determine the enhanced value of each pixel. The neighbourhood can either involve 4 neighbours, as shown in Figure 3.6(a) or 8 neighbours, as in Figure 3.6(b).

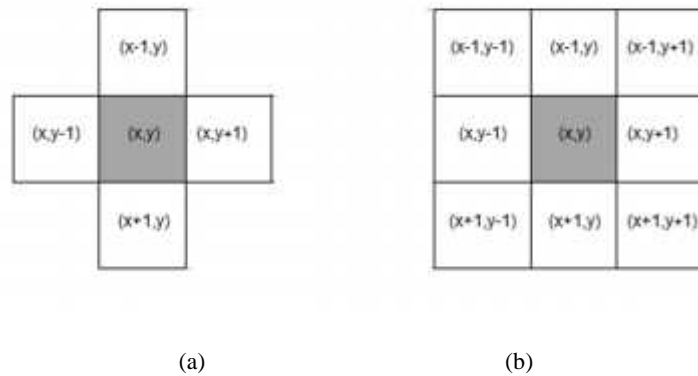


Figure 3.6 Neighbourhood (a) 4 neighbours (b) 8 neighbours

The smoothing techniques use the values of the image in the specified neighbourhood and the corresponding values of a sub-image with the same dimensions. The sub-image is sometimes called a filter or mask. An $n \times n$ mask means that the mask consists of n columns and n rows, and for example, the 8 neighbour mask shown in Figure 3.6(b) is a 3×3 mask.

The process is performed by simply applying the mask from the first top left point of the image rightwards and downwards until the end of the bottom right end of the image. At each point (x,y) , the output is given by a sum of products of each mask value and its corresponding image pixel value. Figure 3.7 on the next page shows the 3×3 masking process on an image.

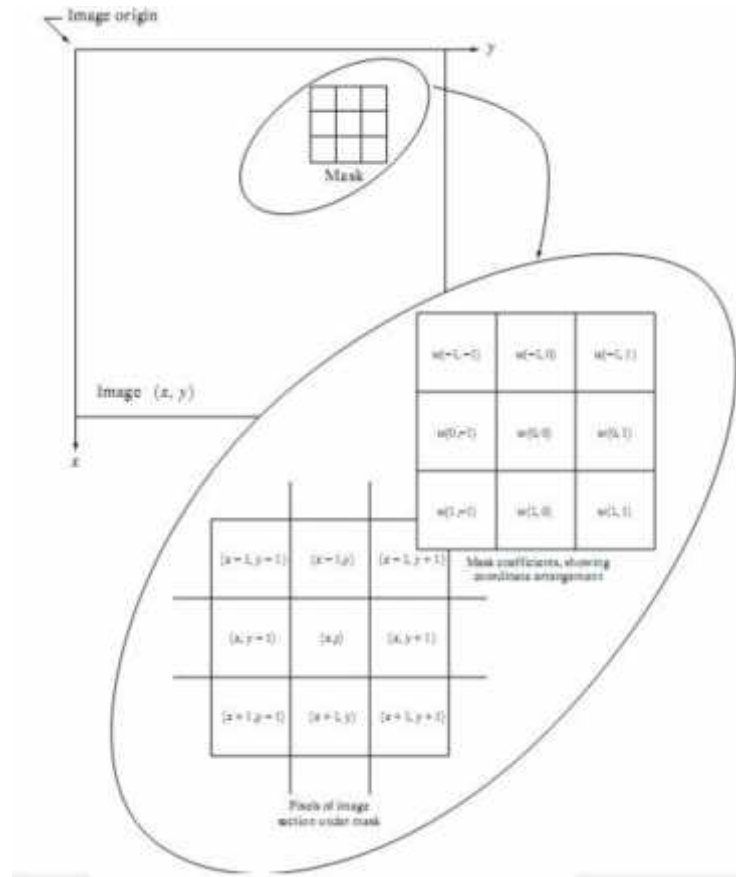


Figure 3.7 3x3 masking process

For a mask $w(x,y)$, with x and y having values from -1 to $+1$ for a 3×3 mask, the centre of the mask, $w(0,0)$, should coincide with the image at $I(x,y)$ indicating that the result $R(x,y)$ value will replace the pixel at (x,y) . The result $R(x,y)$ is calculated using as:

$$\begin{aligned}
 R(x,y) = & w(-1,-1) * I(x-1,y-1) + w(-1,0) * I(x-1,y) + \\
 & w(-1,1) * I(x-1,y+1) + w(0,-1) * I(x,y-1) + w(0,0) \\
 & * I(x,y) + w(0,1) * I(x,y+1) + w(1,-1) * I(x+1,y-1) \\
 & + w(1,0) * I(x+1,y) + w(1,1) * I(x+1,y+1)
 \end{aligned}$$

Mean (average) smoothing mask

The mean smoothing mask is shown in Figure 3.8 where it may be seen that each element makes an equal contribution to the output.

$1/9$	$1/9$	$1/9$
$1/9$	$1/9$	$1/9$
$1/9$	$1/9$	$1/9$

Figure 3.8 3x3 mean smoothing mask

This masks effectively replaces each pixel value in the image with the mean (average) value, which reduce the noise fluctuations leading to a smoother looking image. The averaging process also reduces fine detail and makes the image look less sharp or blurred. In Figure 3.9(a) the original image is shown and the image after applying the mean smoothing mask is shown in Figure 3.9(b).



(a)

(b)

Figure 3.9 Effect of mean smoothing mask

Median smoothing

An alternative to simple averaging is median smoothing, where the pixel values of the image coinciding with the mask are first sorted and the new pixel value is the median (middle) pixel value. An example of this operation is shown for the 3 x 3 mask depicted below.

125	126	133	140	127
122	120	126	123	126
123	123	150	135	133
120	126	125	145	138
125	126	128	144	140

The image values are 120, 126, 123, 123, 150, 135, 126, 125, and 145. These values are sorted to give: 120, 123, 123, 125, 126, 126, 135, 145 and 150. The median is the 5th element, and so the value 126 is the new value which will replace the value 150 (at the centre of the mask). Applying this mask to an image (Figure 3.10(a)), the effect is illustrated in Figure 3.10(b).

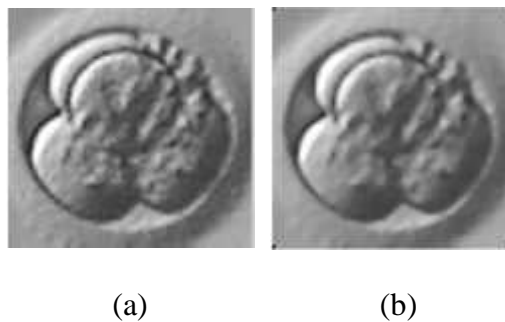


Figure 3.10 Effect of median smoothing

3.2.4 Image segmentation

The objective of the segmentation process is to partition an image into meaningful regions which correspond to part of or the whole of objects within the scene (Awcock et al. 1995). Image segmentation algorithms are generally based on intensity discontinuity or similarity. The first uses the abrupt changes in the pixel values which are usually associated with the edges of an object in the image to define its boundary. The second type partitions the image into regions that are similar according to a set of predefined criteria, such as having values above a thresholding value. These two approaches are described in the following Sections.

3.2.4.1 Edge detection

An edge is a set of connected pixels that lie on the boundary between two regions (Gonzalez et al. 2002). Figure 3.11(a) shows a model of an ideal digital edge which is available at the transition of two different grey levels intensity. However, Figure 3.11 (b) is a practical view of the same image which shows a blurry edge rather than a sharp edge due to many factors such as image acquisition and optical imperfection. The abrupt change in the grey-level is shown in Figure 3.11(c) and Figure 3.11(d) shows the more realistic ramp change in the grey-level intensity. The first derivative of Figure 3.11 (d) is given in Figure 3.11 (e). There is a positive transition at the point of going from the dark side to the lighter side of the image; it is constant for the points in the ramp; and there is another transition at the point from the ramp to the light side of the image. This demonstrates that the first derivative can detect the presence of an edge in an image.

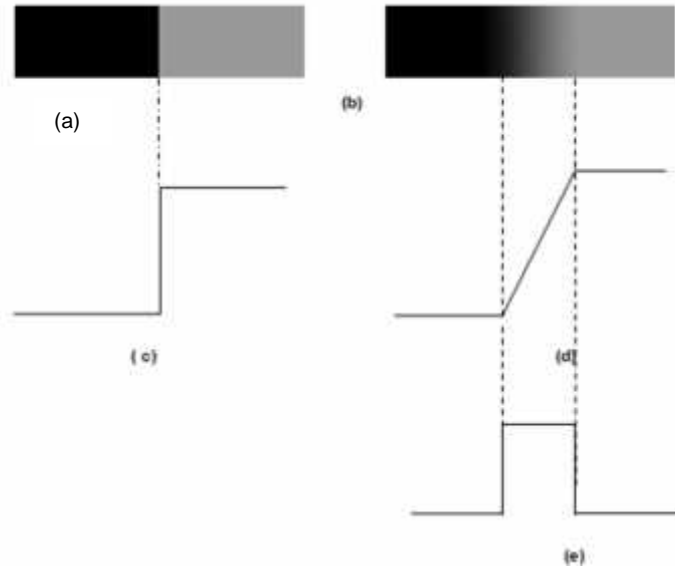


Figure 3.11 Different types of edges (a) ideal image (b) digital image (c) abrupt change in grey level (d) ramp change in the grey level (e) first derivative of the ramp.

The first derivative of an image is based on the 2-D gradient. The gradient $G(x,y)$ of an image depends on both the magnitude and orientation gradients. The magnitude gradient, $|G|$, and orientation angle, α , may be calculated from:

$$|G| = \sqrt{G_x^2 + G_y^2}$$

or

$$|G| = |G_x| + |G_y|$$

$$\alpha = \tan^{-1} \left(\frac{G_x}{G_y} \right)$$

As noise variations will appear as small discontinuities, a pixel in the image is considered to be part of a real edge if its first derivative gradient is greater than a pre-determined threshold value. In many cases the presence of an edge is all that is required and so the orientation angle is not calculated.

Edge detection of an entire image using the magnitude gradient and orientation angle measures can be implemented using masks with the appropriate weights. Typical of these are the Roberts, Sobel and Prewitt edge detectors, where a pair of masks is used which are designed to detect orthogonal components of edges, $|G_x|$ and $|G_y|$, which are then combined to give the $|G|$ and, if necessary and the orientation angle, θ .

Roberts edge detector

The Roberts edge detector uses a pair of 2x2 mask as shown in Figure 3.12. If the pixel grey-level values in a neighbourhood are those in Figure 3.12(a), the values of $|G_x|$ and $|G_y|$ are generated using the pair of masks shown in Figure 3.12(b) and Figure 3.12(c) respectively which are sensitive to diagonal edges.

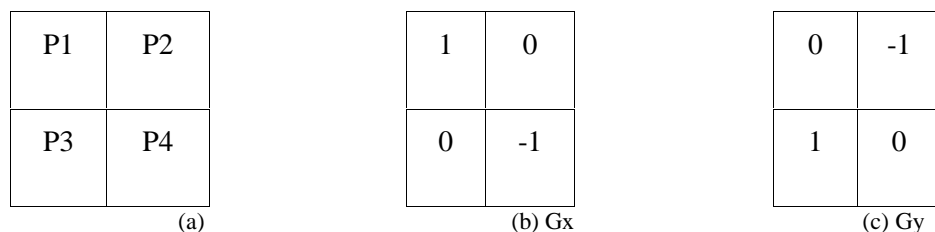


Figure 3.12 Roberts 2x2 masks

$$|G_x| = |P1 - P4|, \quad |G_y| = |P3 - P2|$$

Sobel edge detector

The Sobel edge detector is probably the most popular basic edge detector and uses a pair of 3x3 masks, as illustrated in Figure 3.13(b) and Figure 3.13(c) where G_x is sensitive to vertical edges and G_y sensitive to horizontal edges.

P1	P2	P3	-1	0	1	1	2	1
P4	P5	P6	-2	0	2	0	0	0
P7	P8	P9	-1	0	1	-1	-2	-1

(a) Gx Gy

Figure 3.13 Sobel 3x3 masks

If the pixel grey-level values in a neighbourhood are those in Figure 3.13(a) then

$$|Gx| = |(P3 + 2 * P6 + P9) - (P1 + 2 * P4 + P7)|$$

$$|Gy| = |(P1 + 2 * P2 + P3) - (P7 + 2 * P8 + P9)|$$

Prewitt edge detector

The Prewitt edge detector also uses a pair of 3x3 masks but with different weights values as illustrated in Figure 3.14(b) and Figure 3.14(c) where again Gx is sensitive to vertical edges and Gy sensitive to horizontal edges.

P1	P2	P3	-1	0	1	1	1	1
P4	P5	P6	-1	0	1	0	0	0
P7	P8	P9	-1	0	1	-1	-1	-1

(a) (b) Gx (c) Gy

Figure 3.14 Prewitt 3x3 mask

In this case Gx and Gy are derived from:

$$|Gx| = |(P3 + P6 + P9) - (P1 + P4 + P7)|$$

$$|Gy| = |(P7 + P8 + P9) - (P1 + P2 + P3)|$$

3.2.4.2 Thresholding

Thresholding converts a grey-scale image into a binary image according to a pixel's grey-level value. The basic thresholding technique involves manually selecting a Threshold, T , such that the pixels in the object(s) of interest have grey-level values greater than T , and are set to 1 while the background is set to 0.

A refinement of this technique is to select the Threshold from a histogram of the pixel grey-level values in the image. If the histogram has identifiable peaks and valleys as the histogram shown in Figure 3.15, the threshold T in this case can be chosen automatically as the valley point.

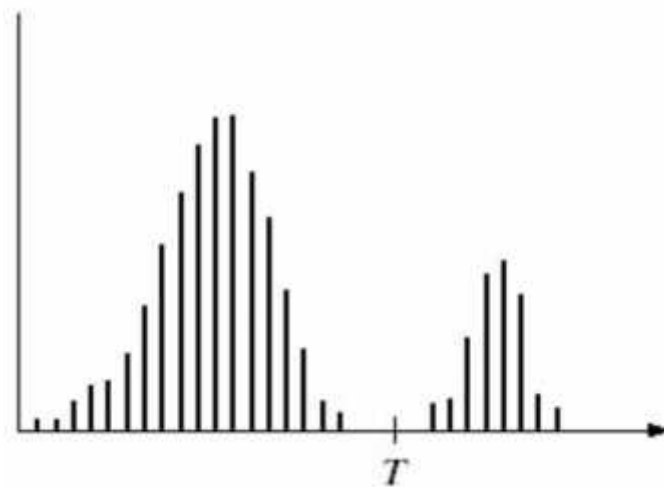


Figure 3.15 Thresholding using histogram

3.3 Object detection

The principle of object detection is to determine the presence or absence of an object that is suspected of being in the image. Some of the commonly used techniques that are particularly appropriate for this study are the Hough Transform and template matching, which was used in the work presented by Mirosław et al. (2005).

3.3.1 Hough Transform

The Hough Transform (Hough et al. 1960) is a technique used to find shapes in a binary digital image. By using Hough Transform it is possible to find all kinds of shapes that can be expressed mathematically such as straight lines, circles and ellipses.

The simple case is the detection of the presence of straight lines in an image. For any point (x,y) in the image, all lines which pass through that pixel have the form $y = mx + c$. However, if this equation was rewritten as $c = -mx + y$ (also called *parametric space*) and the value of x and y were considered as constants, and the value of m and c as variables, each line in parametric space represents a point on the line (x,y) , as shown in Figure 3.16. More importantly, all pixels which lie on the same line in (x, y) space will pass through the same point in (m,c) space.

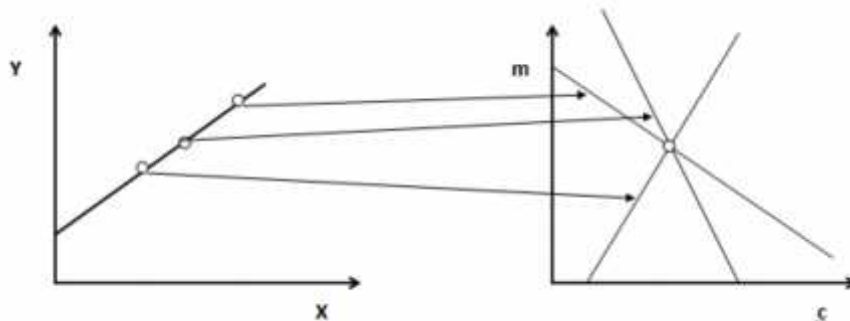


Figure 3.16 The xy plane and the parametric plane

The Hough Transform works by letting each point (x,y) vote in (m,c) space for each possible line passing through it. These votes are added in an accumulator for each (m, c) , and for example, if, after all pixels have been considered, that a particular (m,c) has one vote- this means that there is one point through which this line passes. If a position (m',c') in the accumulator has n votes, this means that n feature points lie on that line, and this is strong evidence for the presence of a line, $y=m'x +c'$ in the image.

Similarly, the Hough Transform can be used to determine the parameters of a circle when a number of points that fall on the perimeter are known. A circle with radius R and centre (a, b) can be described with the following parametric equations:

$$x = a + R \cos(\theta)$$

$$y = b + R \sin(\theta)$$

When the angle θ sweeps through the full 360 degree range the points (x, y) trace the perimeter of a circle. If an image contains many points, some of which are falling on perimeters of circles, then the job of the search program is to find parameter triplets (a,b,R) to describe each circle. The fact that the parameter space is 3D makes a direct implementation of the Hough technique more expensive in computer memory and time. In order to decrease these, known or fixed radii R can be used.

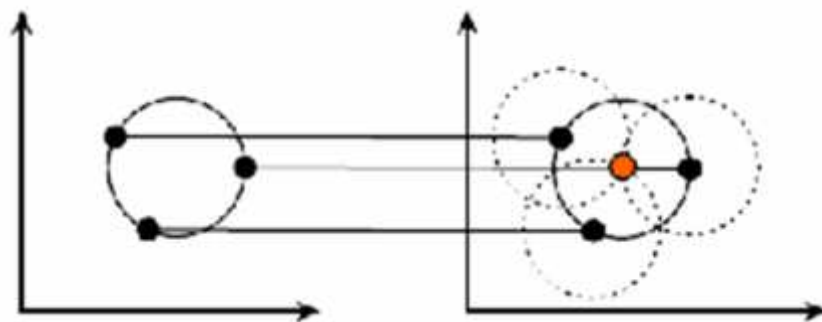


Figure 3.17 Hough transform of a circle with fixed radius

Figure 3.17 shows that each point in the circle (left) with a fixed radius generates a circle in the parameter space (right). The true centre point will be the common point to all parameter circles, and can be found by allocating the maximum value in a Hough accumulation array.

3.3.2 Template matching

Template matching is an extension of the 3 x 3 mask process, but the templates are usually larger and contain an image of the object that is being searched for. The template is moved systematically around the whole image, or a selected region, the degree of similarity, or correlation, between the template and the image at each position is evaluated. If the correlation is high, then the object is considered to have been detected and is positioned at the co-ordinates of this match. The formula used to calculate the values of the correlation array is:

$$S(m,n) = \sum_j \sum_k [IM(j,k)T(j-m,k-n)]$$

where $S(m,n)$ is the similarity measure of point (m,n) , $IM(j,k)$ denotes the image of size (j,k) and T is the template.

This is illustrated in Figure 3.18 for the small template shown in Figure 3.18(a), the image of Figure 3.18(b). The correlation array that is produced is shown in Figure 3.18(c). The highest value in the correlation array is 8 and its position is at the second row in the first column and it corresponds in the image to the starting point at the second row and first column till the fourth row and the third column.

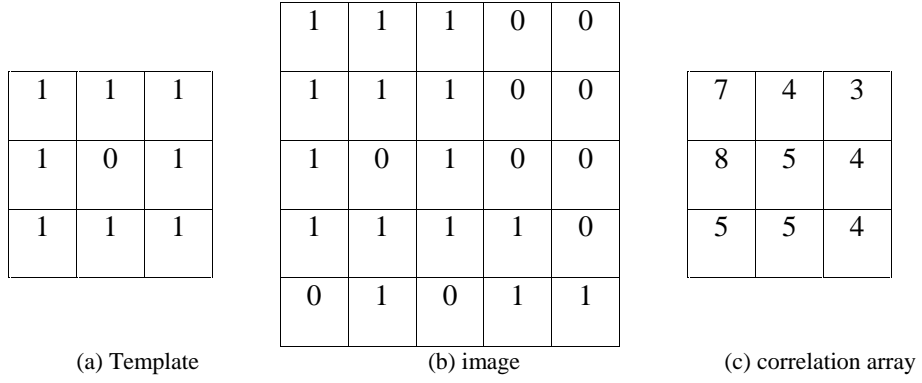


Figure 3.18 Template Matching

However, because the correlation value can go high about a particular coordinate (m,n), the normalized cross-correlation technique is a good solution for such a situation. The normalized cross-correlation has a maximum value of 1 that occurs if and only if the template matches that exact position in the image. This is given below, where the normalized cross correlation is denoted by:

$$NCC(m, n) = \frac{\sum_{m,n} [IM - IM_{mean}][T - T_{mean}]}{\sqrt{\sum_{m,n} [IM - IM_{mean}]^2 \sum_{n,n} [T - T_{mean}]^2}}$$

where IM is the image, IM_{mean} is the mean of the image, T is the template and T_{mean} is the mean of the template. Considering the same example given in Figure 3.18 (a) and (b), when applying the NCC to it the result is given in Figure 3.19.

-0.14	-0.29	0.29
1	-0.29	0.37
-0.21	-0.29	-0.37

Figure 3.19 Results of NCC

3.4 Implementing the Image processing algorithms

Many different programming languages and environments can be used to implement image processing algorithms that have been described, such as C, C++, or Java. However, the MATLAB environment was chosen because it is a high-level technical computing language and interactive environment for algorithm development, data visualization, data analysis, and numeric computation (MATLAB- Mathsworld. 2011). It is used in a wide range of applications, including signal and image processing and many other applications. It also has special toolboxes that contain many built-in functions, including Image Processing libraries that can be easily incorporated into an application. MATLAB also supports vector and matrix operations that are fundamental to engineering and image processing problems. This environment provides a well-supported tool that enables fast development, allowing the user to focus on the extensions to the basic algorithms as required, providing a solution in a particular application.

3.5 Conclusion

A range of image processing techniques have been described in this Chapter, concentrating on those that have been effective in the past for analysing microscope images of cell. The circular nature of the cells being detected and classified in this study would be a good reason for choosing Hough Transform for circle detection initially. However, it is clear that the images would need to be pre-processed to provide the edge-detected images that are required as input to the Hough Transform, possibly with some enhancement to support the edge-detection process. The investigation of the best enhancement and edge-detection techniques for the embryo data is described in the next Chapter.

Chapter 4 Pre-processing of the embryo images

Overview

This chapter covers the investigation and trials of some of the common segmentation and detection techniques on the embryo images as a pre-processing stage. It also includes the algorithm used to overcome the variations in magnification of the images.

4.1 Introduction

The pre-processing process consists mainly of two main operations. The first is to solve the issue of the image having different magnifications. These magnifications are due to the different magnifications of the imaging system, and this step is essential to compensate for this issue. The next is detecting the edges of these images and this step is important for certain techniques that work on edged images rather than the grey scale form. Different approaches are applied and considered for both operations and these are discussed in the following sections.

4.2 Magnification compensation

The size of the cells (blastomeres) in an embryo depends on the age of the embryo itself. According to the research presented by Hnida et al. (2004), the size of the blastomeres of the embryos at Day 1 after fertilization differ from that of Day 2, 3 or even 5. However, since the work proposed in thesis considers the embryo at Day 2, the size of such embryos is taken into consideration. One of the problems found in the set of images available was the difference in the magnification of the images due to the imaging system. Another was that all the research done on Day 2 embryos was done using their potential size (Hnida et al. 2004) while the work here focuses on their pixels equivalence, so a sort of conversion was needed.

The approach taken is to compensate and normalise the different magnifications issue. This was done by detecting the ZP and then estimating its diameter in pixels. As the potential size of the embryo in μm was known, and its equivalent size in pixel was estimated, then the scale of magnification can be calculated. The algorithms used are discussed below.

4.2.1 Detection of the ZP

When investigating the possible techniques and the work done on ZP detection in the Literature Survey, the key research was done by Morales et al. (2008) who aimed to detect the thickness of the ZP. The disadvantage of this approach is that it concentrated on the thickness of the ZP and to do so it used a rather complex technique. The other alternative was using Hough Transform to detect the ZP which has a circular shape. The Hough Transform would be used with an indefinite size of the radius. This requires the accumulator to be a 3D array that corresponds to the x-centre, y-centre and the radius of the circle. The maximum

value of the 3D accumulator will correspond to the radius of the ZP being the biggest circle available.

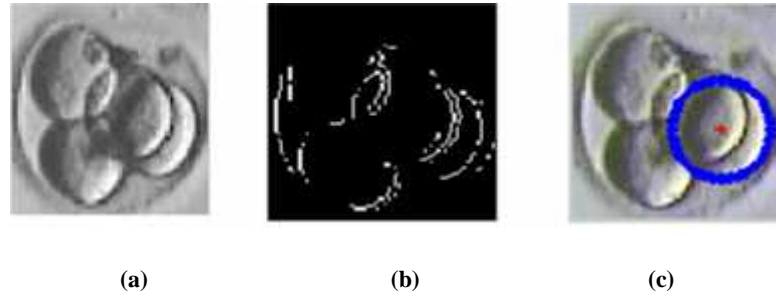


Figure 4.1 Result of detecting the ZP using Hough Transform

Figure 4.1(a) shows an image, the edges of the image is shown in Figure 4.1(b). The ZP is not detected because the intensity variation between the ZP and the surrounding is less than the intensity between the border of the cells and the surroundings. For this reason when the Hough Transform was applied to such an image, a cell was detected rather than the ZP. This is shown in Figure 4.1(c). Since this stage is very important to the rest of the work, failing to detect the ZP size properly was a reason to propose another algorithm that can detect the ZP properly and that is much simpler to implement.

The aim is to detect the ZP simply and then get a rough estimate of its diameter. It was recognized that the ZP can be detected by the presence of a slight difference in the grey level between it and the background and this observation was used to detect the diameter of the ZP.

The initial step of the proposed technique involves the four mid-points of the image at the left, the right, up and down sides as shown in Figure 4.2. These values that are available on the four sides are used as the initial values for an inwards motion towards the centre of the

image. The motion continues at each side separately as long as the intensity difference between that pixel and the next remains smaller than a certain value. This value was determined after investigating the images in the dataset and having a close look at the difference of the grey levels between the border of the ZP and its surrounding. This value was found to be 20 for the available dataset. However, for other images this value might vary.

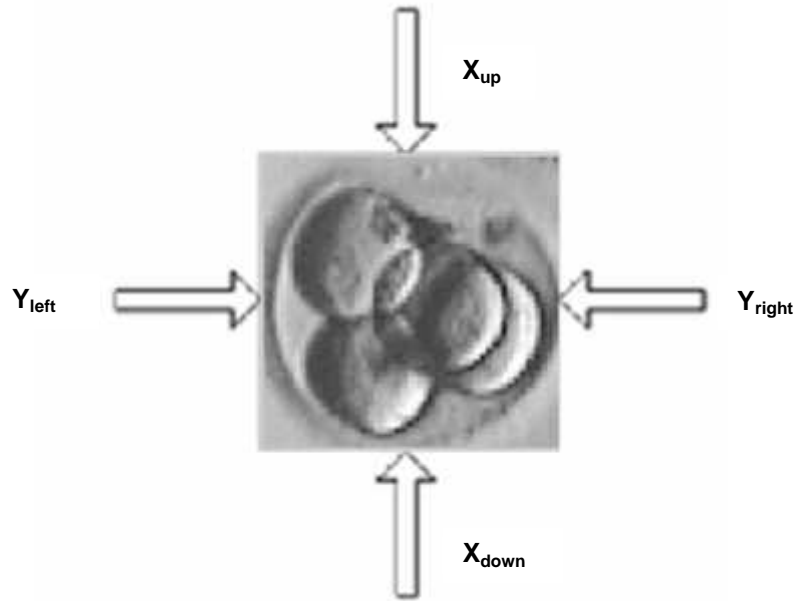


Figure 4.2 Mid-points of the ZP

Eventually, the motion stops at each side yielding four different (x,y) coordinates, and the approximate centre and diameter of the ZP were calculated using

$$X_v = x_{up} - x_{down}$$

$$Y_v = y_{left} - y_{right}$$

$$D = maximum(X_v, Y_v)$$

where x_{up} are the x coordinates of the motion that started from the top of the image,

x_{down} the x coordinates of the motion that started from the bottom of the image. Note that their y coordinates were neglected since they were the same. Similarly, y_{left} and y_{right} are the y coordinates of the motion that started from the left and the right of the image, respectively. D is the estimated diameter of the ZP. Figure 4.3 indicates the result of applying this algorithm on an embryo's image.

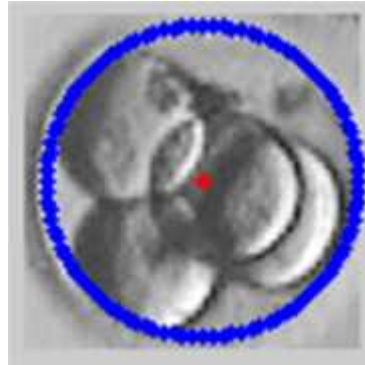


Figure 4.3 The result after ZP detection

4.2.2 The size of ZP

The estimation of the diameter of the ZP is just an initial step towards determining the size of the embryo. The size of the embryo in the image must correspond to its size in reality. Measurements on the images are done in pixels and converted to actual physical units by knowing the scale of conversion. However, knowing that the size of Day 2 embryo to be about 0.15 mm and the size of the ZP in pixels, the required scale was calculated by .

$$S = \text{size of zona pellucida} / \text{Actual size}$$

The scale S was calculated by dividing the size of the ZP which represented the size of the image of the embryo in pixels by the actual size of the embryo given in μm . According to the work done by Hnida et al. (2004), the expected blastomeres diameter of a 4-cells

embryo was $64.9 \pm 8.5 \mu\text{m}$. This meant that the expected blastomeres ranged from $56.4 \mu\text{m}$ to $73.4 \mu\text{m}$. However, to know the size of such blastomeres in an image (in pixels) these values should be multiplied by the scale value S that was previously calculated. This gives the minimum diameter (in pixels) D_{\min} and the maximum diameter D_{\max} of the expected blastomeres.

Assume that the images had a diameter of 95 pixels. Knowing that actual size of the Day 2 embryo should be about 0.15 mm, the scale S can be calculated by dividing 95 by 0.15mm or $150 \mu\text{m}$ which will give a value of 0.63 pixels/ μm . However, to calculate D_{\min} the value of S was multiplied by the minimum value of the blastomere which was $56.4 \mu\text{m}$, this gave a value of 36 pixels. Similarly the value of D_{\max} was 46 pixels.

4.3 Edge detection

The second pre-processing operation that was considered important following the Literature Survey is edge-detection. Several algorithms were tried out, some of which gave acceptable results while others gave very weak edges and a further enhancement was required. These are described in the following sections and the results after applying different edge detection techniques to the embryo data are shown.

4.3.1 Edge detection using basic techniques

Different edge detection techniques such as Sobel and Prewitt that were described in the previous Chapter were implemented. The results are illustrated in Figure 4.4 for a typical embryo image. Neither techniques were particularly successful and only detected the stronger fragments of the cell edges. In some images the edges detected were very weak to the extent

that they were barely visible.



Figure 4.4 Image after applying Sobel and Prewitt

Different threshold were chosen, as shown in Figure 4.5, to try and improve clarify these edges but they did not improve the results. Upon increasing the threshold the edges became much lighter, while decreasing the threshold introduced more fragment and false edges due to noise in the image .



Figure 4.5 Using different thresholds on Sobel

4.3.2 Edge detection using a new approach

In order to try and overcome these drawbacks and hence produce an edge which was more clear, a new algorithm was developed. The idea behind this algorithm was based on the observation that the difference between the blastomere and its border was simply the difference in the grey level intensity. This is shown in Figure 4.6, where it may be seen that

the border was usually darker in colour than the rest of the blastomere.

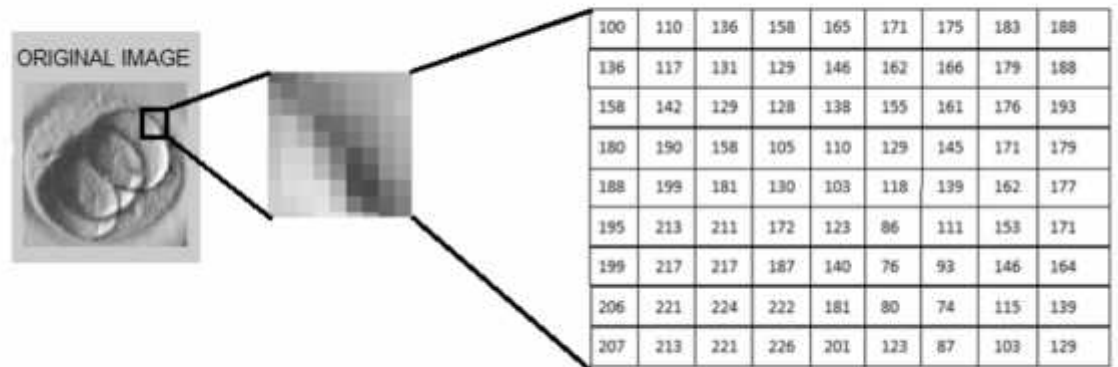


Figure 4.6 Intensity of the border

To distinguish this difference, subtracting the intensity of each pixel from its neighbour was performed, and if the difference was greater than a certain value, this point was considered a border. The border of the blastomere was darker than that of the ZP and this caused the value of the difference to be bigger. The value was found to be 25 for the available dataset. This was found after having a close view (Figure 4.6) to the value of the intensities between the border of the cell and the background. However, this value might change with a different image dataset. This process was performed in two directions. The first from left to right, that is the subtraction occurs between the pixel and its left neighbour. The other one occurs from top to bottom, which is where the subtraction occurs between the pixel and its below neighbour. As a result of merging these two results together, the border of the blastomere was achieved. Part of the image shown in Figure 4.6 that shows a border is illustrated Figure 4.7(a). This sample illustrates the left to right subtraction. Notice that the absolute value of the subtraction is the value to be considered rather than the signed value of it and this is given in Figure 4.7(b). The value at each location was examined, the location

that had a value above the threshold was given the value of 1 which represented a possible edge point otherwise it was given a 0. This is shown in Figure 4.7(c). The value of the threshold chosen was evaluated after several trials on the available images data set.

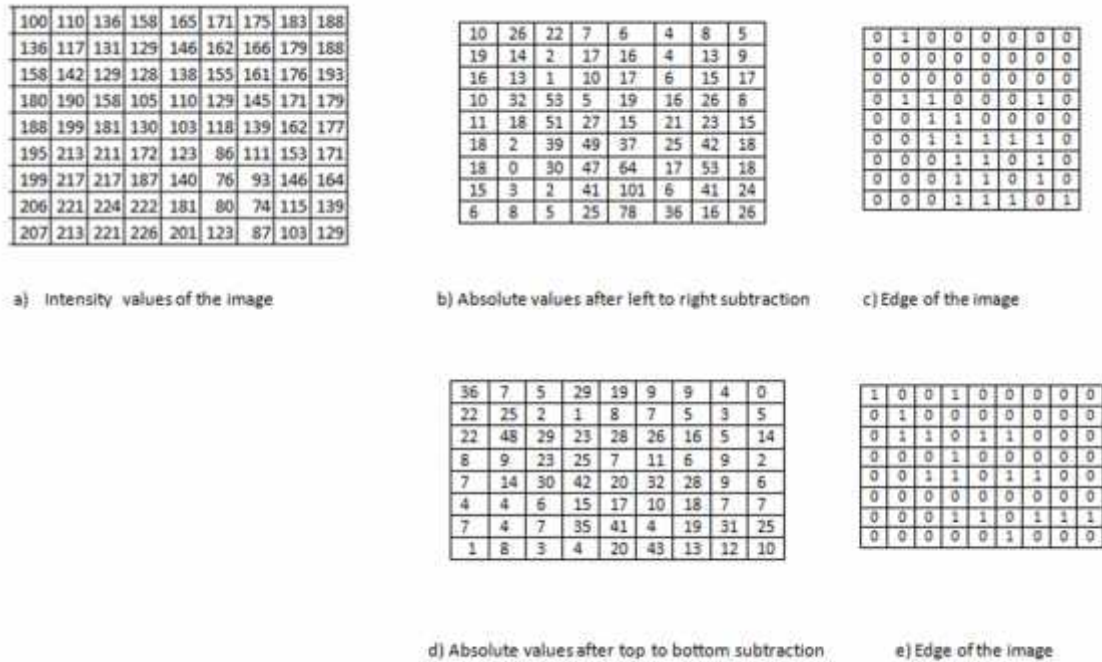


Figure 4.7 Difference between the intensity

Similarly, the subtraction was also performed from the top of the image towards the bottom as shown in Figure 4.7(d) and hence the edges in the vertical direction were detected as shown in Figure 4.7(e). Having these two results of the possible edges, one in the horizontal direction (Figure 4.7(c)) and the other in the vertical direction (Figure 4.7(e)) combining them together achieved the final edges of the image. This is shown in Figure 4.8.



Figure 4.8 Merging the two results

The result of this new algorithm (Elshenawy algorithm) is illustrated below in Figure 4.9. Comparing this result to the previous one in Figure 4.5, it was clearly shown that this method detected thicker edges rather than the thin edges that appeared after using Sobel edge detector.

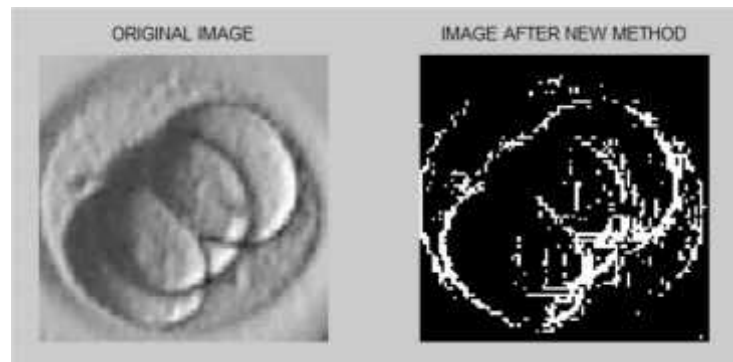


Figure 4.9 Edge detected using Elshenawy method

4.3.3 Edge detection using convolution mask

Another approach for getting the edges of the image was using masks similar to the ones used by Sobel, Prewitt or any other type but with different mask values. Figure 4.10 shows the convolution kernel used.

-3	0	3
-3	1	3
-3	0	3

Figure 4.10 Convolution kernel

The result of applying such a mask all over the image yielded an output image such as the one given in Figure 4.11(a) below. Upon studying the output image, it was obvious that

the edges of the image are the ones having darker grey intensity (closer to 0, so a simple thresholding technique was used. It changed the image into a binary image as shown in Figure 4.11(b).

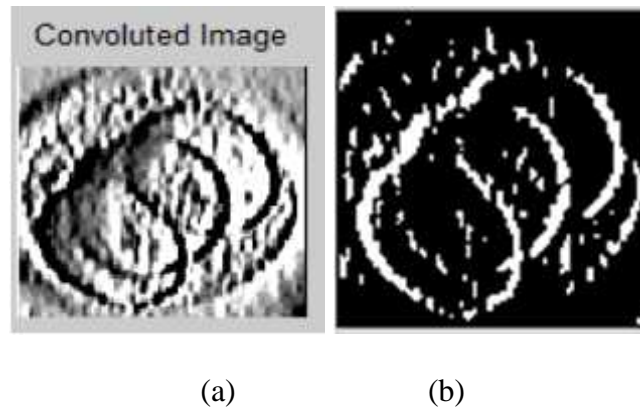


Figure 4.11 Image after applying the convolution kernel

4.4 Conclusion

The two main pre-processing operations consisted of resolving the magnification problem of the image and detecting the edges of the cells too. Resolving the magnification problem depended on the size of the ZP which was detected by the designed algorithm rather than Hough Transform or the work done by Morales et al. (2008). In the edge detection phase, the common algorithms such as Sobel and Prewitt showed poor edges and hence a new algorithm was essential. Two algorithms were designed, the first (Elshenawy) used the difference in grey level to detect the edge while the second used a convolution mask to do so. Both algorithms gave promising edges as a result and the next phases will show which algorithm is more efficient.

Chapter 5 Embryo Detection using the Hough Transform

Overview

The nature of the blastomere being circular leads to the initial approach of detecting them using common circle detection techniques such as Hough Transform. This chapter covers the implementation of the circular Hough Transform and its application to the embryo images. The technique will use some of the pre-processing stages discussed in the previous chapter, including three different edge-detection algorithms. The results obtained for each of these edge-detection algorithms are compared and discussed in terms of their robustness for cell detection.

5.1 Introduction

One of the common techniques used for detecting circles in an image is Hough Transform. The three parameters that such a technique must return are the centre x and y and the radius of the circle. However, with the increase in the number of parameters compared with the straight line detection, the complexity of the process also increases. For this reason, it was better to fix one of these parameters, and the natural one to constrain was the radius of the circle, which represents the radius of the cell. In order to apply Hough Transform the image

has to be in its edge form rather than the original image, this will reduce the time complexity of applying the Hough Transform. Since the input to the Hough transform is the x and y coordinates, it will be much better to feed the algorithm with the points that represent the edge of the image rather than all the points in the image. For this reason it was required to apply the two pre-processing stages discussed in the previous Chapter, which were the magnification compensation and the edge detection on the image before applying the Hough Transform.

5.2 Proposed technique

The proposed technique consists of two phases, the first of which is the pre-processing phase while the second is the Hough Transform phase. Figure 5.1 demonstrates the sequence and the output of these phases.

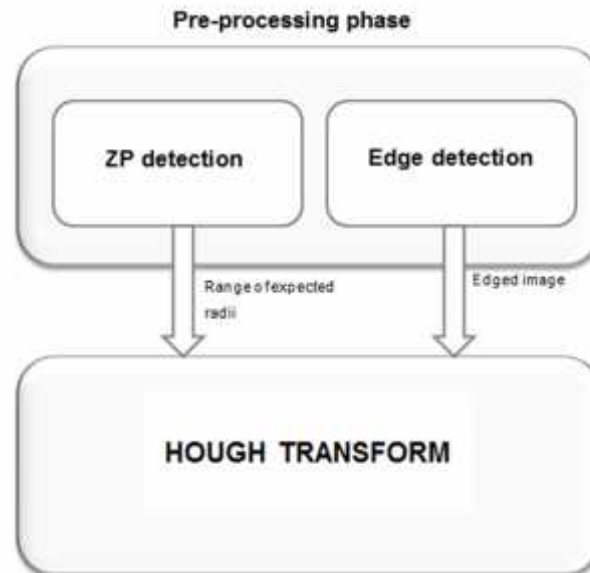


Figure 5.1 Algorithm used for applying Hough Transform

The ZP detection stage generates the range of expected diameters of Day 2 blastomeres, corresponding to the range having the minimum value of the diameter (in pixels)

D_{min} and the maximum diameter D_{max} . These are used as the diameter size to the Hough Transform in order to decrease the number of variables and hence the complexity of the algorithm. The other stage is the edge detection phase which detects the edges of the image using the three techniques mentioned earlier that were the Sobel edge detector, the new algorithm and finally the convolution mask. The outputs of these two phases are then fed to the Hough Transform algorithm.

Upon approaching this phase, the size of the radii needed in the transform would have been calculated along with the edges of the image. The Hough Transform was then applied to each of the edge detected images.

The number of iterations needed to apply the transform on the same image depended on the range of the radii available from previous calculations that were discussed in previous sections. These are the value of D_{min} and D_{max} in Algorithm 5-1 below.

Algorithm 5-1 Steps of applying Hough Transform

For $i = D_{min}$ to D_{max}

- *Apply Hough Transform using the value of i .*
- *Store the maximum value of the Hough Transform in an array x*

End for

Remove all the redundant values from x .

As discussed before, the result of applying the Hough Transform was the generation of a 3D accumulation array representing the x-centre, y-centre and the radius of the circle, but since the radius used is fixed, then a 2D accumulation array is generated instead. Each value in this array corresponded to the vote value of detecting a circle (of the specified radius) at this point. For example if the X and Y coordinates of the array had n votes this meant that n possible points passed through this point. The X and Y coordinate that were found to have the highest count, was considered to be the position of the strongest circle. However, since the image had more than one cell, detecting the one cell that had the maximum accumulator count was not appropriate for this application.

To compensate this problem all possible maximum values were considered and found. Figure 5.2 shows the difference between detecting only one peak value and detecting all peak values that that could indicate the presence of additional cells in the image.

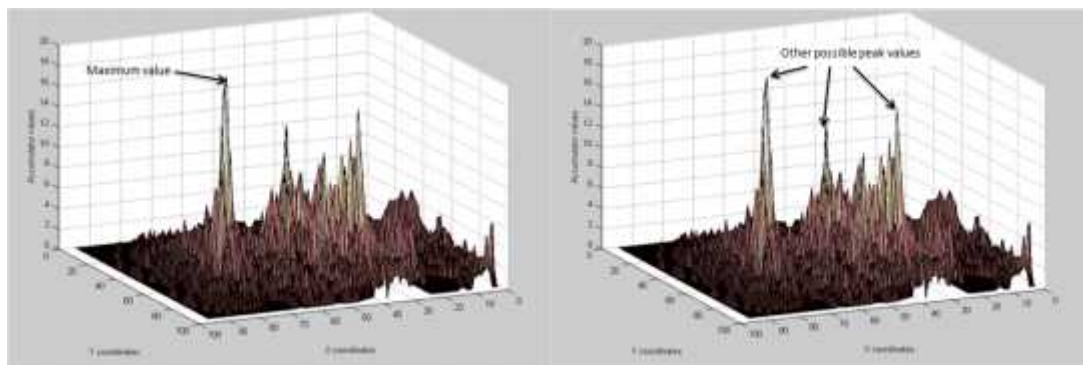


Figure 5.2 The accumulator values

The next step that followed applying Hough Transform involved storing the values that corresponded to the peak values in an array. Each time the transform was applied the results were appended at the end of this array. At the end of all the iterations this array held

all possible values of detected cells with the values of their radii .Table 5.1 gives the values of such an array, and corresponds to the image given in Figure 4.3. The first column contains the value of the radius used for applying the transform, whereas the second and the third columns are the X and Y coordinates of the centre of the cell. The last column contains the matching value of the transform which is the accumulator count and so is a measure of the strength of the circle.

Table 5.1 The value of the array

Size of radius	Center (X)	Center (Y)	Matching value
19	72	36	25
19	44	66	19
21	43	64	26
23	73	32	38
23	43	62	30
25	53	44	46
25	43	60	43

On inspection of this array, it was found that some of these values were redundant as they corresponded to the same circle. This can be clearly shown after plotting the X and Y values of the centres. Figure 5.3 shows that these values can be clustered only into three groups rather than the seven in the Table. The cluster size however, varied according to the size of the embryo which differed according to the magnification that was used on the images. The cluster size was chosen in a way to eliminate the redundant points but at the same time take into consideration the possibility of overlapping cells. Therefore, it was chosen to be 50% of the radius of the smallest cell, which was determined by the size of the ZP determined earlier.

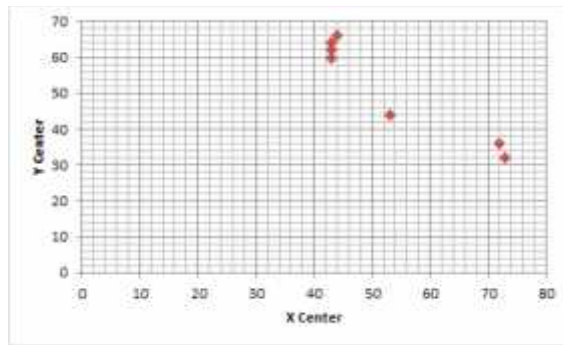


Figure 5.3 Plot of X and Y coordinates

The elimination of the redundant values was implemented using the steps indicated below: Assume that the data in Table 5.1 is in array 'a', the output is kept in array 'x', mask size 21x21.

Step #	Function of the step	Result of the round 1	Result of the round 2	Result of the round 3																																																																																				
1	Get the maximum matching value in 'a'	46																																																																																						
2	Place the corresponding value in array 'x'	$x =$ <table><tr><td>25</td><td>53</td><td>44</td><td>46</td></tr></table>	25	53	44	46	$x =$ <table><tr><td>25</td><td>53</td><td>44</td><td>46</td></tr><tr><td>25</td><td>43</td><td>60</td><td>43</td></tr></table>	25	53	44	46	25	43	60	43	$x =$ <table><tr><td>25</td><td>53</td><td>44</td><td>46</td></tr><tr><td>25</td><td>43</td><td>60</td><td>43</td></tr><tr><td>23</td><td>73</td><td>32</td><td>38</td></tr></table>	25	53	44	46	25	43	60	43	23	73	32	38																																																												
25	53	44	46																																																																																					
25	53	44	46																																																																																					
25	43	60	43																																																																																					
25	53	44	46																																																																																					
25	43	60	43																																																																																					
23	73	32	38																																																																																					
3	Replace the maximum matching value in 'a' with zero	$a =$ <table><tr><td>19</td><td>72</td><td>36</td><td>25</td></tr><tr><td>19</td><td>44</td><td>66</td><td>19</td></tr><tr><td>21</td><td>43</td><td>64</td><td>26</td></tr><tr><td>23</td><td>73</td><td>32</td><td>38</td></tr><tr><td>23</td><td>43</td><td>62</td><td>30</td></tr><tr><td>25</td><td>53</td><td>44</td><td>0</td></tr><tr><td>25</td><td>43</td><td>60</td><td>43</td></tr></table>	19	72	36	25	19	44	66	19	21	43	64	26	23	73	32	38	23	43	62	30	25	53	44	0	25	43	60	43	$a =$ <table><tr><td>19</td><td>72</td><td>36</td><td>25</td></tr><tr><td>19</td><td>44</td><td>66</td><td>19</td></tr><tr><td>21</td><td>43</td><td>64</td><td>26</td></tr><tr><td>23</td><td>73</td><td>32</td><td>38</td></tr><tr><td>23</td><td>43</td><td>62</td><td>30</td></tr><tr><td>25</td><td>53</td><td>44</td><td>0</td></tr><tr><td>25</td><td>43</td><td>60</td><td>0</td></tr></table>	19	72	36	25	19	44	66	19	21	43	64	26	23	73	32	38	23	43	62	30	25	53	44	0	25	43	60	0	$a =$ <table><tr><td>19</td><td>72</td><td>36</td><td>25</td></tr><tr><td>19</td><td>44</td><td>66</td><td>0</td></tr><tr><td>21</td><td>43</td><td>64</td><td>0</td></tr><tr><td>23</td><td>73</td><td>32</td><td>0</td></tr><tr><td>23</td><td>43</td><td>62</td><td>0</td></tr><tr><td>25</td><td>53</td><td>44</td><td>0</td></tr><tr><td>25</td><td>43</td><td>60</td><td>0</td></tr></table>	19	72	36	25	19	44	66	0	21	43	64	0	23	73	32	0	23	43	62	0	25	53	44	0	25	43	60	0
19	72	36	25																																																																																					
19	44	66	19																																																																																					
21	43	64	26																																																																																					
23	73	32	38																																																																																					
23	43	62	30																																																																																					
25	53	44	0																																																																																					
25	43	60	43																																																																																					
19	72	36	25																																																																																					
19	44	66	19																																																																																					
21	43	64	26																																																																																					
23	73	32	38																																																																																					
23	43	62	30																																																																																					
25	53	44	0																																																																																					
25	43	60	0																																																																																					
19	72	36	25																																																																																					
19	44	66	0																																																																																					
21	43	64	0																																																																																					
23	73	32	0																																																																																					
23	43	62	0																																																																																					
25	53	44	0																																																																																					
25	43	60	0																																																																																					
4	Let x_c be the corresponding x-centre value and y_c the corresponding y-centre value	$x_c=53, y_c=44$	$x_c=43, y_c=60$	$x_c=73, y_c=32$																																																																																				
5	Clear all the matching value in 'a' whose x-centre value and y-centre value are between the following range, x-centre between (x-centre value -N , x-centre value +N) y-centre between (y-centre value -N , y-centre value +N)	$a =$ <table><tr><td>19</td><td>72</td><td>36</td><td>25</td></tr><tr><td>19</td><td>44</td><td>66</td><td>19</td></tr><tr><td>21</td><td>43</td><td>64</td><td>26</td></tr><tr><td>23</td><td>73</td><td>32</td><td>38</td></tr><tr><td>23</td><td>43</td><td>62</td><td>30</td></tr><tr><td>25</td><td>53</td><td>44</td><td>0</td></tr><tr><td>25</td><td>43</td><td>60</td><td>43</td></tr></table>	19	72	36	25	19	44	66	19	21	43	64	26	23	73	32	38	23	43	62	30	25	53	44	0	25	43	60	43	$a =$ <table><tr><td>19</td><td>72</td><td>36</td><td>17</td></tr><tr><td>19</td><td>44</td><td>66</td><td>0</td></tr><tr><td>21</td><td>43</td><td>64</td><td>0</td></tr><tr><td>23</td><td>73</td><td>32</td><td>38</td></tr><tr><td>23</td><td>43</td><td>62</td><td>0</td></tr><tr><td>25</td><td>53</td><td>44</td><td>0</td></tr><tr><td>25</td><td>43</td><td>60</td><td>0</td></tr></table>	19	72	36	17	19	44	66	0	21	43	64	0	23	73	32	38	23	43	62	0	25	53	44	0	25	43	60	0	$a =$ <table><tr><td>19</td><td>72</td><td>36</td><td>0</td></tr><tr><td>19</td><td>44</td><td>66</td><td>0</td></tr><tr><td>21</td><td>43</td><td>64</td><td>0</td></tr><tr><td>23</td><td>73</td><td>32</td><td>0</td></tr><tr><td>23</td><td>43</td><td>62</td><td>0</td></tr><tr><td>25</td><td>53</td><td>44</td><td>0</td></tr><tr><td>25</td><td>43</td><td>60</td><td>0</td></tr></table>	19	72	36	0	19	44	66	0	21	43	64	0	23	73	32	0	23	43	62	0	25	53	44	0	25	43	60	0
19	72	36	25																																																																																					
19	44	66	19																																																																																					
21	43	64	26																																																																																					
23	73	32	38																																																																																					
23	43	62	30																																																																																					
25	53	44	0																																																																																					
25	43	60	43																																																																																					
19	72	36	17																																																																																					
19	44	66	0																																																																																					
21	43	64	0																																																																																					
23	73	32	38																																																																																					
23	43	62	0																																																																																					
25	53	44	0																																																																																					
25	43	60	0																																																																																					
19	72	36	0																																																																																					
19	44	66	0																																																																																					
21	43	64	0																																																																																					
23	73	32	0																																																																																					
23	43	62	0																																																																																					
25	53	44	0																																																																																					
25	43	60	0																																																																																					
6	Get the maximum matching value in 'a'	43	38	0																																																																																				
7	Goto step 2 while the maximum matching value \neq zero			stop																																																																																				

The first group contains the sixth value, while the second group contains the second, third, fifth and seventh values and the rest are in the third group. It was noticeable that the first group did not contain any redundant values unlike the second and the third groups. However, to remove the redundant values from the first group, the point having the maximum matching value was the only one taken while all the rest were eliminated. The same action was done on all the points of the array. After this process, the seven elements in Table 5.1 would be reduced to three elements as shown in Table 5.2 below, indicating the centres and the radii of all possible cells in the image.

Table 5.2 Values after elimination

Size of radius	Center (X)	Center (Y)	Matching value
23	73	32	38
25	53	44	46
25	43	60	43

These values were plotted on the original image giving the result shown in Figure 5.4.



Figure 5.4 Plotted results on the image

5.3 Results of applying Hough Transform

The results that were achieved when following this procedure were found to depend heavily on the edge-detection algorithm that was used. Three sets of results were obtained for each

image, and these are discussed in the following Sections. In this Section samples of these results will be given, while the rest will be found in Appendix B (p.154).

Results of applying the Sobel detector

When the Hough Transform was applied to the images obtained using the Sobel edge detector, the algorithm generally managed to detect some true cells but found many false ones. In some images, the algorithm had completely failed to detect any true cells, and this will be clearly shown in the following section.

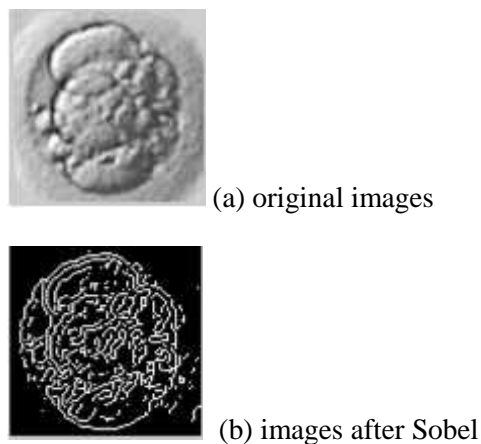


Figure 5.5 Image samples after applying Sobel

In some of the images, such as the one in Figure 5.15, the cells were clearly distinguishable, but after applying the Sobel edge detector the circular outline of the cells was not that clear, because of the noise that had appeared in the edge-detected images. This was found to be a major problem with the Hough Transform approach; the effects of the noise gave rise to many false cells.





Edged Image	Result	Diameter (pixels)	X center	Y center	Matching factor
		46	50	57	32
		42	56	68	29
		46	33	25	25

Figure 5.6 Sample of result on image 3

The results of the image shown in Figure 5.6 were good because it had less noise in it. In the above image, the Hough Transform managed to detect only three cells but they were the true ones.









Edged Image	Result	Diameter (pixels)	X center	Y center	Matching factor
		46	33	62	32
		50	37	32	26
		38	66	46	25
		50	45	68	24
		38	61	57	21
		38	65	31	20
		38	25	51	19

Figure 5.7 Sample of result on image 26

The effect of increased noise on the cell detection process is clearly shown in the results illustrated in Figure 5.7. The algorithm managed to detect the three cells in the previous figure, but then it detected other false ones because of the noise in the image. In this Figure, the results in the fourth and lower rows show false cells, although they had high matching values.








Edged Image	Result	Diameter (pixels)	X center	Y center	Matching factor
		48	57	19	24
		48	43	62	24
		48	30	48	22
		48	59	62	22
		36	70	63	16
		36	58	30	15

Figure 5.8 Sample of result on image 10

Investigating the results of another image (Figure 5.8), it was found that the proposed technique has detected some true cells, such as the ones shown in the fifth and sixth rows. However, it also detected some false cells that even had matching values greater than those of the true cells, and this was considered as a misleading result.















Edged Image	Result	Diameter (pixels)	X center	Y center	Matching factor
		46	57	47	26
		42	40	64	25
		50	40	39	24
		42	75	40	23
		50	65	22	23
		50	60	60	23
		50	52	20	22
		42	71	52	21
		50	40	21	21
		38	67	10	20
		46	43	50	20
		50	51	34	20
		38	64	36	19

Figure 5.9 Result of image 14

When images were processed with higher noise levels, the results of applying the Hough Transform were not satisfactory at all. The results of Figure 5.9 show that the algorithm detected cells with matching factors very close to the ones detected in Figure 5.6, Figure 5.7 and Figure 5.8 but this time they were false cells. This was because of the very noisy image that was produced after applying the Sobel edge detector.

Results of applying Elshenawy algorithm

The second edge-detection technique that was evaluated is Elshenawy algorithm discussed in Chapter 4. Two samples of the results are shown in Figure 5.10, and when compared visually with the results of the Sobel algorithm in Figure 5.5(b), it is clear that these results have thicker and clearer edges, which might be helpful when applying the Hough Transform, although, the noise was still present.

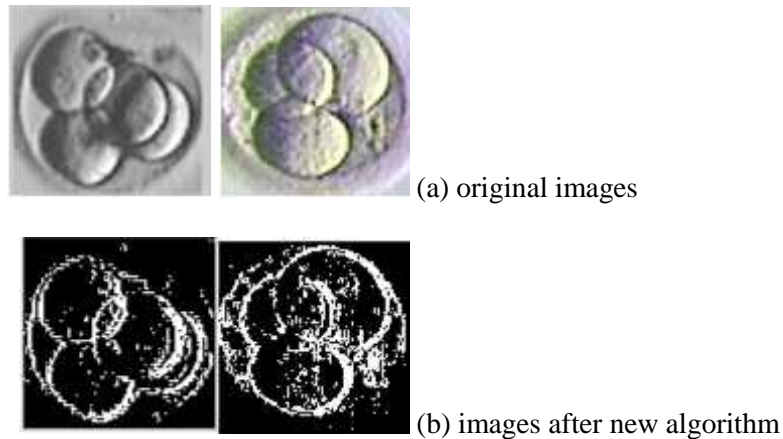


Figure 5.10 Sample of images after applying Elshenawy algorithm

The thick and clear edges that yielded from using Elshenawy algorithm enabled the Hough Transform to find the true cells better, as shown in Figure 5.11. The four cells in the image were correctly detected, and with higher matching factors.






Edged Image	Result	Diameter (pixels)	X center	Y center	Matching factor
		46	56	65	42
		50	49	52	40
		46	32	25	34
		38	72	35	23

Figure 5.11 Image 3 result after using Elshenawy algorithm

Looking at the images that had more noise, such as the one in Figure 5.12, many false cells were detected, also with high matching ratios, due to the noise.






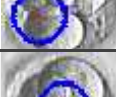

Edged Image	Result	Diameter (pixels)	X centre	Y centre	Matching factor
		50	33	59	48
		42	67	44	38
		42	38	36	36
		50	44	68	35
		42	56	29	25
		42	48	51	25

Figure 5.12 Result of image 26

In the results depicted below in Figure 5.13, the true cells detected also had the lowest matching point as the case in the results of Figure 5.8. The false cell detected in the fourth row had a matching point higher than the true cells in the fifth and sixth rows. On the other hand, the results of the false cells in the first, second and third rows had detected the cells but with improper sizes.




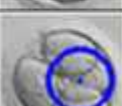
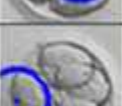
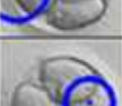
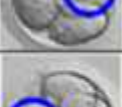
Edged image	Result	Diameter (pixels)	X centre	Y centre	Matching factor
		48	40	61	38
		48	29	48	35
		48	51	61	34
		48	57	15	31
		36	47	69	30
		40	54	26	23

Figure 5.13 more results using Elshenawy algorithm on image 10

With images that had even more noise, the algorithm also failed to detect any true cells or even give a low matching factor to indicate a weak detection value. As shown in Figure 5.14, the result gave a matching factor of 45, which was considerably high if compared to the other results stated above. Taking a closer look at the result, the detected cell was not a true cell.








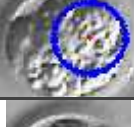
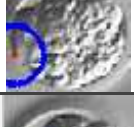

Edged Image	Result	Diameter (pixels)	X centre	Y centre	Matching factor
		50	56	44	45
		50	63	56	42
		50	57	32	40
		46	76	37	37
		50	44	31	37
		50	36	42	37
		50	48	63	37
		42	67	8	29
		46	68	25	29

Figure 5.14 Results of image 14

Results of applying the convolution mask detector

The results of the third technique are shown in Figure 5.15, where it can be seen that the edge-detected image had also thick and clear edges but the noise was less than the previous types, because of the smoothing process introduced by the larger 3x3 template. The

results showed the detection of the three cells correctly in the first three rows. The fourth result showed the detection of the same cell as the first one but with different dimension, and the fifth row indicates the detection of the fourth cell but with an incorrect dimension. The matching factors of these results were considerably high in comparison with the previous techniques.







Edged image	Result	Diameter (pixels)	X center	Y center	Matching factor
		50	56	63	40
		50	35	25	39
		46	51	54	38
		38	56	71	35
		50	70	28	33

Figure 5.15 Results of convolution mask on image 3

The noisy edge-detected image, such as that shown in Figure 5.16, that was not processed well by the two earlier techniques, gave much better results using this technique, as can be seen in Figure 5.16. This technique managed to detect all the true cells in the image, with high matching factor, and found no other false ones.

Edged image	Result	Diameter (pixels)	X center	Y center	Matching factor
		50	33	59	45
		42	67	43	36
		38	37	38	35

Figure 5.16 Results of the image 26 using convolution mask

The image shown in Figure 5.17 when applying the convolution mask edge-detector have properly detected only two cells and one on false cell. This was because the image after edge detection had less noise than the others. Yet, the false cell also had a matching value higher than the detected true cells.


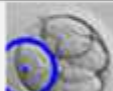

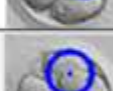
Edged image	Result	Diameter (pixels)	X centre	Y centre	Matching factor
		48	57	19	37
		36	47	67	32
		36	32	54	28

Figure 5.17 More results using the convolution mask

However, this approach still detected false cells in the very noisy images, although the matching factors were lower than for the true ones, as may be seen in Figure 5.18.








Edged image	Result	Diameter (pixels)	X center	Y center	Matching factor
		46	54	43	33
		46	56	64	33
		50	40	60	33
		42	36	43	31
		50	42	31	28
		50	54	31	28

Figure 5.18 Result of image 14

5.4 Results using the Hough Transform.

Table 5.3 shows the cell count for the 30 images in the training dataset derived using the Hough-based technique. This technique managed to detect around 60 out of 94 actual true cells in these images. Although the Sobel technique had the highest percentage in detecting potential cells, it also had the highest count of false cells detection, which was 226. The convolution technique reduced the number of false cells considerably, but was not quite as accurate as the Sobel technique for finding the true cells.

Table 5.3 Hough-based technique results

Edge detector technique	Total cell count	Potential detected cells		False cells
		count	%	
Sobel	94	62	65.9	226
New algorithm		61	64.8	155
Convolution mask		57	60.6	161

5.5 Conclusions

This Chapter described the use of the circular Hough Transform for detecting the cells inside the images. The transform used a fixed radius in its detection to compensate the errors found when the same technique was used for the ZP detection and to make use of the knowledge about the likely range and similarity of diameters of the cells that would make them suitable for implantation.

Three different edge-detectors were considered, for pre-processing the image data for the Hough Transform. The Sobel edge-detector gave the poorest results with the lowest matching factors compared to the other two techniques. In the noisy images, the process found false cells with similar matching factors to those of the true cells, and for particularly noisy images, the technique failed to detect true cells and detected false cells with high matching factors. The lowest numbers of false cells that were found was using the 3x3 template, although it detected slightly fewer true cells than for the Sobel edge-detector.

The overall performance of the Hough Transform was 60-66% and this was not considered sufficiently reliable to meet the objectives of the study. Consequently it was necessary to consider other cell detection techniques. These are described in the next two Chapters, and these results are reconsidered in comparison with those obtained using the alternative techniques.

Chapter 6 Embryo detection using template matching

Overview

In this Chapter a second technique is introduced to detect the blastomere in the embryo. This involves template matching, with templates being designed to match the acceptable sizes of the blastomeres at Day 2. The template design strategy is described first, followed by the implementation of the template matching process. Two measures of the degree of match are investigated, and the results that were obtained with the image dataset are presented and discussed.

6.1 Introduction

When using the circular Hough Transform the edge-detected fragments that could contribute to the circular boundary of a blastomere were added into the accumulator corresponding to the centre of that boundary. Unfortunately, noise tended to break up the real edge, reducing effectiveness of detecting true edges, but also gave rise to false edges. However, the decision to focus on the circular shape of the blastomeres with a range of acceptable diameters that would be suitable for implantation was still considered to be most promising way forward. Consequently, the second technique that is considered to detect the

cells in the images involves template matching using templates with the same circular shape and size as the blastomeres. The position in the image that gives the best match, or as in the case of the Hough Transform, positions of the highest matches indicate the locations of blastomeres. Since acceptable blastomeres could have a range of sizes, a variety of templates are used in this process.

6.2 The proposed algorithm

The main issue with the template matching approach is the design of the template, in particular, the size, contents and shade (grey-scale or monochrome) of the template. These factors are discussed in the next Section, followed by the implementation of the template matching process, and then the results.

6.2.1 Templates generation

Size of the template

As for the Hough Transform process, the size of the template is relative to the size of the ZP and the acceptable range of sizes of the blastomere. This is resolved by using the pre-processing phase (ZP detection only). The range of diameters of the rings varied as discussed in Chapter 4 from 36 to 52 pixels, each having a thickness of 2 pixels, and templates were generated from each of these sizes.

Contents of the template

Although the template could have contained a disk, whose size corresponds to the size of the blastomeres, it was expected that the matching process would be confused by the overlap of the cells, and so it was decided to design a template with a ring to

match the edge of the blastomere, Figure 6.1 shows a sample of such a template. The thickness of the ring was created to be similar to the thickness of the cell.

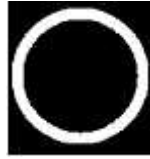
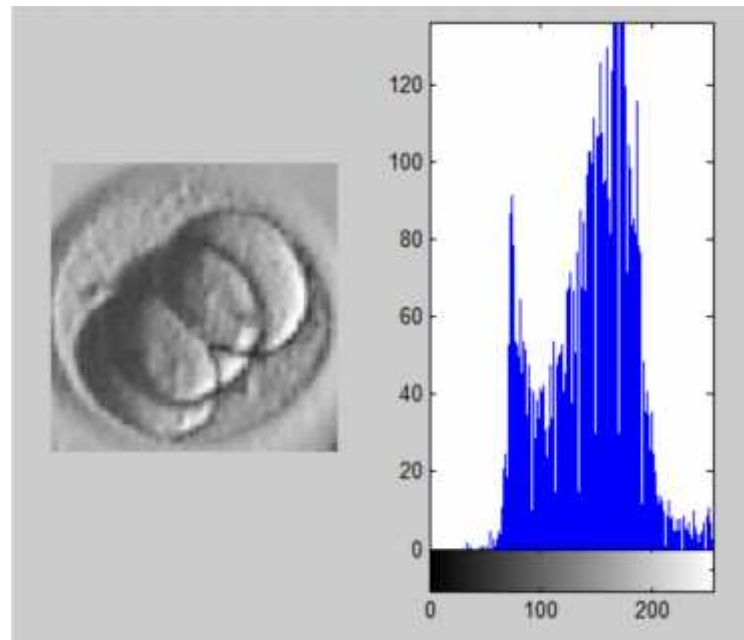


Figure 6.1 Template contents

Shade of the template

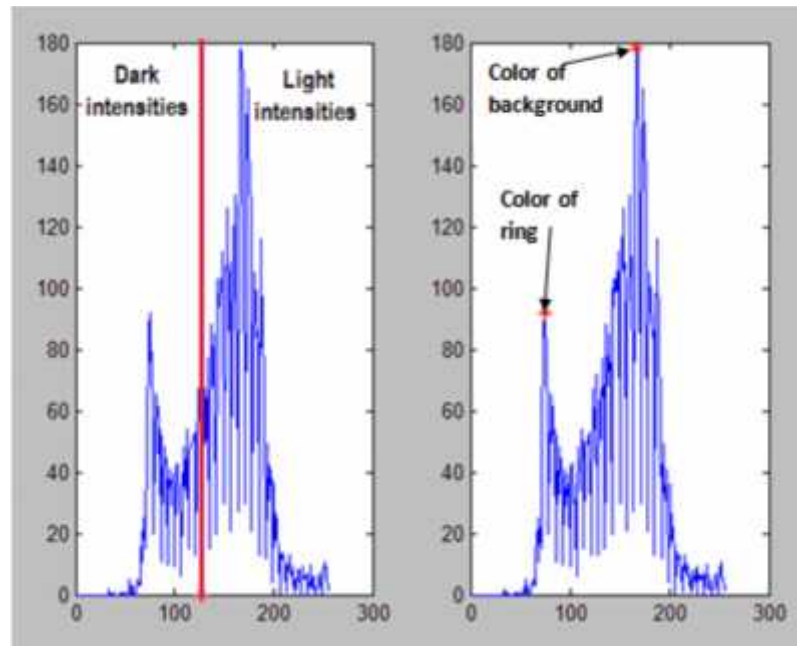
While a monochrome template could have been used, it was considered that a grey-scale template that matched the average background and interior of the blastomere, with a dark grey ring similar to that of the blastomere, would give the best matches. However, it was observed that the brightness values differed from one image to another, which consequently required the shades in the template to be determined separately for each image, prior to the matching procedure. The method used to determine the shades in the templates involved building a grey-level histogram for the original image, and then selecting grey-level values for the background/interior of the template, and the shade of the ring of the blastomere. Figure 6.2(b) illustrates the histogram analysis of the image in Figure 6.2(a). The histogram shows the distribution of grey-level values in the image, with higher grey-level values corresponding to bright shades in the image, as shown by the shaded horizontal axis in the Figure.



(a) (b)

Figure 6.2 Histogram analysis. (a) Original image (b) histogram of the image

In order to decide upon the shades of background/interior and the ring, the histogram was divided into two equal halves as shown in Figure 6.3(a) and the peaks in each half were found (Figure 6.3 (b)). The grey-level value of the peak in the dark half was selected to be the value of the ring and the value of the peak found in the second half (the bright half) was selected to be the value of the background/interior for that image.



(a)

(b)

Figure 6.3 Peak values

The values that appeared in Figure 6.3(b) that corresponded to the value of the ring and the background are shown in Figure 6.4 when used to create the template. The background of the template had the grey value of 167 while the ring had the value of 76.

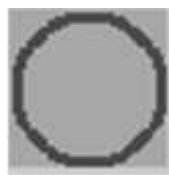


Figure 6.4 Sample of the template

6.2.2 Correlation process

Once the templates had been generated, the correlation process takes place as indicated in Figure 6.5

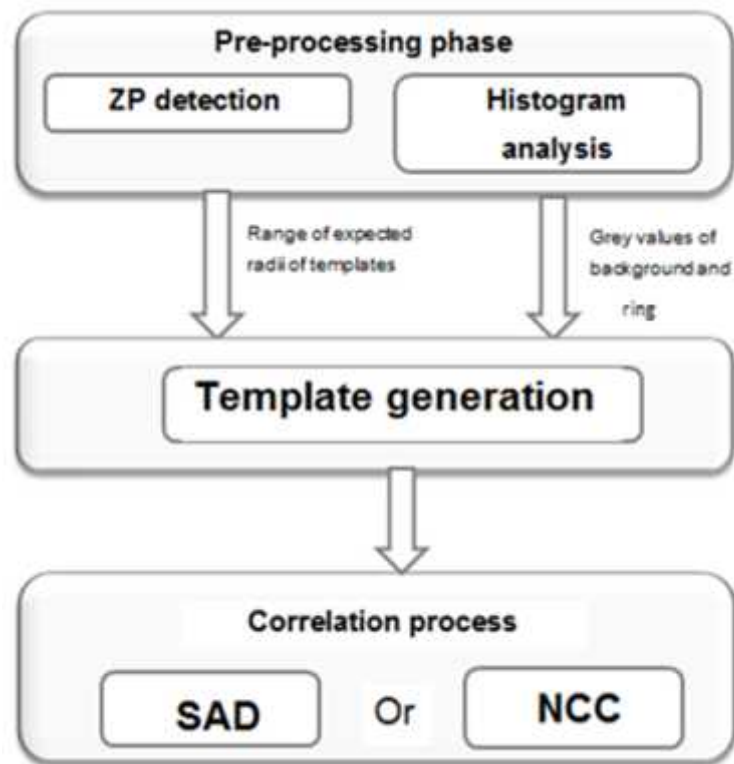


Figure 6.5 Correlation procedure

Two correlation techniques were investigated; the Sum of Absolute Differences (SAD) and the Normalised Correlation Coefficient (NCC). The potential advantage of the SAD technique is considerably reduced computational times, compared with the NCC algorithm. These are discussed in the following Sections.

SAD technique

The SAD technique is based on calculating the difference between each point in the image and the corresponding point in the template used for comparison. Then, the magnitude of these differences are added together to measure the similarity between two images. This process is defined as:

$$SAD(IM, T) = \sum \sum |IM(i, j) - T(i, j)|$$

Where IM is the image and T is the template generated, and is demonstrated in Figure 6.6.

167	167	164	165	165	165	166	165	165	162
163	165	164	161	163	164	162	164	165	160
165	165	165	164	164	158	160	162	163	162
164	163	162	162	162	163	163	160	162	162
163	163	163	163	161	161	162	161	160	158
162	165	163	161	162	160	163	163	161	160
163	162	162	161	161	161	161	161	161	156
161	163	162	160	163	158	163	160	160	155
157	164	161	157	162	160	159	162	159	150
159	162	163	161	157	160	158	155	153	151

(a)

142	142	142	142	142	142	142	142	142	142
142	142	142	142	142	142	142	142	142	142
142	142	142	142	142	142	142	142	142	124
142	142	142	142	142	142	142	142	142	124
142	142	142	142	142	142	142	124	124	124
142	142	142	142	142	124	124	124	124	124
142	142	142	142	124	124	124	124	124	142
142	142	142	142	124	124	124	124	142	142
142	142	142	124	124	124	124	142	142	142
142	142	124	124	124	124	142	142	142	142

(b)

25	25	22	23	23	23	24	23	23	20
21	23	22	19	21	22	20	22	23	18
23	23	23	22	22	16	18	20	21	38
22	21	20	20	20	21	21	18	38	38
21	21	21	21	19	19	20	37	36	34
20	23	21	19	20	36	39	39	37	36
21	20	20	19	37	37	37	37	37	14
19	21	20	18	39	34	39	36	18	13
15	22	19	33	38	36	35	20	17	8
17	20	39	37	33	36	16	13	11	9

(c)

25	25	22	23	23	23	24	23	23	20
21	23	22	19	21	22	20	22	23	18
23	23	23	22	22	16	18	20	21	38
22	21	20	20	20	21	21	18	38	38
21	21	21	21	19	19	20	37	36	34
20	23	21	19	20	36	39	39	37	36
21	20	20	19	37	37	37	37	37	14
19	21	20	18	39	34	39	36	18	13
15	22	19	33	38	36	35	20	17	8
17	20	39	37	33	36	16	13	11	9

(d)

Figure 6.6 SAD technique (a) image (b) template (c) the differences (d) the value of the SAD

Figure 6.6(a) shows part of the image with its corresponding grey level values while the template is shown in Figure 6.6(b). The two grey levels of the template have the grey values of 142 for the background and 124 for the ring according to the image as discussed earlier. The difference between these two is given in Figure 6.6(c), and the

magnitudes of these differences was added together in order to reach the sum of absolute differences (SAD) 2456, as given in Figure 6.6(d). The mask of the template is moved one pixel to the right and the same technique is done with the new part of the image. This process continues until the template has been applied to all pixels in the image. The location having the minimum SAD value is considered to be the position of the best match between the template and the image.

NCC technique

The NCC method is based on Pearson's correlation theory, and is calculated from:

$$NCC(x,y) = \frac{\sum_{x,y} [IM - IM_{mean}][T - T_{mean}]}{\sqrt{\sum_{x,y} [IM - IM_{mean}]^2 \sum_{x,y} [T - T_{mean}]^2}}$$

where IM is the image, IM_{mean} is the mean of the image, T is the template and T_{mean} is the mean of the template. The correlation coefficients values range from -1.0 to 1.0; 1.0 indicates a high value and consequently a very good match, and this reduces to zero for poor matches, 0.0 indicating no similarity between the template and the image values at the particular at position, 0.0 is obtained if there is no match. This is illustrated using Figure 6.7 below, where the same part of the image and template were those used earlier in Figure 6.6.

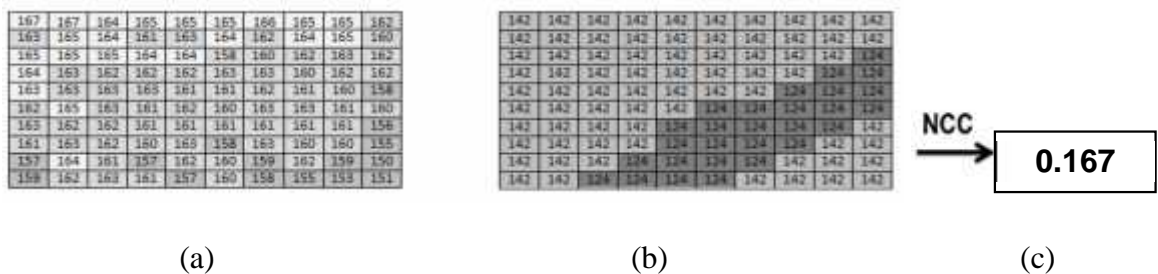


Figure 6.7 NCC technique (a) image (b) template (c) the value after applying NCC

The result of applying the NCC technique gave a value of 0.167. This was a very poor value that indicated a weak similarity between the above image and the template. In the regions of the blastomere, where the template and image had a good match the NCC typically exceeded 0.4. The template was moved systematically around the whole image, as with the SAD method, and in this case the location having the maximum NCC was considered to be the position of the best match between the template and the image.

6.3 Results using the SAD and NCC correlation techniques

6.3.1 Considering one peak value

This section will show samples of the results obtained by the SAD and the NCC correlation techniques while the rest of the results will be available in Appendix C (p.173) . The diameter of the ring in the templates sizes ranged from 38 to 52 pixels. The results obtained for a sample image are shown in Figure 6.8.

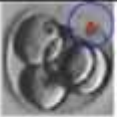
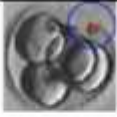
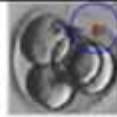
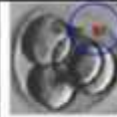
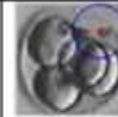
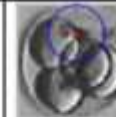
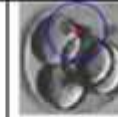





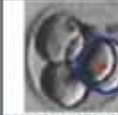
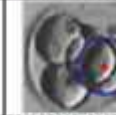


		Diameter (pixels)							
		38	40	42	44	46	48	50	52
SAD									
		Center(20,76) Value=48112	Center(21,75) Value=55544	Center(22,74) Value=64197	Center(23,73) Value=73600	Center(24,72) Value=83359	Center(25,50) Value=92914	Center(26,49) Value=100443	Center(27,49) Value=109657
NCC									
		Center(73,38) Value=0.3461	Center(35,34) Value=0.358	Center(34,33) Value=0.388	Center(34,33) Value=0.4139	Center(56,70) Value= 0.3755	Center(56,69) Value=0.3113	Center(37,36) Value=0.2707	Center(36,37) Value=0.2296

Figure 6.8 Results of image 3

It may be seen from the figure that results obtained using the SAD technique were absolutely inappropriate, as they only found false cells. The NCC technique gave much better results and showed a unique detection of a cell centred at point (73,38) and had a diameter of 38 pixels. The value of the NCC was 0.3461 only. The results for the second, third, fourth, seventh and eighth ring diameters all showed the detection of the same cell. The centres were nearly the same but the diameters were different. The diameter of the cell with the highest NCC value was considered to be the best one, and in this case it was the fourth one, which had a value of NCC of 0.4139. A third cell was detected with the fifth and the sixth ring diameters. Again the highest similarity value was considered the best result, which was that of the fifth ring diameter, and had a value 0.3755.

As shown, the NCC algorithm managed to detect only three cells out of four clear ones. This was because only one maximum was considered as a result of applying each diameter. This problem was solved by considering all the peak values and eliminating the redundant points (as discussed in Section 5.2) instead of just taking one maximum value. An example of the results of considering all the peak values will be shown in the later section.



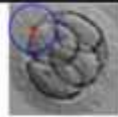
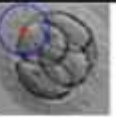
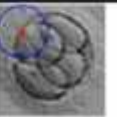

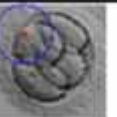
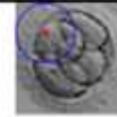

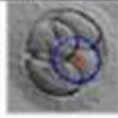
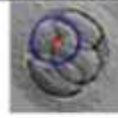
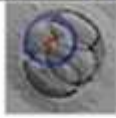
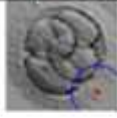
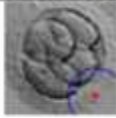
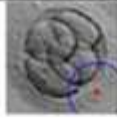
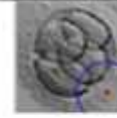
		Diameter (pixels)							
		37	39	41	43	45	47	49	51
SAD									
	Center(20,20) Value=23506	Center(21,21) Value=28147	Center(22,22) Value=34038	Center(23,23) Value=41391	Center(24,24) Value=49304	Center(25,25) Value=56605	Center(26,26) Value=64170	Center(27,27) Value=71755	
NCC									
	Center(64,46) Value=0.3621	Center(51,60) Value=0.3338	Center(34,40) Value=0.3499	Center(34,39) Value=0.3591	Center(80,79) Value= 0.2865	Center(81,58) Value=0.2633	Center(78,78) Value=0.2523	Center(78,78) Value=0.2438	

Figure 6.9 Results of a sample of image 13

The image in Figure 6.9 had four clear cells, but again the SAD techniques failed to detect any true cells. In the case of the NCC, only three cells were detected as seen for the first three ring diameters, with NCC values almost the same as the previous example image. The results for the fourth to the seventh ring diameters show the detection of false cells, but with relatively low NCC values, which were indicative of the matches being false.

An example of an image that had only one cell is shown in Figure 6.10, which meant that these techniques should not give any matches, or at least if they did it should be with very low NCC values.





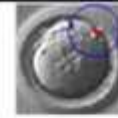
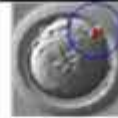


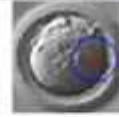
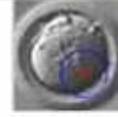
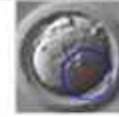
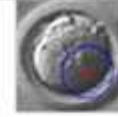


		Diameter (pixels)						
		36	38	40	42	44	46	48
SAD								
	Center(19,77) Value=35679	Center(20,76) Value=40991	Center(21,75) Value=46518	Center(22,74) Value=51958	Center(23,57) Value=58307	Center(24,57) Value=64258	Center(25,56) Value=71888	
NCC								
	Center(28,35) Value=0.35585	Center(50,70) Value=0.33418	Center(64,61) Value=0.39414	Center(63,61) Value=0.3898	Center(62,61) Value=0.3333	Center(62,59) Value=0.3502	Center(62,57) Value=0.3533	

Figure 6.10 Results of image 7

As with the previous results, the SAD technique only found false cells. The NCC technique also found false cells detection, but with high NCC values which was problematic because these cells had NCC values which were close to the previously detected true cells. As it was intended to use a threshold NCC value to distinguish between true and false cells, this would lead to errors in the classifications.

With images that had significant noise as for the example shown in Figure 6.11, the results of the SAD technique were the same as the previously discussed examples. On the other hand, the results of the NCC were all considered as false cells and their values were considerably low in comparison with the previous results.




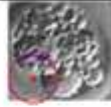

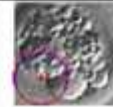




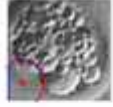
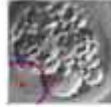
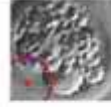
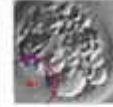
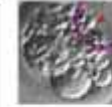

		Diameter (pixels)							
		38	40	42	44	46	48	50	52
SAD									
		Center(76,20) Value=32875	Center(75,21) Value=39204	Center(74,22) Value=45638	Center(73,23) Value=53511	Center(72,24) Value=61248	Center(71,25) Value=68779	Center(70,26) Value=76801	Center(69,27) Value=84347
NCC									
		Center(48,71) Value=0.2776	Center(48,21) Value=0.2696	Center(79,14) Value=0.2475	Center(79,13) Value=0.2437	Center(79,15) Value=0.2367	Center(79,15) Value=0.2185	Center(18,77) Value=0.2084	Center(18,78) Value=0.2112

Figure 6.11 Result of image 16

The failure of the SAD technique to detect any true cells was a reason to exclude this technique from any further enhancement in the approach. The enhancement needed in this approach was considering more than one peak value rather than only one peak value per diameter size. This case was similar to that found in the previous Chapter when applying the Hough Transform. The same approach to detect more than one peak value hence was used in this enhanced technique too but this approach was used with the NCC technique only.

6.3.2 Considering peak values

An example of the results of considering all the peak NCC values in an image is shown in Figure 6.12 (The SAD approach was not investigated in view of the poor earlier results).

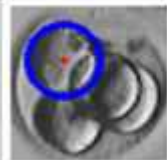

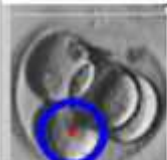
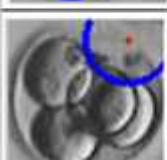

Image	X-center	Y-Center	Radius	Value
	34	33	22	0.41386
	57	71	22	0.40203
	73	38	19	0.34607
	13	74	26	0.22797
	79	115	26	0.22252

Figure 6.12 Sample of results with more than one peak of image 3

Although it was thought that this approach might detect the fourth cell in this image it was unsuccessful. However, the three cells that were detected using the earlier process shown in Figure 6.8 were also detected here. The difference here was that they were only detected once with the best similarity values. However, the drawback of this method was that it had detected false cells, unlike the previous one, although the false cells had low NCC values.

An example of an image that contained more noise is shown in Figure 6.13. The NCC approach found false cells, and these had high NCC values. The rest of the results are placed in Appendix D (p.179).

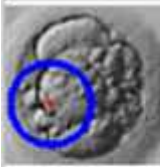
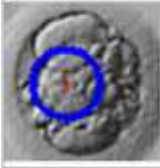
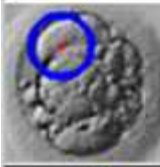
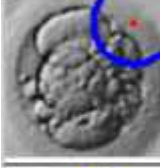
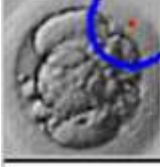
Image	X-center	Y-Center	Radius	Value
	59	28	24.5	0.41367
	49	38	20.5	0.39341
	26	34	18.5	0.34092
	16	78	24.5	0.24952
	16	78	25.5	0.2317

Figure 6.13 Sample of image 24

The other extreme of the results of an image where a true cell was found, but with a low NCC value is shown in Figure 6.14.

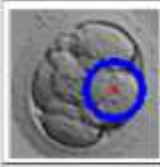
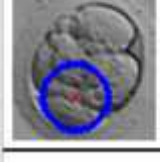
	52	67	18	0.446514
	68	42	21	0.288909

Figure 6.14 Another misleading result of image 12

These results highlight the difficulties and failings of the basic template match approach. In the case of the SAD technique, simply subtracting each value in the template from its corresponding grey-level value in the image, led to the process determining the brightest location in the image, because the majority of the values template corresponded to the background, which had the brighter values. That is the value of the background was dominant over the value of the template.

In the case of the NCC technique, when only the (one) maximum peak value was used, true cells were detected with NCC values that ranged from 0.4 till 0.3. It is believed that values did not exceed the 0.4 range simply because the template used consisted of the two selected grey levels, whereas the image had 256 grey levels, and so the similarity value could not be very high even at the positions of best match. Also, there was a problem in that some of the false cells that were detected also had similar NCC values to the true ones. The other drawback of this technique was that each size of the template gave only one result. Some images had more cells that were not detected because of this issue. The attempt to solve this drawback was to try to take more than a peak value in order to detect more cells in the image.

6.4 Summary of template matching results

Two approaches were considered using the template matching technique: SAD and the NCC. These approaches were used to detect the cells either by considering one peak value of the correlation coefficient or by all available peak values. The results obtained using these approaches are demonstrated in Table 6.1 and Table 6.2.

Table 6.1 One peak template matching results

Approach	Total cell count	Potential detected cells		False cells
		count	%	
SAD	94	0	0	219
NCC		44	46.8	175

It can be seen from the Table that the SAD technique showed complete failure in detecting any potential cells, while the NCC technique had detected only 46.8%.

The trials that considered more than one peak value excluded the SAD approach since it gave 0% of potential cells detection. Table 6.2 shows that this enhancement produced a slight increase in the potential cell detection but a great improvement in false cell detection count.

Table 6.2 Multi-peak template matching results

Approach	Total cell count	Potential detected cells		False cells
		count	%	
NCC	94	45	47.8	69

6.5 Conclusion

The idea of using the template matching technique to solve the drawbacks that were found with the Hough Transform techniques yielded drawbacks itself and gave more poor results than expected. The SAD technique failed to detect any true cells available in any of the images. The performance of the NCC technique was much better than the SAD, but the separation of true and false cells was problematic, because in many cases the NCC value of the false cells was similar to that of the true cells, and so a classification based on an NCC threshold was inaccurate. There were also examples of true cells being detected with a low NCC value. The other drawback of the basic technique was that each of the templates gave only one result, the best match with that particular ring diameter, and this led to some images containing cells that were not detected.

The attempt to solve this drawback was to try to examine all the NCC peak values in order to detect more cells in the image. However, this approach did not improve the situation, and in most cases the same cells were detected as in the previous technique. Not only that but it had also found additional false cells in the images.

While the template matching approach with a range of ring diameters was expected to give more accurate results than with the Hough Transform, this was not found to be the case. It was thought that the main problem was matching a two shade template with grey-scale, and an enhancement to this approach, where the number of grey levels in the images was reduced for the matching process would yield more accurate classifications. This enhancement is described in the following Chapter.

Chapter 7 Embryo detection using Binary Template Matching

Overview

After investigating the Hough Transform and the template matching techniques in the previous Chapters, an enhanced template matching technique is developed in this Chapter in an attempt to improve on the poor classifications that were obtained. The rationale for the enhancements, the implementation of the new techniques and the results that were achieved when applied to the image data set are described.

7.1 Introduction

The poor results obtained with the techniques described in the previous Chapter were attributed largely to matching a two-shade template with the values in a grey-scale. The approach taken in this Chapter is to reduce the images to binary, using the edge-detection techniques used to pre-process the images for the Hough Transform. As a consequence of this the bi-level ring templates can also be reduced to the binary ones avoiding the need to determine the average background/interior, and the value for the cell border in each image.

7.2 The binary template matching technique

In this technique the first step is the detection of the ZP which determines the size of the ring templates used. The templates here are generated but in their binary form. The binary version of the ring template takes the form shown in Figure 7.1.



Figure 7.1 Binary ring template

Each image is converted to its binary form after detecting its edges using the proposed algorithms discussed in Chapter 4, and Figure 7.2 shows the images after applying the different edge detection techniques described.

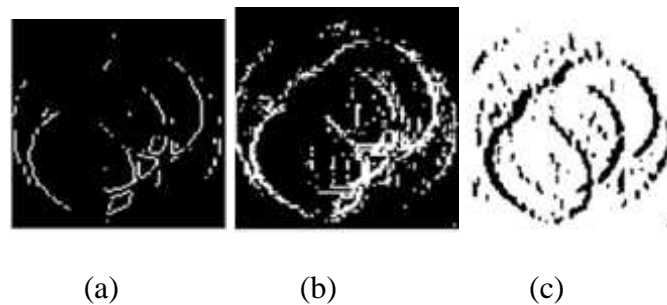


Figure 7.2 Binary representation of the images after applying different edge detection algorithms (a)

Sobel (b) Elshenawy algorithm (c) convolution mask

The output from the convolution mask technique is converted to its binary form. But the conversion caused the edges to be black and the background to be white, which is opposite to the desired output. This result is inverted such that the edges are white, while the background is black as shown in Figure 7.3.

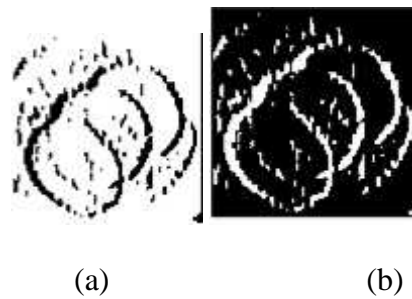


Figure 7.3 Output from convolution mask technique (a) original (b) inverted

As both the image and template are now in binary form, it is less complex and simpler to perform a simple AND operation between the two arrays, and then count the number of matches (1s). In this case, the maximum value indicates the position of the best match. As with the previous techniques, all peaks are found for each image when processed with a particular ring diameter, and the redundant ones are eliminated. The summary of this technique is depicted below in Figure 7.4.

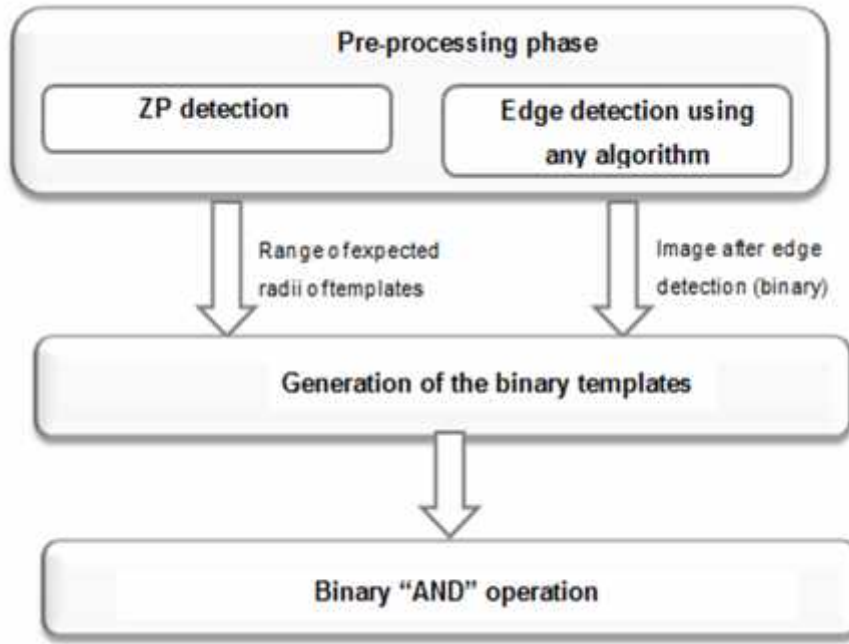


Figure 7.4 Summary of the algorithm

This process was performed on the image dataset for each of the three edge detection techniques described above. The results obtained for each of these techniques, and a discussion about the advantaged and disadvantages of each are discussed in the next Section.

7.3 Results for the binary templates matching technique

A sample of the results is shown in Figure 7.5. The results are illustrated as follows: the columns show the results of applying each of the three different edge-detectors on an example image. The adjacent numbers correspond to the x and y coordinates of the peak similarity value, the diameter of the ring, and finally the similarity value. The similarity value was calculated from the ratio of the number of the matches (1s) to the number of pixels in the ring then multiplying it by 100 to convert it to a percentage. If there was a perfect match with the ring the percentage similarity value would be 100%. The rows are ordered in terms of the similarity values found for the different peaks for each technique. Some of the results are

discussed and shown below in this Section while the rest of the images are placed in Appendix E (p.187).

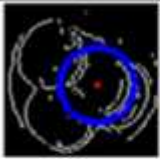
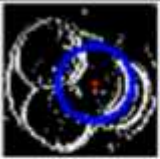
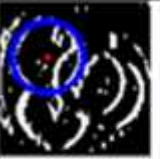
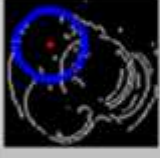
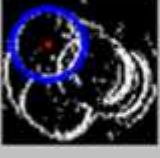

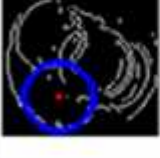
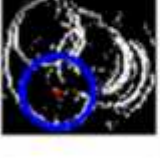
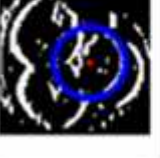
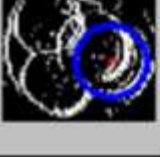
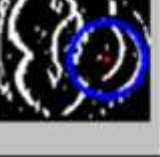
Sobel edge detection		Elshenawy detection		Convolution edge detection	
Image	Results	Image	Results	Image	Results
	x_centre=51 y_centre=58 radius=23 value=26.8%		x_centre=50 y_centre=57 radius=23 value=55.2%		x_centre=35 y_centre=31 radius=22 value=68.1%
	x_centre=33 y_centre=29 radius=21 value=25.7%		x_centre=33 y_centre=29 radius=22 value=48.3%		x_centre=70 y_centre=35 radius=22 value=55.7%
	x_centre=71 y_centre=35 radius=21 value=21.8%		x_centre=69 y_centre=35 radius=22 value=44.2%		x_centre=51 y_centre=57 radius=22 value=55.7%
			x_centre=58 y_centre=68 radius=22 value=44.2%		x_centre=57 y_centre=68 radius=23 value=55.2%

Figure 7.5 Results obtained from an example image

In this example, the Sobel edge detector gave the lowest similarity percentages. This was because the edges that were derived were very thin and hence the match count was not high compared to the thicker edges that were generated by the two other techniques. Three cells were detected; the fourth being missed due to the absence of a part of cell's edge. However, the results of the other two techniques gave much higher similarity percentages and also managed to detect all the four cells in this image, although the cell with the highest similarity percentage was different for the two techniques.

Figure 7.6 is the same as Figure 7.5 but with the results for each technique colour coded according to the coordinates of the detected cell centre. The first cell detected in the Sobel technique was coded using a red rectangle, this same cell was also detected in Elshenawy algorithm and the convolution techniques and hence given the same red rectangle code.

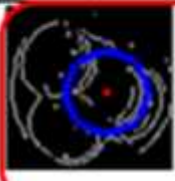
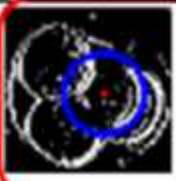

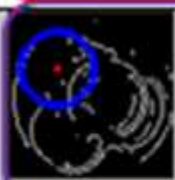
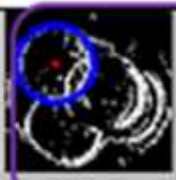

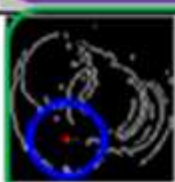
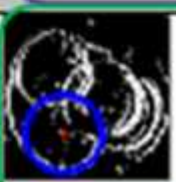

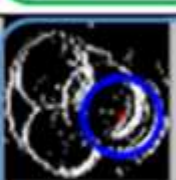

Sobel edge detection		Elshenawy detection		Convolution edge detection	
Image	Results	Image	Results	Image	Results
	x_centre=51 y_centre=58 radius=23 value=26.8%		x_centre=50 y_centre=57 radius=23 value=55.2%		x_centre=35 y_centre=31 radius=22 value=68.1%
	x_centre=33 y_centre=29 radius=21 value=25.7%		x_centre=33 y_centre=29 radius=22 value=48.3%		x_centre=70 y_centre=35 radius=22 value=55.7%
	x_centre=71 y_centre=35 radius=21 value=21.8%		x_centre=69 y_centre=35 radius=22 value=44.2%		x_centre=51 y_centre=57 radius=22 value=55.7%
			x_centre=58 y_centre=68 radius=22 value=44.2%		x_centre=57 y_centre=68 radius=23 value=55.2%

Figure 7.6 Corresponding cells colour-coded

The first cell (red rectangle) that was detected using the Sobel edge detector, with a similarity percentage of 26.8%, was found using Elshenawy algorithm detector but with a higher similarity of 55.2%, and was found by the convolution edge-detector with an even higher percentage that reached 55.7%. Note that the centres and the radii of the three results are so close that they could be considered the same. This was shown again with the rest of the detected cells (purple, green and blue rectangles) except for the fourth cell (blue rectangle) that was not detected by the Sobel detector as mentioned above. It should be noted that the convolution edge-detector technique gave the highest similarity percentage.

Another sample of the results achieved is given in Figure 7.7. The detected cells are also colour coded by rectangles for simplicity in comparisons.

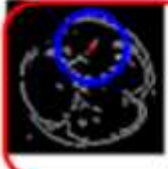
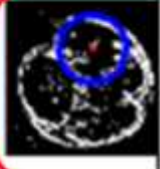
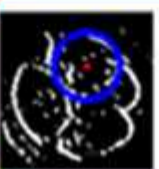

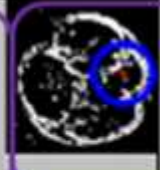
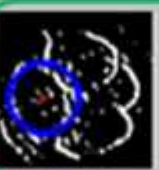
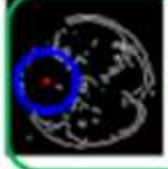
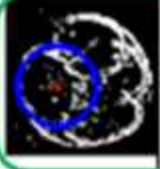
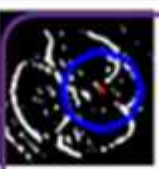
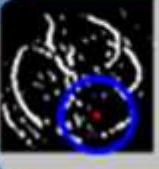
Sobel edge detection		Elshenawy detection		Convolution edge detection	
Image	Results	Image	Results	Image	Results
	x_centre=31 y_centre=52 radius=21 value=28.9%		x_centre=31 y_centre=53 radius=20 value=59%		x_centre=33 y_centre=54 radius=20 value=41.1%
	x_centre=51 y_centre=65 radius=23 value=20%		x_centre=47 y_centre=72 radius=18 value=41.7%		x_centre=53 y_centre=29 radius=21 value=40.1%
	x_centre=51 y_centre=25 radius=18 value=18.3%		x_centre=54 y_centre=32 radius=24 value=36%		x_centre=49 y_centre=63 radius=23 value=38.9%
					x_centre=73 y_centre=60 radius=22 value=31.4%

Figure 7.7 Results of image 10

The first detected cell (red) was found by all three techniques with centres and radii more or less alike, but with different similarity percentages. This time the highest percentage similarity was achieved by Elshenawy technique. In the case of the second detected cell (purple), the highest percentage similarity was, again, that of Elshenawy technique, but its radius was different from that found by the two other techniques.

Taking a closer look at this, it was found that this result was the correct one, as the two other techniques gave a larger radius because the cell overlapped other cells. The third cell (green) was detected with the highest percentage by the convolution technique and was a case similar to that of the second cell (purple). Finally the forth cell (blue) was only detected by the convolution technique.

An example of a more noisy image is shown in Figure 7.8, where it can be seen that the cells were not as clearly defined in the results achieved by Sobel and Elshenawy as for the convolution technique.


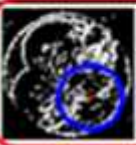


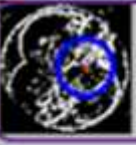
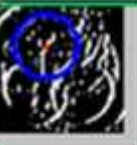

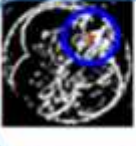






Sobel edge detection		Elshenawy detection		Convolution edge detection	
Image	Results	Image	Results	Image	Results
	x_centre=66 y_centre=64 radius=23 value=30.7%		x_centre=66 y_centre=64 radius=23 value=69%		x_centre=65 y_centre=65 radius=23 value=57.3%
	x_centre=50 y_centre=61 radius=19 value=29.1%		x_centre=48 y_centre=62 radius=20 value=58%		x_centre=32 y_centre=38 radius=23 value=51.8%
	x_centre=30 y_centre=39 radius=24 value=25.9%		x_centre=31 y_centre=64 radius=19 value=48.8%		x_centre=62 y_centre=27 radius=20 value=47.8%
	x_centre=31 y_centre=64 radius=19 value=25%		x_centre=33 y_centre=40 radius=26 value=48.7%		x_centre=44 y_centre=59 radius=25 value=42.1%
	x_centre=51 y_centre=73 radius=22 value=23.6%				x_centre=46 y_centre=72 radius=19 value=37.7%

Figure 7.8 Results of image 15

This time the results were different from the earlier examples. Each technique has managed to find cells that were not be detected by the other techniques. For, example, the cell detected and enclosed with the blue rectangle was only detected by the Sobel technique, and Elshenawy algorithm, while the cell enclosed with the black rectangle which was only detected by the Sobel and the convolution. There was also a cell (not coloured) detected by the convolution technique that was not detected by the other two techniques. The similarity percentage in this case was higher than the above results, but unfortunately some of those were false cells. However, the true cells in this image were the ones shown by the red, green, black and the uncoloured rectangles.

With images that had even more noise, the results were not satisfactory because false cells were with high similarity percentages. This is clearly illustrated in Figure 7.9.

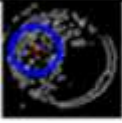
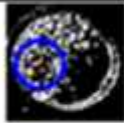

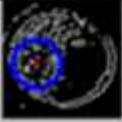
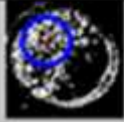

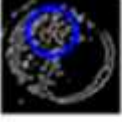
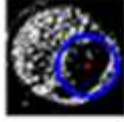

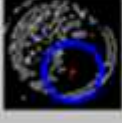


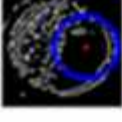



Sobel edge detection		Elshenawy detection		Convolution edge detection	
Image	Results	Image	Results	Image	Results
	x_center=41 y_center=27 radius=19 value=30%		x_center=50 y_center=27 radius=19 value=60.5%		x_center=58 y_center=67 radius=23 value=52.7%
	x_center=52 y_center=28 radius=19 value=28%		x_center=34 y_center=33 radius=19 value=54.4%		x_center=48 y_center=24 radius=19 value=49.7%
	x_center=30 y_center=41 radius=19 value=26.3%		x_center=56 y_center=65 radius=24 value=43.2%		x_center=50 y_center=36 radius=23 value=48%
	x_center=65 y_center=58 radius=23 value=22.9%		x_center=36 y_center=44 radius=26 value=39.8%		x_center=32 y_center=35 radius=21 value=46.6%
	x_center=48 y_center=67 radius=25 value=21.3%				x_center=38 y_center=57 radius=19 value=43.8%
					x_center=66 y_center=56 radius=22 value=42%
					x_center=46 y_center=71 radius=21 value=41.4%

Figure 7.9 Result of image 9

In this image there were no cells that could be identified, but the three techniques managed to find potential cells.

These results suggest that the binary template matching technique compensated for some of the difficulties with the template matching algorithm developed in the previous Chapter although false cells were still being detected with high similarity percentages to those of the true cells. However, this technique did appear to manage to detect more true cells than the template matching algorithm. It was observed in the examples shown that the lowest

percentage similarities were obtained using the Sobel edge detector, and this occurred because the edges were very thin compared with the thickness of the rings in the ring templates. In the cases of the noisy images there was a tendency to find a large number of pixels that overlapped the template ring, which caused the high similarity percentage, and hence the detection of a false cell.

7.4 Summary of the binary template matching results

The results obtained using the binary template matching approach on the image dataset using the three edge-detection techniques used to pre-process the images for the binary template matching are given in Table 7.1.

Table 7.1 Binary template matching technique results

Edge detector technique	Total cell count	Potential detected cells		False cells
		count	%	
Sobel	94	68	72.3	92
Elshenawy algorithm		67	71.2	83
Convolution mask		74	78.7	117

This approach produced significantly better results than the earlier grey-scale template matching approach. The convolution mask approach detected the most true cells, but at the same time found many more false cells than the other technique. Elshenawy algorithm has the same overall accuracy as the Sobel edge detector but found fewer false cells.

7.5 Conclusion

The idea of using binary rather than the grey levels images and templates have increased the number of potential cells detected. This increase was available in all types of edge detection techniques. On the other hand, the number of false cells has also increased, and this will cause the system to misclassify the embryos. Another improvement and refinement was essential to try to decrease number of the false cells detected. This refinement will be introduced in the following Chapter.

Chapter 8 Refining the Binary Template Matching

Overview

In this Chapter a refinement on the binary template matching technique is made. This refinement was essential to decrease the number of false cells detected by the previous binary template matching technique.

8.1 Introduction

The previous results of the binary template matching technique had increase the number of potential cells detected. On the other hand, the number of false cells detected had also increased. Refinements will be introduced in this Chapter to decrease the number of false cells detected. These refinements will include applying a filter to smooth the image in order to eliminate some of the available noise which might be the reason of the false cells detection. The other refinement will be trying to introduce another mask to measure the level of noise within the detected cell. These two approaches will be discussed in details in the following sections.

8.2 Refining the binary template matching results

8.2.1 Applying filters

The results obtained using the binary template matching approach on the image dataset showed an improvement on the detection of true cells, but there were still a large number of false cells being found, particularly in the noisier images. In order to reduce this noise, applying a filter was essential. Its aim was to smooth the image before using the edge-detectors. Although smoothing causes the image to be blurry and might eliminate part of the edges along with the available noises, but the intensity of the present edges of the cells are much darker than that of the noise so the effect in eliminating the noise will be more visible than that of the dark edges. However, decreasing the noise in the image will hence decrease the number of false cells detected. Figure 8.1 on the next page shows an image in its actual form, and then the edges detected using the three different techniques of this image. The median filter was then applied to this and its edges were detected and finally the mean filter was applied to the same image and then the edges were detected too. This step was made to choose among these filters. However, it was observed that the effect of applying the median filter gave better results than before, especially when applying both Elshenawy and the convolution mask techniques. On the other hand, the mean filter gave very noisy results upon applying the Sobel technique and produced both weak and discontinuous edges when using Elshenawy technique and satisfactory results when applying the convolution mask technique. Hence the median filter was applied on the images to resolve the problem of the noise, aiming to improve the results.

Technique	Actual Image	Image after edge detection	Image after median filter	Edges of filtered image	Image after mean filter	Edges of filtered image
Sobel						
Elshenawy algorithm						
Convolution mask						

Figure 8.1 Example images after edge detection, with and without the different filters

The summary of the algorithm is now look like the one illustrated in Figure 8.2 and is different from the one previously shown in Figure 7.4. The pre-processing phase now includes the stage of smoothing the image before applying any of the three edge detection techniques that were previously mentioned.

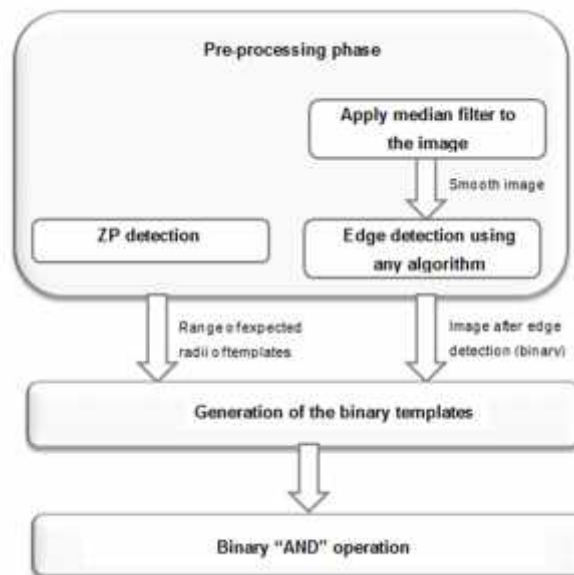












Figure 8.2 Summary of the algorithm when applying the median filter

Samples will be shown in the following pages while the rest of the results are placed in Appendix F (p. 202) and Appendix G (p. 215). The results depicted in Figure 8.3(a) illustrate the output of using the refined algorithm when applying the median filter prior to detecting the edges by the Sobel technique. Comparing these results to the previous results displayed in Figure 7.6, that are also shown in Figure 8.3(b), it was obvious that the number of potential cells that were detected using this approach has increased from three to four cells. However, two drawbacks appeared; the first was the presence of a detected false cell and the second was the low percentages of the results. Although the fourth cell was detected, the percentage of all the results seemed to decrease.

Image	Image after edge detection	Radius	x-centre	y-centre	Result (%)
		22	33	30	21.4
		23	51	58	21.1
		21	71	35	19.5
		22	58	69	16.9
		18	47	21	14.2

(a)

Image	Image after edge detection	Radius	x-centre	y-centre	Result (%)
		23	51	58	26.8
		21	33	29	25.7
		21	71	37	21.8

(b)

Figure 8.3 Results when using Sobel (a) with median filter (b) without median filter on image 3

In the figure, the detected cell that is marked with the red rectangle was detected in the two approaches. In the approach that used the median filter the percentage of detection was 21.4 % while in the other approach this percentage reached 25.7%. Similarly, the

percentages of the other cells that were marked with the purple and green rectangles have decreased from 26.8% to 21.1% and from 21.8% to 19.5%, respectively. On the other hand, the centres and radii of both techniques were very close to each other.

Upon changing the edge-detection technique, the results also changed. The results of using Elshenawy algorithm are shown in Figure 8.4. As shown in the Figure, the four potential cells were detected by both techniques; with applying the median filter (Figure 8.4(a)) and without the median filter (Figure 8.4(b)).








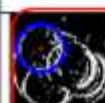


Image	Image after edge detection	Radius	x-centre	y-centre	Result (%)
		22	34	29	62.5
		24	51	58	59.3
		22	70	35	56.5
		18	55	73	50.2

Image	Image after edge detection	Radius	x-centre	y-centre	Result (%)
		23	50	57	55.2
		22	33	29	48.3
		22	69	35	44.2
		22	58	68	44.2

(a)
(b)






Figure 8.4 Results when using Elshenawy algorithm (a) with median filter (b) without median filter on image 3

Unlike the results achieved by using the Sobel technique, the percentages of detection using Elshenawy algorithm have increased by using the median filter. When studying all the results of both approaches in the Figure, it was observed that the results of the two approaches were very close to each other and yet no false cells were detected in neither of





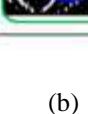
them.

The last edge-detection technique was the convolution mask. The results of this technique are illustrated in Figure 8.5 below. No false cells were detected in both approaches and all four potential cells were detected. The percentage results however varied from one cell to another. Some results of the detected cells were higher in the approach using the median filter (red rectangle) while the results of the rest decreased.

It was obvious in the results of the previous embryo that due to the noise reduction after applying the median filter, some of the results percentages would have decreased in some cells due to the removal of some pixels during the filtering process.

Image	Image after edge detection	Radius	x-centre	y-centre	Result (%)
		22	35	31	66.1
		21	70	35	55.9
		23	57	68	52.9
		23	51	56	52.7

(a)

Image	Image after edge detection	Radius	x-centre	y-centre	Result (%)
		22	35	31	68.1
		22	70	35	55.7
		22	51	57	55.7
		23	57	68	55.2

(b)

Figure 8.5 Results when using convolution mask (a) with median filter (b) without median filter on image 3

Further trials and investigations were taken concerning the images that had more noise (Figure 7.8) than the previous one. Figure 8.6 shows a sample of this image. It gives the

results of such an image when using the Sobel edge detector with and without applying the median filter.




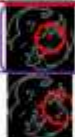
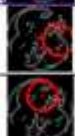


















Image	Image after edge detection	Radius	x-centre	y-centre	Result (%)
		23	66	65	26.2
		24	30	39	21.6
		19	60	61	18.8
		21	62	74	18.7
		21	29	51	16.9
		19	75	51	16.3
		19	32	64	16.3
Image	Image after edge detection	Radius	x-centre	y-centre	Result (%)
		23	66	64	30.7
		19	60	61	29.1
		24	30	39	25.9
		19	31	64	25
		22	51	73	23.6







Figure 8.6 More results when using Sobel (a) with median filter (b) without median filter on image 15

It was obvious that the results achieved with applying the median filter (Figure 8.6(a)) contained many false cells compared to the other approach (Figure 8.6(b)). On the other hand the three potential cells were detected using both approaches. The size and the position of the detected cells were similar in both approaches but again the percentage of detection decreased when the median filter was applied.

When applying Elshenawy algorithm to the same image the results depicted in Figure 8.7 were achieved. It was observed that all of the four potential cells were found through both techniques with very close similarity of position, size and even percentage. It was also noted that the percentage of detection of the Sobel technique was lower than the two other techniques.

Image	Image after edge detection	Radius	x-centre	y-centre	Result (%)
		23	65	65	69
		23	30	38	61.9
		19	50	61	53.6
		19	31	64	50
		19	76	52	49.7
		19	54	76	48
		20	29	51	47.5
		19	60	26	45

(a)

Image	Image after edge detection	Radius	x-centre	y-centre	Result (%)
		23	66	64	69
		20	48	62	58
		19	31	64	48.8
		26	33	40	48.7
		26	33	40	48.7

(b)

Figure 8.7 More results when using Elshenawy algorithm (a) with median filter (b) without median filter on image 15

The results that were achieved by the convolution mask were exactly the same except for the value of the percentages. Again, the values of the percentages decreased when the filter was applied because of the loss of some of the borders that were removed as part of the smoothing process. The results are given below in Figure 8.8.








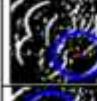

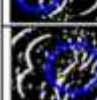


Image	Image after edge detection	Radius	x-centre	y-centre	Result (%)
		23	65	65	55.5
		23	32	38	51.1
		20	62	27	43.0
		25	44	59	34.5
		19	46	72	31.9

Image	Image after edge detection	Radius	x-centre	y-centre	Result (%)
		23	65	65	57.3
		23	32	38	51.8
		20	62	27	47.6
		25	44	59	42.1
		19	46	72	37.7

(a)
(b)

Figure 8.8 More results when using convolution mask (a) with median filter (b) without median filter on image 15

The results obtained using the binary template matching approach on the image dataset when the median filter was applied to reduce the noise levels prior to the edge-detection techniques is shown in Table 8.1.

Table 8.1 Results when applying median filter

Edge detector technique	Total cell count	Potential detected cells		False cells
		count	%	
Sobel	94	69	73.4	119
Elshenawy algorithm		76	80.8	105
Convolution mask		85	90.4	100

This approach improved on the detection of the true cells, but still found a large number of false cells.

Upon applying the median filter on the images and trying to detect the cells using the Hough Transform instead, the following results shown in Table 8.2 were achieved. Comparing the results in Table 8.1 and Table 8.2, the number of potential cells detected using the Sobel technique had slightly increased when using the Hough transform but the false cells detected had increased too. As for the other edge detection techniques, the potential detected cells have decreased upon using the Hough transform without any improvement in the number of false cells detected. Therefore, the second approach of refinement will be applied on the binary template matching technique.

Table 8.2 Results when using Hough Transform on filtered imaged

Edge detector technique	Total cell count	Potential detected cells		False cells
		count	%	
Sobel	94	71	75.5%	143
Elshenawy algorithm		56	59.5%	101
Convolution mask		53	56.3%	147

8.2.2 Applying two templates

A second refinement was to introduce a second set of binary templates, which took the form of a disk which had the ranges of sizes as the cells, and the ring template. This template measures the noise within a cell and rejects the result if the amount of noise within the cell exceeds certain limits. The two templates are shown in Figure 8.9.

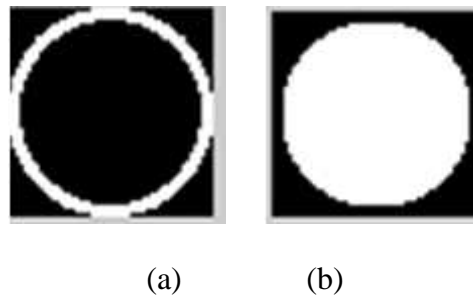


Figure 8.9 Ring (a) and disk (b) binary templates

A cell that was found was considered as a true cell if its border was detected using the ring template (a) and its interior did not contain a considerable amount of noise which was measured by using template (b).

Two percentage sensitivity values were then calculated, one using the ring template as before, giving an indication of the match between the image and the ring template, the ‘border percentage sensitivity’ (BPS), and the second, giving an indication of the match of the disk template and the 1s in the interior of the cell, the ‘interior percentage sensitivity’ (IPS), which would be high for noisy images and low otherwise. There was an inverse relationship between these two percentage sensitivity measures in the sense that a high BPS gave a strong indication of the presence of a true cell, while a high IPS gave a strong indication of noise in the image, and would reduce the indication of the cell being a true cell.

The task of combining these sensitivity values to decide if a potential cell was a true cell was not straightforward. One solution that was investigated was to construct a mathematical equation where the variables were the BPS and the IPS and the output was the likelihood of true cell. The surface shown in Figure 8.10 has the desired characteristics:

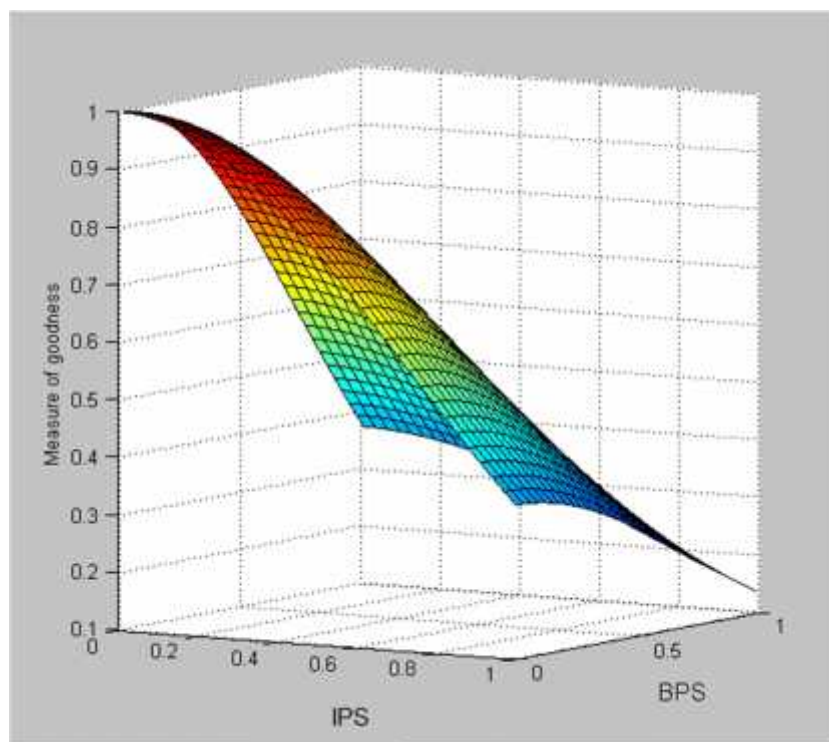


Figure 8.10 Surface of the desired equation

The equation of such a curve:

$$Z = \exp (-X.^2 - Y.^2)$$

where Z is the likelihood of a potential cell being a true cell, and X and Y are the BPS and IPS respectively. The maximum value of Z was then used to detect the position of the best match of the cells. The same rules that were used in the previous techniques for redundant points elimination were applied in this technique too. However, any value of Z that was less than 0.5 was not considered. This was considered to neglect the points that had likelihood less than 50% which were a weak chance of being a cell. The steps taken to apply this algorithm are summarized in Figure 8.11 found on the next page.

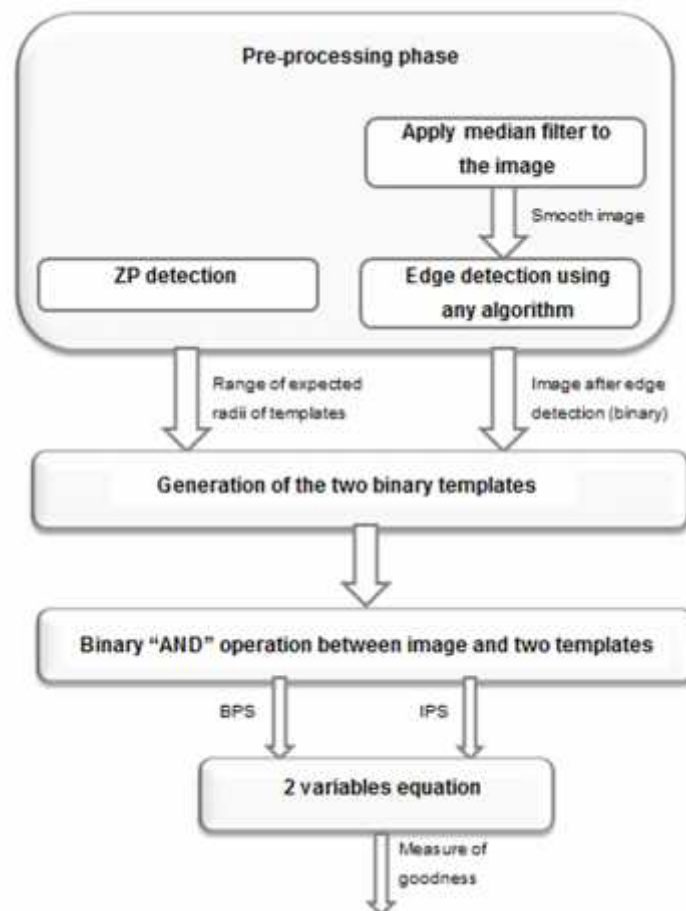


Figure 8.11 Summary of the algorithm

Samples of the results are given on the next page and discussed while the rest are placed in Appendix H (p.226) and Appendix I (p.232). Figure 8.12 shows a sample image with the new edge-detection technique.


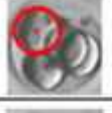
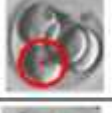

Image	Radius	x-centre	y-centre	BPS	IPS	Measure of goodness
	23	50	57	0.5	0.17	0.75
	22	34	29	0.48	0.15	0.74
	22	70	34	0.44	0.1	0.72
	23	57	68	0.41	0.24	0.67

Figure 8.12 Sample of results using Elshenawy detector algorithm on image 3

The results show that the two template classification algorithm managed to detect all of the four available cells correctly with no false ones. As for the measure of goodness it varied from 0.75 to 0.67 which is considerably high. These values varied due to the variation in the values of both the BPS and the IPS values. In the results of the first row, the BPS was 0.5 while the IPS was 0.17 which gave a measure of goodness 0.75. As the value of the IPS decreased, it was expected that the measure of goodness would increase as they were inversely proportional, but the opposite happened because the value of the BPS decreased, as can be seen in the results of the second and third rows. Note that the slight decrease in the measure of goodness in the second and third rows was not as prominent as the decrease in the result of the fourth one. This was because there was a big increase in the value of the IPS.

As the noise increased in the image, the tendency of the algorithm to detect false cells also increased. This was because noise increased the BPS and hence the measure of goodness. Note that the IPS, which was meant to be the noise measure, was also high because of the noise. This is seen in the example shown in Figure 8.13 where the result of applying the convolution mask to an image is seen. The only true cell available in the second row has a measure of goodness of 0.71 which was very high. Although the result in the first row had a higher measure of goodness, the detected cell was a false one; this high value was a result of the high value of the BPS compared to that of the second row.


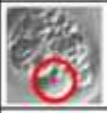




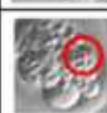
Image	Radius	x-centre	y-centre	BPS	IPS	Measure of goodness
	25	48	30	0.48	0.23	0.72
	20	73	49	0.43	0.13	0.71
	18	58	44	0.42	0.21	0.68
	25	31	32	0.41	0.24	0.66
	21	38	45	0.35	0.23	0.62
	20	20	36	0.34	0.22	0.61
	18	37	70	0.34	0.25	0.61

Figure 8.13 Results using convolution mask on image 16

When trying to apply this technique on the images that used the Sobel edge

detector, the algorithm did not give any significant results. Further investigation showed that the reason was that the edges produced were very thin and weak; this caused the BPS to be very low. On the other hand, the images lacked noise which caused the IPS to be very low too. Upon combining the values of the BPS and the IPS, the achieved value of the measure of goodness was below the desired value.

In summary, the enhanced “AND” technique used two templates instead of one to detect the cells. The first detected the presence of the border while the other measured the noise inside the detected cell. The outputs of these two templates were then applied to a 2 variable equation to evaluate the measure of goodness of the detected cell. The results of this technique are illustrated in

Table 8.3. Although the number of detected cells decreased slightly, this approach did lead to a considerable drop in the number of false cells.

Table 8.3 Enhanced "AND" technique results

Edge detector technique	Total cell count	Potential detected cells		False cells
		count	%	
Sobel	94	0	0	0
Elshenawy algorithm		72	76.5	42
Convolution mask		71	75.5	91

8.3 Conclusion

In this chapter the template matching algorithm was modified to process on binary images rather than grey level images. The modification made consisted of two phases: the first involved applying the median filter to the image before the edge detection process, while the second introduced a second template to get a measure of the noise inside the cell, which was considered to be responsible for the large number of false cells being detected. These two values were then combined in a two variable equation to give a single value which gave the likelihood of a potential cell being a true cell.

The modifications to the template matching approach to convert the images to binary, and then using a median filter to reduce the noise before applying the edge detection algorithms gave the better results. The introduction of a second binary template to get a measure of the noise in the cells led to a slightly reduced detection of the true cells, but a considerable reduction in the number of false cells detected. A summary of all the results is given in the next Chapter with the best algorithm developed in this Chapter applied to the test image dataset to investigate the robustness of the algorithm.

Chapter 9 Results and Discussion

Overview

The results of the previous techniques are provided in this chapter together with a measure of performance of each. The technique having the best results will be the used to test the other images that were left as a test dataset. Measures will also be provided for these results.

9.1 Introduction

All of the previous algorithms that were used aimed to detect the presence of cells in Day 2 embryos. Different results were achieved from each technique. To distinguish between them and decide which one was more effective, a measure of robustness was essential. The same measure was used for all techniques. This measure consisted of two parts. The first involved counting the number of potential cells that were effectively detected by the algorithm compared to the total available cell count in all the images that is 94 cells. The second involved counting the number of false cells that the technique has detected. The following section will present the results obtained using each technique.

9.2 Summary of Previous Results

The results will be displayed in order of the algorithm was investigated:

- **Hough Transform technique.**

The Hough Transform approach was described in Chapter 5. Three different edge-detection techniques were applied to each of the images in the dataset, and the accuracy of these in detecting true cells, and number of false cells detected, primarily as a result of noise in the images was discussed. The results obtained were presented in Table 5.3, which has been copied below as Table 9.1:

Table 9.1 Hough-based technique results

Edge detector technique	Total cell count	Potential detected cells		False cells
		count	%	
Sobel	94	62	65.9	226
Elshenawy algorithm		61	64.8	155
Convolution mask		57	60.6	161

- **Template matching technique**

The two template matching techniques that were considered SAD and the NCC, were described in Chapter 6. These approaches were used to detect the cells either by selecting one value (minimum SAD, or maximum NCC) or by considering all the available peak values. The results obtained using these approaches were presented in Table 6.1 and 6.2, which have been copied below in Table 9.2 and Table 9.3:

Table 9.2 One peak template matching results

Approach	Total cell count	Potential detected cells		False cells
		count	%	
SAD	94	0	0	219
NCC		44	46.8	175

Table 9.3 Multi-peak template matching results

Approach	Total cell count	Potential detected cells		False cells
		count	%	
NCC	94	45	47.8	69

- **Binary template matching technique**

This technique was described in Chapter 7 and used template matching, but instead of working on the image in its grey scale form, both the image and the template were converted into its binary form. This required the application of the three edge detection algorithms on the image before applying the template matching process, which used a logical AND operation, and used the ratio of the number of matches (1s) to the number of pixels in the template ring to generate a percentage similarity measure of the match between the image and the template. Table 9.4 shows the results that were presented in Table 7.1.

Table 9.4 Enhanced template matching technique results

Edge detector technique	Total cell count	Potential detected cells		False cells
		count	%	
Sobel	94	68	72.3	92
Elshenawy algorithm		67	71.2	83
Convolution mask		74	78.7	117

- **Refining the Binary template matching technique**

Applying median filter

The first approach of refinement was by using the median filter to smooth the image and hence decrease the number of false cells detected. The median filter was applied to the original image before applying any of the three edge detection techniques after which the binary template matching and the Hough Transform approaches were applied to the edges of the images. Table 9.5 and Table 9.6 are copied from Table 8.1 and Table 8.2 represented in the previous Chapter.

Table 9.5 Results when applying median filter

Edge detector technique	Total cell count	Potential detected cells		False cells
		count	%	
Sobel	94	69	73.4	119
Elshenawy algorithm		76	80.8	105
Convolution mask		85	90.4	100

Table 9.6 Results when using Hough Transform on filtered imaged

Edge detector technique	Total cell count	Potential detected cells		False cells
		count	%	
Sobel	94	71	75.5%	143
Elshenawy algorithm		56	59.5%	101
Convolution mask		53	56.3%	147

Comparing the results in Table 9.5 and

Table 9.6, it is shown that using the Hough Transform decreased the number of detected cells and increased the number of false cells detected too.

Enhanced “AND” technique

The enhanced “AND” technique used two templates instead of one to detect the cells. The first detected the presence of the border while the other measured the noise inside the detected cell. The outputs of these two templates were then applied to a 2 variable equation to evaluate the measure of goodness of the detected cell. However, the results of this technique are illustrated on the next page in Table 9.7. Although the number of detected cells decreased slightly, this did lead to a considerable drop in the number of false cells.

Table 9.7 Enhanced "AND" technique results

Edge detector technique	Total cell count	Potential detected cells		False cells
		count	%	
Sobel	94	0	0	0
Elshenawy algorithm		72	76.5	42
Convolution mask		71	75.5	91

9.3 Results for the testing dataset

Each of the approaches introduced gave different results, the best of which was that of the enhanced “AND” technique using Elshenawy algorithm as an edge detector technique. To measure the performance of this approach to detect cell in different images, this technique was used on the 10 testing images that were kept aside. These consisted of 5 images which were taken with a lower magnification than the images in the larger dataset and 5 taken with a higher magnification. The results will be introduced and discussed in detail in the following sections showing the compensation measures that were designed to overcome the magnification issue and the size of the ZP.

9.3.1 Applying the algorithm

The first step, which was part of the pre-processing stage, was the detection of the ZP. This was detected using the technique described earlier in Chapter 4. This technique mainly used the information about the difference in the grey level of the border of the ZP and the background. This information was a product of the close investigation that was made on the nature of the embryos images that showed that this difference was 20. Using this technique

to detect the ZP of the testing images, a sample of these results is depicted below in Figure 9.1.



Figure 9.1 ZP detection of a testing image

The image in Figure 9.1 is one of the images that have a smaller magnification than the images that were used in all of the previous work. The size of this image is 80x80. Upon applying the ZP detection algorithm on this image, the algorithm detected the ZP properly as illustrated in the Figure and the size of the diameter was 76 pixels. From this the scale factor was simply calculated by dividing the diameter of the ZP by the size of the Day 2 embryo, giving a value of 0.5 pixel/ μm .

According to the work done by Hnida et al. (2004) and introduced in Chapters 2 and 4, the expected size of the cells (blastomeres) of Day 2 embryos ranged from 56.4 μm to 73.4 μm . To convert these values into pixels, the scale factor was used. These ranges were equivalent to 28 pixels to 37 pixels. These values were the D_{\min} and the D_{\max} (respectively) values of the templates to be generated. In this approach two templates were generated having the same size each time. The first template had the ring in it in order to detect and measure the existence factor of the border of the cell, whereas the second template was a solid flood-filled circle that was used to measure the noise factor inside the cells. These two factors gave their results as a percentage to the actual size of the template and for this they were named BPS and IPS.

The second step of the pre-processing phase involved detecting the edges of the image after applying the median filter. The edge detection algorithm that gave the best results was Elshenawy algorithm that was introduced and designed in this work. This technique used the same idea that was used in the ZP detection, but this time the threshold value was 25 due to the darker colour of the border of the cell compared to that of the ZP.

The idea of this technique was based on using the two templates that were generated and moved along the whole image by a simple logical “AND” operation. This operation developed the two factors that were BPS and IPS. These factors were used to measure the percentage of existence of the border and the noise inside the cells. These values were then substituted in an equation which was introduced in Chapter 7. The choice of this equation was based on the 3D surface required, taking BPS and IPS as the X-Y axis, respectively, while the Z axis was the indicator of the measure of goodness of the detected cell. For this reason any result that was below 50% was neglected.

The results of using this technique gave some redundant values that had to be removed. These redundant values were removed using the clustering technique developed and discussed before in chapter 5. This technique worked to remove the redundant values that belonged to a mask size around the maximum value. The size of this mask depended on the size of the image, which was again subject to changes and depended on the size of the ZP, as mentioned before. For this image the D_{\min} was 28 pixels, which made the radius equal to 14 pixels, and since 50% of the radius value was 7, the mask size for the clustering process was 15x15. This mask removed the redundant size but at the same time tried to keep the cells that were nearly overlapping.

The results are shown in Figure 9.2 below. The table shows that the algorithm has detected 3 of the 4 potential cells available.

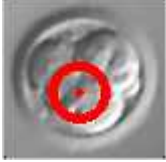



Image	Radius	x-centre	y-centre	BPS	IPS	Measure of goodness
	14	48	38	0.45	0.16	0.72
	16	24	42	0.45	0.24	0.69
	16	35	24	0.38	0.21	0.65
	14	50	48	0.35	0.24	0.62

Figure 9.2 results of the enhanced "AND" technique

Another sample taken from the available images is given in the next page in Figure 9.3. This image has a higher magnification scale than that of the other images that were used in the previous work. The size of this image is 180 x 180. Upon applying the ZP detection technique to this image, the ZP was properly detected as depicted in the Figure.

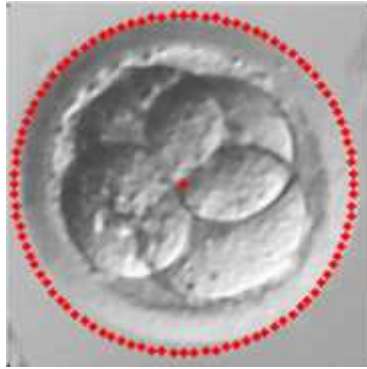


Figure 9.3 sample of another image

The image shown in the Figure had a ZP diameter of 168 pixels. The magnification scale S of this image came from dividing the diameter of the image, which is 168 by the expect size of the embryo which is $150\mu\text{m}$, to give $1.12 \text{ pixels}/\mu\text{m}$. However, the values of D_{\min} and the D_{\max} were 62 pixels and 82 pixels, respectively. Another value that was dependent on the size of the ZP and the magnification scale was the size of the clustering mask. As explained before the size of the mask would be calculated from the radius of the smallest template which for this image was 31. The mask size for this image was 33×33 .

The results of applying the algorithm to this image are shown on the next page in Figure 9.4. The algorithm managed to detect all of the 4 cells without any false ones. The results of the rest of the 10 images are depicted in Appendix J (p.238).




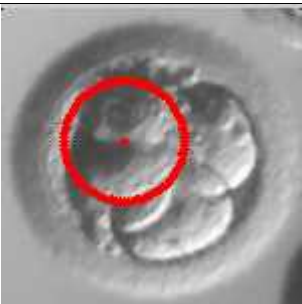
Image	Radius	x-centre	y-centre	BPS	IPS	Measure of goodness
	31	87	59	0.33	0.14	0.62
	33	96	87	0.32	0.17	0.61
	33	66	100	0.29	0.14	0.59
	32	67	62	0.26	0.08	0.58

Figure 9.4 Results of the image

9.3.2 Results

The 10 images that were kept aside as a test sample to measure the robustness of the enhanced “AND” algorithm gave 80% of potential cells detection. It can be seen in Table 9.8 that out of the 35 cells that were present in the 10 images, the algorithm has properly detected 30 cells. On the other hand, only 6 false cells were detected.

Table 9.8 summary of the results

Edge detector technique	Total cell count	Potential detected cells		False cells
		count	%	
Elshenawy algorithm	35	30	85	6

The enhanced “AND” technique along with all the compensation solutions that were designed have proven that together they detected the potential cells of a new image dataset with a percentage of 80%. These compensations included detecting the ZP with different magnification scales, evaluating the different ranges of the templates used and even the size of the clustering mask.

9.4 Classification results

Table 9.9 presents all the cell counts of all the images. The information in this table consists of the cell count which gives the actual cell available in the image, the number of potential cells that the algorithm managed to detect and finally the false cells detected. The optimum case is where the number of cell counts was all detected with no false cells, such as the result of image 3. Image 3 contains 4 cells, these cells were all properly detected with no false cells, likewise images 4, 11, 13, 16, 21, 30 and 34. These 8 results are shown in Table 9.10(a) and are the only ones that can be used for classification.

Table 9.9 Classification results

Image #	Cell count	Potential cells detected	False cells detected
1	4	2	0
2	3	2	0
3	4	4	0
4	3	3	0
5	4	1	3
6	4	3	1
7	1	0	4
8	3	1	1
9	2	0	4
10	4	4	1
11	5	5	0
12	4	3	0
13	4	4	0
14	0	0	4
15	4	4	1
16	1	1	0
17	5	3	1
18	0	0	5
19	4	2	4
20	4	2	0

Image #	Cell count	Potential cells detected	False cells detected
21	3	3	0
22	4	4	1
23	3	3	1
24	4	4	1
25	4	2	2
26	3	3	2
27	3	3	2
28	4	4	3
29	3	2	1
30	4	4	0
31	4	2	0
32	4	3	0
33	2	1	1
34	4	4	0
35	3	3	1
36	3	3	1
37	4	4	1
38	3	3	1
39	4	3	1

Table 9.10 results used for classification**(a)**

Image #	Cell count	Potential cells detected	False cells detected
3	4	4	0
4	3	3	0
11	5	5	0
13	4	4	0
16	1	1	0
21	3	3	0
30	4	4	0
34	4	4	0

(b)

Image #	Cell count	Potential cells detected	False cells detected
3	4	4	0
13	4	4	0
30	4	4	0
34	4	4	0

Considering the classification issue of these cells and according to the grading technique used in this work of Day 2 embryo, the only images that can be re-implanted are those having 4 properly detected cells as in images 3, 13, 30 and 34 as depicted in Table 9.10(b). Although the images 4, 11, 16 and 21 have properly detected cells, neither of them have the desired number of cells that should be available according to the grading system used, that is why these are not to be re-implanted again.

In some cases detecting false cells or even failing to detect all potential cells in the image causes an improper classification result. Table 9.9 shows that some images contain 4 cells, which means that they can be re-implanted but because of false cells detected/failure of detecting all the potential cells, they were classified as inappropriate. These images are 1, 10, 12, 15, 19, 20, 22, 24, 28, 31, 32, 37 and 39. On the other hand, some results detected 4 cells while they are not present and this will also cause misleading classification. Such images were 5, 6, 7, 14, 17, 23, 25, 35, 36 and 38.

9.5 Conclusion

Among all the different approaches used, the enhanced “AND” technique gave the best results that had high percentage of correct cell detection as well as low false cells detection. The importance of trying to detect all the available potential cells and none of the false cells has appeared clearly during the classification process. The total number of detected cells was not as important as managing to clarify if this number consists of all the potential cells, some false cells or a combination of both.

Given the size criteria that was used to detect the cells that met the template used, the aims and objectives became to select correctly the identified images having 4 cells. However, the aims and objectives of this Thesis were completely met for those images that were correctly analysed.

Chapter 10 Conclusions

Overview

This Chapter contains the summary of the work done in this thesis. It reviews the main aims and objectives and the results and the findings obtained. Finally suggestions for future work are provided.

10.1 Summary of the aims and objective and work done

The aim of this work was to develop a prototype automated image analysis system that is able to detect and classify Day 2 human embryo cells as suitable for implantation. To accomplish this, there were many stages which this work had to perform. This work has managed to:

- Map the characteristics and key features of the Day 2 embryo cells that would make them suitable for implantation into features that can be detected by the system. These features were the blastomere number and size. Day 2 embryos must have 4 blastomeres that are even in size.
- Pre-process the image to compensate for magnification and illumination variations in the microscope images. This was achieved by developing a novel approach to detect the size of the ZP, which was then used to estimate the

magnification of the image and hence adjust the measurements of the anticipated sizes of the cells to tune the detection algorithms.

- Develop and compare different image segmentation and feature extraction techniques appropriate to these images: the Hough Transform and template matching. These techniques were carried out using the information from the pre-processing stage, as it was essential to compensate for the magnification and illumination variations in the images. Certain modifications were made to these techniques which involved the production of novel techniques for the edge detection along with the new approaches that were based on the Hough Transform and the template matching. These modifications used a disk as a template that matched the cell sizes and grey scale. The template was used in further modifications but in its binary form.
- Identify the most accurate image processing techniques for classifying the embryo as suitable for implantation and this was done after investigating all the results from all different techniques and approaches available.
- Investigate the performance of the approach using images of embryos taken with different microscope magnifications.

10.2 Summary of the results and findings

The work done in this thesis involved applying different techniques aiming to detect and classify Day 2 embryos. The first of which was a Hough-based technique that managed to detect potential cells with a percentage that varied from 60.8% to 65.9% according to the edge detection technique used.

The template matching based techniques were carried out using two approaches. The first only took into consideration a unique peak value and gave a detection percentage of 46.8% when using the NCC method while the SAD gave 0%. The second approach that detected all the peak values gave 47.8%.

Enhancing the template matching technique by converting both the image and the templates into their binary form made the percentage of detection increase to reach 71.2% to 78.7%, depending on the type of edge detection technique used which was either Sobel, Elshenawy algorithm or the algorithm that used the convolution mask. When the median filter was used to this technique, the edges produced by using the Sobel edge detector produced a percentage of 73.4%. However, the percentages of the two other techniques reached 80.8% and 90.4% respectively.

A final modification was made to the technique; the result of this modification gave a percentage of Elshenawy algorithm and the convolution mask of 75.5% and 76.5%, while the Sobel gave 0%. This final technique was further used on another dataset of images that contained 10 images that had different magnifications, 5 of which had smaller magnification and the other 5 had a higher magnification. These images gave a percentage of detection of 85%.

As shown from all the previous results, the numbers of potential cells detected along with the number of the false cells detected were the main factors that will affect the classification. The optimum case for the classification is where the number of cell counts are all properly detected with no false cells. Considering the classification issue of these cells and

according to the grading technique used in this work of Day 2 embryo, the only images that can be re-implanted are those having 4 properly detected cells

In some cases detecting false cells or even failing to detect all potential cells in the image causes an improper classification result. Such as detecting 4 cells upon which 2 of them are potential cells and the other 2 were false ones. According to the classification issues this image can re-implanted, but in reality 2 of the detected cells are false. Other cases had 4 cells but the detected results showed more than that because of the false ones which made the classification result to consider not re-implanting it.

As for the classification of the detected images of the latter technique, 39 images were tested on the system, 8 images were found suitable for the classification process, that is all the available cells were properly detected with the absence of false cells. Among these 8 images, 4 images had their 4 cells and hence were appropriate to be re-implanted again, while the other 4 images had their cells properly detected too but they were not considered to be appropriate for re-implantation due to their cell count which was not equal to the desired number.

10.3 Future work

The fact that the system has detected only 8 images properly with their real cells and no false cells out of the whole dataset was a key issue to consider if the system is to be robust enough for clinical use. Further work is required to correctly identify only the true cells in the images. The current algorithms have detected 80% of the true cells, and considerable work was required to reduce the false cells down to minimum.

The work done measured some of the thresholds according to the images available. These thresholds might slightly change with the change of the clinic. Creating a system before the proposed detection system to automatically adjust these thresholds will make this system more effective to work on any image from any clinic.

If accuracy of the detected Day 2 cells can be sufficiently improved for clinical use it will be possible to implement this on an embedded system that can be placed inside the incubator. The system will take pictures of the embryos while they are inside the incubator at the appropriate time (at Day 2), and then detect, classify and finally grade the embryos.

The work in this thesis focused on the detection of cells of Day 2 embryos. However, work can be done to automatically measure the fragmentation percentage, which can be used along with the number of cells count detected in order to perform an automatic grading system for embryos at other stages of development.

Finally, the merger between BPS and IPS can be tried out using the concept of fuzzy logic. These two values can be considered as the variables of the fuzzy system and an appropriate membership function can be developed to produce the desired output, which in this case would be the measure of goodness.

Bibliography

Awcock, G. & Thomas, R. 1995, *Applied Image Processing*, Macmillan.

Beuchat, A. & Thevenaz, P, 2008, 'Quantitative morphometrical characterization of human pronuclear zygotes.', *Human Reproduction*, vol 23, no. 9, pp. 1983-1992.

Bikhet, S., Darwish, A. & Tolba, H. 2000, 'Segmentation and classification of white blood cells', *ICASSP '00*.

Bqczkowski, T., Kurzawa, R. & W., G. 2004, 'Methods of embryo scoring in in vitro fertilization', *Reproductive Biology*, vol 4, no. 1, pp. 5-22.

Canny 1986, 'A Computational Approach to Edge Detection', *IEEE Transactions on Pattern Analysis and Machine Intelligence*, vol 8, pp. 679-714.

Cummins, J., Breen, T. & Harison, K, 1986, 'A formula for scoring human embryo growth rates in in vitro fertilization: its value in predicting pregnancy and in comparison with visual estimates of embryo quality.', *In vitro Fertilization and Embryo Transfer*, vol 3, no. 5, pp. 284-295.

Dokras, A., Sargent, I. & Barlow, D. 1993, 'Human blastocyst grading: an indicator of development potential?', *Human Reproduction.*, vol 8, no. 12, pp. 2119-2127.

Filho, E., Noble, J. & Wells, D. 2010, 'A review on automatic analysis of human embryo microscope images.', *The open Biomedical Engineering*, vol 4, pp. 170-171.

Gardner D.K., SE,MD 2005, 'Single blastocyst transfer: a prospective randomized trial', *Fertility and Sterility*, no. 81, pp. 551-555.

Giusti, A, Corani, G & L.M, G 2009, 'Segmentation of human zygotes in hoffman modulation contrast images.', *Medical Image Understanding and Analysis (MIUA'09)*.

Gonzalez, R. & Woods, R. 2002, *Digital Image Processing (2nd ed.)*., Prentice Hall.

Heske T., HJN 1999, *Fuzzy logic for real world design*, Annabooks, San Diego.

Hnida, C., Engenheiro, E. & Ziebe, S. 2004, 'Computer-controlled, multilevel, morphometric analysis of blastomere size as biomarker of fragmentation and multinuclearity in human embryos.', *Human Reproduction*, vol 19, no. 2, pp. 288-293.

Hough, P. V. C., Method and Means for Recognizing Complex Patterns, *US Patents* 3969654, 1996

Kass M., WA,TD 1988, 'Snakes: active Contour Model', *International journal of Computer Vision*, pp. 321-331.

Lau, T. & Bischof, W. 1991, 'Automated detection of breast tumors using the asymmetry approach.', *Computers and Biomedical Research.*, vol 24, no. 3, pp. 271-295.

Mirolaw, L, Chorazyczewski, A, Buchholz, F & Kittler, R 2005, 'Correlation-based Method for Automatic Mitotic Cell Detection in Phase Contrast Microscopy', in *Computer Recognition Systems*.

Morales, DA., Bengoetxea, E. & Larranaga, P. 2008, 'Automatic segmentation of zona pellucida in human embryo images applying an active contour model.', *Medical Image Understanding and Analysis (MIUA'08)*.

Prat, W. 2001, *Digital Image Processing*, 3rd edn.

Puissant, F., Rysselberge, M. & Barlow, P, 1987, 'Embryo scoring as a prognostic tool in ivf treatment.', *Human Reproduction.*, vol 2, no. 8, pp. 705-708.

Ross, N., Pritchard, C. & Rubin, D. 2006, , *Medical and Biological Engineering and Computing.*, vol 44, no. 5, pp. 427-436.

Sallam, H 2001, *Infertility and Assisted Conception.*

Scott, L., Alvero, R. & M., L. 2000, 'The morphology of human pronuclear embryos is positively related to blastocyst development and implantation.', *Human Reproduction.*, vol 15, no. 11, pp. 2394-2403.

Staessen, C., Camus, M. & Bollen, N. 1992, 'The relationship between embryo quality and the occurrence of multiple pregnancies.', *Fertility and Sterility.*, vol 57, no. 3, pp. 262-630.






























Steer, C., Mills, C. & Tan, S. 1992, 'The cumulative embryo score: a predictive embryo scoring technique to select the optimal number of embryos to transfer in an in vitro fertilization and embryo transfer programme.', *Human Reproduction.*, vol 7, no. 1, pp. 117-119.

Vromen, J. & McCane, B. 2009, 'Red blood cell segmentation from sem images.', *Image and Vision Computing IVCNZ '09.*, New Zealand.

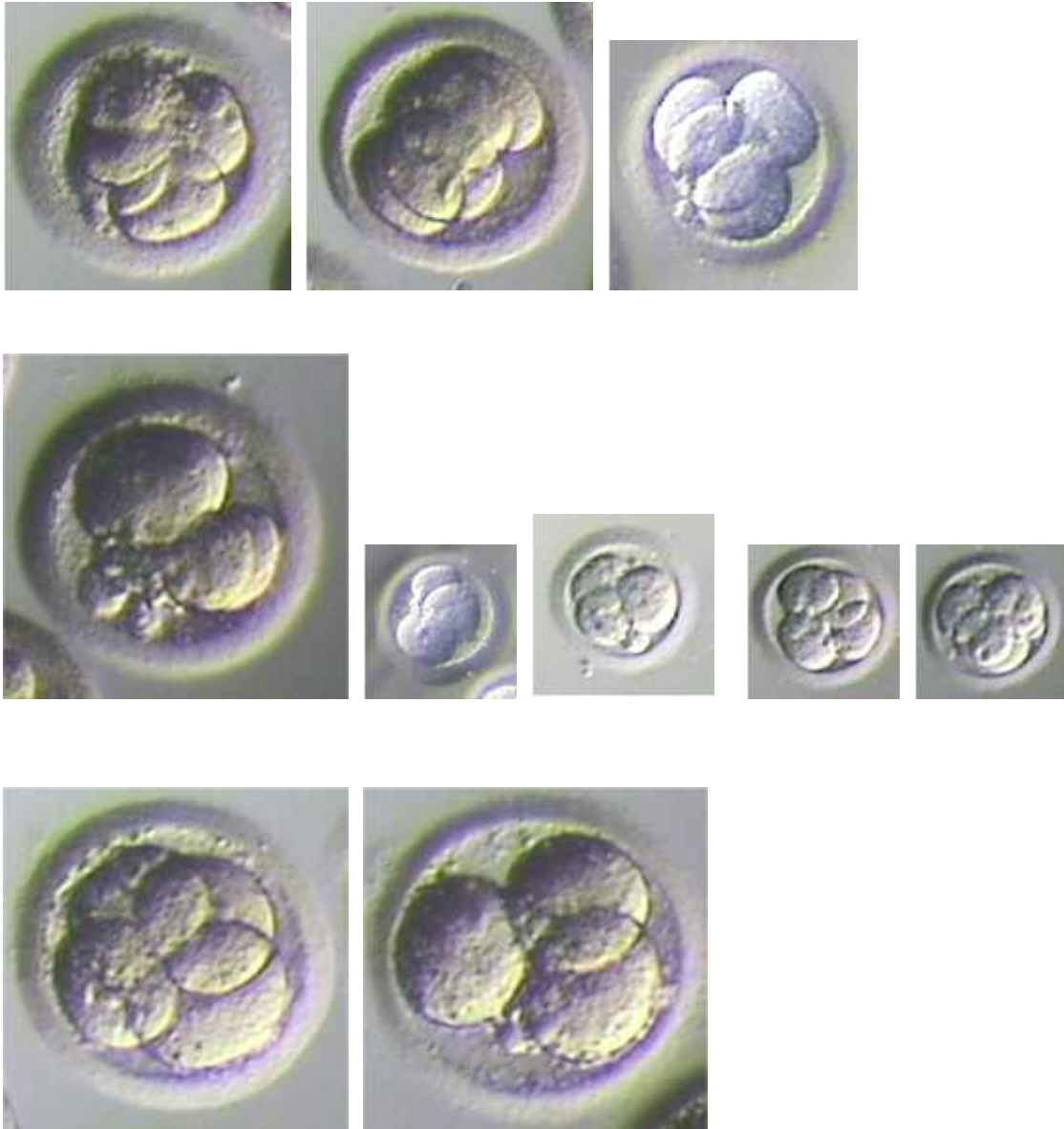
Zeibe, S., Peterson, K. & Lindenberg, S. 1997, 'Embryo morphology or cleavage stage: how to select the best embryos for transfer after in vitro fertilization.', *Human Reproduction.*, vol 12, no. 7, pp. 1545-1549.

APPENDIX A

Images Dataset

Image 1		Image 9		Image 17		Image 25	
Image 2		Image 10		Image 18		Image 26	
Image 3		Image 11		Image 19		Image 27	
Image 4		Image 12		Image 20		Image 28	
Image 5		Image 13		Image 21		Image 29	
Image 6		Image 14		Image 22			
Image 7		Image 15		Image 23			
Image 8		Image 16		Image 24			

Testing Dataset


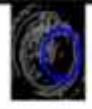


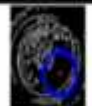





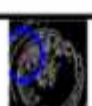





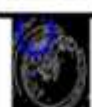




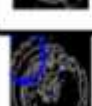






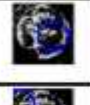

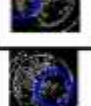





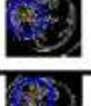


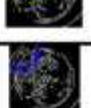





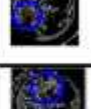









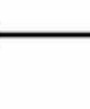




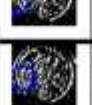


APPENDIX B












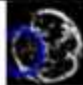




This Appendix contains the results of the Hough Transform technique that was discussed in Chapter 5. Some of these results were depicted in the Chapter while the rest are shown in the tables in the following pages.

The results of the detected cells of each of the three types of edge detectors (Sobel, new algorithm and convolution mask) are given in each table. However, these results include the x-centre, y-centre, radius and finally the matching value which corresponds to the value of accumulator. The detected cell is also shown as a blue circle plotted on the image.

[illegible][illegible]

Original image	Sobel edge detection					New algorithm edge detection					Convolution edge detection				
	Image	Results				Image	Results				Image	Results			
		x-gradient	y-gradient	gradient	threshold value		x-gradient	y-gradient	gradient	threshold value		x-gradient	y-gradient	gradient	threshold value
		50	66	24	24		57	51	24	31		48	66	24	34
		62	65	20	23		67	52	22	30		48	31	24	32
		39	31	22	22		3	26	24	26		59	63	24	30
		31	19	22	19		29	38	24	26		41	66	22	29
		51	22	24	19		16	19	22	23		54	8	22	28
		14	29	20	18		41	26	22	22		26	17	22	28
		27	6	22	17							47	39	18	27
		19	17	22	17							54	75	20	25
		23	41	18	15										

Original image	Sobel edge detection				New algorithm edge detection				Convolution edge detection						
	image	Results				image	Results				image	Results			
		x-gradient	y-gradient	gradient	threshold value		x-gradient	y-gradient	gradient	threshold value		x-gradient	y-gradient	gradient	threshold value
		55	62	22	23		64	53	24	33		54	66	24	34
		52	52	28	21		52	26	24	32		51	24	22	30
		54	64	28	21		52	52	24	31		65	21	22	29
		31	17	22	20		64	41	24	31		65	24	22	29
		45	26	22	20		20	43	24	28		50	4	24	29
		32	35	24	19		52	36	24	27		40	32	24	29
		30	17	28	18		52	36	24	21		26	14	22	26
		36	26	24	18		20	25	24	21		9	6	38	23
		58	26	18	15		2	17	24	29		45	12	18	21
		27	46	20	15		33	27	24	22		56	29	18	22
							55	62	24	22		34	63	18	23
							44	25	22	20		61	5	18	23
												58	17	18	23
												34	77	18	23

Original image	Sobel edge detection					New algorithm edge detection					Convolution edge detection				
	image	Results				image	Results				image	Results			
		x coordinate	y coordinate	radius	vector		y coordinate	x coordinate	radius	vector		x coordinate	y coordinate	radius	vector
		57	19	24	24		61	40	24	38		57	19	24	37
		63	62	24	24		48	29	24	35		47	67	18	32
		90	48	24	22		61	51	24	34		32	54	18	28
		59	62	24	22		15	57	24	31					
		70	63	18	16		69	47	18	30					
		58	30	18	15		26	54	20	28					





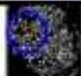


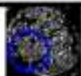


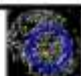



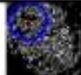








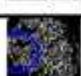





[illegible]

[illegible]
















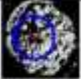







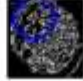


[illegible][illegible]






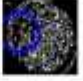


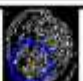
[illegible][illegible]


























[illegible]







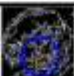
Original Image	Sobel edge detection					New algorithm edge detection					Convolution edge detection				
	Image	Results				Image	Results				Image	Results			
		entropy	contrast	radius	detecting time		entropy	contrast	radius	detecting time		entropy	contrast	radius	detecting time
		69	45	23	25		45	68	23	42		32	3	25	33
		38	26	25	26		36	34	25	42		38	3	25	32
		59	29	25	25		54	46	23	41		68	4	25	32
		51	55	25	25		26	37	25	39		39	4	25	30
		24	38	23	23		17	17	25	34		43	6	25	30
		35	34	23	23		62	65	21	33		66	6	23	29
		40	2	25	23		54	33	23	30		53	5	25	29
		48	15	25	23		2	39	25	28		53	2	19	28
		34	43	25	23		26	8	25	27		24	2	25	28











[illegible]











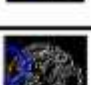


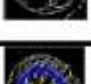


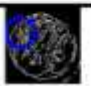








Original image	Sobel edge detection					New algorithm edge detection					Convolution edge detection				
	Image	Results				Image	Results				Image	Results			
		x centre	y centre	radius	matching rate		y centre	x centre	radius	matching rate		x centre	y centre	radius	matching rate
		39	47	25	27		50	66	23	40		52	58	25	34
		40	60	25	27		30	49	25	38		32	31	25	33
		27	48	23	26		61	57	23	37		69	47	25	33
		57	39	25	26		40	70	25	37		66	70	25	31
		43	58	25	26		40	47	25	38		53	31	25	30
		63	22	25	25		18	66	23	31		45	67	21	28
		41	35	25	24		40	39	25	31		70	24	23	28
		25	36	25	23		68	41	23	29		31	57	23	28





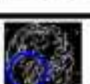


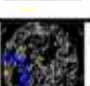


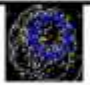
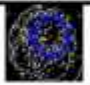


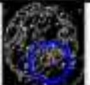











		31	39	21	22		40	21	25	27		18	1	21	26
		74	24	29	22		11	74	25	26					
		44	22	25	22										
		71	49	25	22										
		39	11	25	21										
		68	38	25	21										



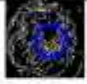

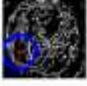

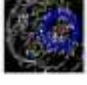

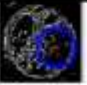











Original image	Sobel edge detection					New algorithm edge detection					Convolution edge detection				
	Image	Results				Image	Results				Image	Results			
		x-center	y-center	radius	threshold value		x-center	y-center	radius	threshold value		x-center	y-center	radius	threshold value
		27	65	19	28		62	56	25	40		67	32	25	40
		56	65	25	28		27	67	25	37		56	62	25	40
		42	70	23	26		37	33	25	37		27	60	23	37
		63	25	23	23		48	56	25	36		52	30	25	36
		71	38	19	22		69	57	19	34		29	38	25	35
		55	68	23	22		27	52	25	32		47	66	25	34
		42	32	25	22		19	34	25	28		57	70	19	33
		30	37	25	21		55	55	19	37		73	48	25	31




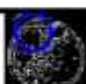




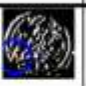
		45	8	25	39		2	56	23	26					
		24	25	25	19		55	62	19	25					
		33	48	25	19		55	38	19	24					
		44	52	25	19										








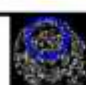


Original image	Sobel edge detection					New algorithm edge detection					Convolution edge detection				
	Image	Results				Image	Results				Image	Results			
		x-center	y-center	radius	Matching rate		x-center	y-center	radius	Matching rate		x-center	y-center	radius	Matching rate
		37	36	24	24		4	26	24	30		43	17	22	24
		46	3	24	23		38	33	22	28		56	16	24	24
		24	30	22	22		49	39	22	28		52	67	24	33

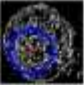























		52	63	24	22		13	35	24	26		49	3	22	32
		39	47	20	19		65	52	22	25		35	47	18	31
		96	17	22	10		55	35	30	24		25	28	24	31
		35	8	20	18		29	24	27	23		51	53	24	31
		90	44	24	18		48	31	22	22		38	2	22	30
		32	19	18	16		13	29	34	20		32	15	22	29
		70	41	20	16		21	7	24	19		40	26	24	29
		36	60	20	18							35	55	20	27



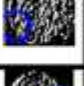

Original image	Sobel edge detection					New algorithm edge detection					Convolution edge detection				
	Image	Results				Image	Results				Image	Results			
		x-centre	y-centre	radius	Min-Max value		x-centre	y-centre	radius	Min-Max value		x-centre	y-centre	radius	Min-Max value
		29	43	25	31		42	28	25	35		55	24	25	35
		62	30	23	26		30	61	23	31		25	32	23	34
		63	7	23	21		2	30	23	31		61	6	25	33
		39	55	23	21		21	44	23	25		49	47	23	31
		69	55	23	21							61	32	19	28
		30	2	23	20		11	67	23	24		49	56	21	28
		55	41	21	18		50	41	21	23		40	42	21	26
		47	17	19	17		60	47	25	22		40	61	21	26











		26	54	19	16						47	17	19	25	
		50	57	19	16						63	56	19	25	
		66	19	19	15						34	2	21	25	
		47	68	19	15										
Original Image	Sobel edge detection				New algorithm edge detection				Convolution edge detection						
	Image	Results				Image	Results				Image	Results			
		x-centre	y-centre	radius	Masking value			x-centre	y-centre	radius		Masking value		x-centre	y-centre
		54	67	22	24		24	33	24	34		52	67	24	33
		34	28	24	22		62	52	24	33		38	53	24	31
		61	24	20	20		32	23	20	30		51	53	24	31
		47	22	22	20		18	60	24	25		45	32	24	30









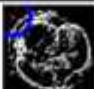










		39	60	22	20		5	68	18	10		53	26	22	28
		21	33	20	17							64	33	20	27
		60	3	20	15							36	28	22	27
												45	2	20	24
												65	17	22	24
















Original image	Sobel edge detection				New algorithm edge detection				Convolution edge detection						
	image	Results				Image	Results				Image	Results			
		x-centre	y-centre	radius	Masking value		x-centre	y-centre	radius	Masking value		x-centre	y-centre	radius	Masking value
		41	59	25	28		40	48	23	32		30	40	25	35
		59	62	21	28		54	48	23	32		44	27	23	33
		27	44	23	24		2	46	25	32		63	32	25	33

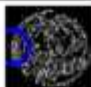









		58	37	25	24		30	62	23	28		56	43	25	33
		39	27	25	22		47	36	25	28					
		69	48	25	22		47	68	25	28		41	2	25	30
		52	8	23	21		64	37	21	26		30	2	21	29
		78	10	23	20		18	57	25	24		56	4	25	29
		37	2	19	19		10	84	19	19		32	48	21	28
		54	49	19	18							55	25	23	28
		54	19	19	18							40	35	23	28
		41	16	23	18							72	36	23	28
												48	46	21	27





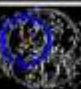

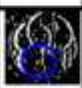
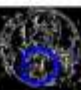



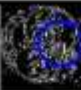








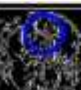


											36	60	19	26
											64	54	19	25
											68	15	19	24
											51	76	19	24





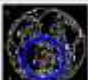





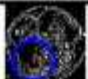


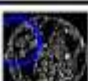




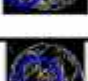

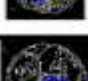
Original image	Sobel edge detection					New algorithm edge detection					Convolution edge detection				
	Image	Results				Image	Results				Image	Results			
		x-coords	y-coords	radius	Masking value		y-coords	x-coords	radius	Masking value		x-coords	y-coords	radius	Masking value
		32	46	24	25		64	46	24	38		30	46	20	37
		49	66	22	24		32	37	24	31		52	67	24	33
		35	32	24	22		1	41	20	29		38	53	24	31





		47	1	22	18		46	32	24	29		51	53	24	31
		31	2	18	16		32	25	34	24		45	32	24	30
		48	37	18	16		10	13	18	19		53	26	22	28
		21	27	20	18		1	24	30	19		64	33	20	27
												36	28	22	27
												45	2	20	24
												65	17	22	24


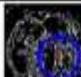





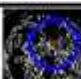

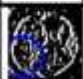
Original image	Sobel edge detection					New algorithm edge detection					Convolution edge detection				
	Image	Results				Image	Results				Image	Results			
		x-centre	y-centre	radius	Matching value		x-centre	y-centre	radius	Matching value		x-centre	y-centre	radius	Matching value
		42	63	24	28		62	42	24	44		30	40	25	35
		53	25	24	23		21	48	24	29		41	61	22	34
		34	36	18	22		28	37	22	27		63	32	25	33
		69	21	24	22		48	44	22	26		56	43	25	33
		57	62	24	22		5	42	20	23		45	25	25	31
		39	21	24	21		36	74	18	22		58	54	20	30
		39	50	20	20		5	35	20	21		64	40	23	30
		74	32	22	19		12	23	18	20		41	2	25	30

		46	7	18	17								46	16	22	29		
		47	37	18	17													
		54	50	20	16									53	8	24	29	
		68	50	20	16									46	46	24	29	
														61	9	24	28	
													72	36	23	28		
													58	66	24	27		

Original image	Sobel edge detection					New algorithm edge detection					Convolution edge detection				
	Image	Results				Image	Results				Image	Results			
		x-centre	y-centre	rad us	Matching value		y-centre	x-centre	rad us	Matching value		x-centre	y-centre	rad us	Matching value
		33	62	23	32		59	33	25	48		33	59	25	45
		37	32	25	26		44	67	21	38		67	43	21	36
		66	46	19	25		68	44	25	35		37	38	19	35
		45	68	25	24		36	38	21	36					
		61	57	19	21		29	56	21	25					
		65	31	19	20		51	48	21	25					
		25	51	19	19										

Original image	Sobel-edge detection					New algorithm edge detection					Convolution edge detection				
	Image	Results				Image	Results				Image	Results			
		x-centre	y-centre	radius	Matching value		y-centre	x-centre	radius	Matching value		x-centre	y-centre	radius	Matching value
		50	69	25	26		46	64	25	41		62	43	23	36
		62	47	23	25		63	33	23	40		37	61	25	35
		31	68	19	24		53	56	21	38		61	61	23	33
		66	36	23	23		33	66	25	38		35	18	25	29
		32	17	25	22		17	32	25	33		66	1	19	26
		59	24	25	21		24	55	25	33					
		47	39	25	21		70	45	23	30					
		63	58	19	19										

		77	25	19	18										
		23	53	19	18										
		51	54	21	18										

Original image	Sobel edge detection					New algorithm edge detection					Convolution edge detection				
	Image	Results				Image	Results				Image	Results			
		x-centre	y-centre	radius	Matching value		y-centre	x-centre	radius	Matching value		x-centre	y-centre	radius	Matching value
		59	61	23	26		58	37	23	43		36	55	25	40
		62	17	25	26		17	69	25	38		55	62	25	39
		37	56	25	24		49	66	25	34		65	19	25	37

[illegible][illegible]

APPENDIX C

This Appendix contains the results of the proposed technique in Chapter 6. These results are the results of applying the correlation technique and getting the values of the maximum correlation coefficient. The two techniques used were the SAD and the NCC.








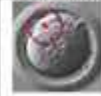






		Diameter (pixels)							
		36	38	40	42	44	46	48	50
SAD	NCC								
		Center(77,19) Value=41989	Center(76,20) Value=49562	Center(75,21) Value=55361	Center(74,22) Value=61742	Center(73,25) Value=69651	Center(72,27) Value=75679	Center(71,27) Value=82022	Center(70,26) Value=89294
SAD	NCC								
		Center(66,62) Value=0.3264	Center(66,62) Value=0.3120	Center(66,69) Value=0.2843	Center(61,63) Value=0.2391	Center(66,55) Value=0.2851	Center(67,56) Value=0.2293	Center(116,84) Value=0.2288	Center(116,84) Value=0.2255

















		Diameter (pixels)							
		38	40	42	44	46	48	50	52
SAD	NCC								
		Center(20,76) Value=28397	Center(21,75) Value=33277	Center(22,74) Value=39100	Center(23,73) Value=46281	Center(24,72) Value=53993	Center(25,71) Value=62063	Center(26,70) Value=70784	Center(27,69) Value=80034
SAD	NCC								
		Center(62,23) Value=0.3828	Center(62,24) Value=0.3609	Center(65,25) Value=0.3877	Center(43,67) Value=0.9729	Center(42,66) Value=0.3776	Center(41,65) Value=0.3707	Center(40,65) Value=0.3366	Center(53,46) Value=0.3303







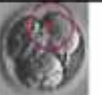







		Diameter (pixels)							
		38	40	42	44	46	48	50	52
SAD	NCC								
		Center(26,76) Value=48112	Center(21,75) Value=55544	Center(22,74) Value=64197	Center(23,73) Value=73600	Center(24,72) Value=83359	Center(25,50) Value=92914	Center(26,49) Value=100443	Center(27,49) Value=109657
SAD	NCC								
		Center(73,38) Value=0.3461	Center(36,34) Value=0.3158	Center(34,33) Value=0.3888	Center(34,33) Value=0.4139	Center(66,70) Value=0.3755	Center(66,69) Value=0.3113	Center(37,36) Value=0.2707	Center(36,37) Value=0.2296

















		Diameter (pixels)							
		38	40	42	44	46	48	50	52
SAD	NCC								
		Center(20,66) Value=32927	Center(21,66) Value=36099	Center(22,67) Value=40317	Center(23,66) Value=45341	Center(24,66) Value=50695	Center(25,70) Value=56444	Center(26,70) Value=61820	Center(27,69) Value=68159
SAD	NCC								
		Center(67,29) Value=0.3849	Center(29,38) Value=0.3838	Center(30,38) Value=0.4299	Center(29,39) Value=0.3917	Center(56,65) Value=0.3360	Center(56,65) Value=0.3405	Center(55,64) Value=0.2715	Center(26,30) Value=0.2968



		Diameter (pixels)							
		38	40	42	44	46	48	50	52
SAD	NCC								
		Center(76,20) Value=28672	Center(75,26) Value=32464	Center(74,27) Value=35828	Center(73,26) Value=39304	Center(72,26) Value=43083	Center(71,25) Value=47075	Center(70,26) Value=52119	Center(69,26) Value=56489
SAD	NCC								
		Center(31,38) Value=0.3422	Center(73,38) Value=0.3093	Center(32,44) Value=0.3093	Center(33,44) Value=0.3649	Center(33,43) Value=0.3485	Center(33,42) Value=0.2977	Center(35,41) Value=0.269	Center(37,40) Value=0.2984



		Diameter (pixels)						
		36	38	40	42	44	46	48
SAD								
		Center(19,77) Value=35679	Center(20,76) Value=40991	Center(21,75) Value=46518	Center(22,74) Value=51958	Center(23,57) Value=58307	Center(24,57) Value=64258	Center(25,56) Value=71888
NCC								
		Center(28,36) Value=0.35585	Center(50,70) Value=0.33418	Center(64,61) Value=0.39414	Center(83,61) Value=0.3888	Center(82,61) Value=0.3333	Center(82,69) Value=0.3502	Center(82,57) Value=0.3533



		Diameter (pixels)							
		37	39	41	43	45	47	49	51
SAD									
		Center(20,77) Value=29983	Center(21,76) Value=36566	Center(22,75) Value=43899	Center(23,74) Value=52342	Center(24,73) Value=61279	Center(25,72) Value=69943	Center(26,71) Value=78935	Center(27,70) Value=88069
NCC									
		Center(38,26) Value=0.3428	Center(37,29) Value=0.3407	Center(37,30) Value=0.2998	Center(78,78) Value=0.2826	Center(79,78) Value=0.2905	Center(14,15) Value=0.2803	Center(41,32) Value=0.2099	Center(37,46) Value=0.2080



		Diameter (pixels)						
		36	38	40	42	44	46	48
SAD								
		Center(19,77) Value=25018	Center(20,76) Value=30464	Center(21,75) Value=36536	Center(22,74) Value=43669	Center(23,57) Value=49971	Center(24,57) Value=54776	Center(25,56) Value=60634
NCC								
		Center(70,55) Value=0.4425	Center(70,54) Value=0.4409	Center(70,53) Value=0.3549	Center(70,38) Value=0.3045	Center(67,35) Value=0.3113	Center(66,36) Value=0.3309	Center(66,36) Value=0.3294



		Diameter (pixels)							
		38	40	42	44	46	48	50	52
SAD									
		Center(20,76) Value=38000	Center(21,75) Value=43956	Center(22,74) Value=49234	Center(23,73) Value=56188	Center(24,72) Value=63112	Center(25,71) Value=71807	Center(26,66) Value=78294	Center(27,67) Value=84411
NCC									
		Center(94,80) Value=0.3860	Center(63,61) Value=0.3747	Center(61,62) Value=0.33673	Center(66,64) Value=0.3532	Center(66,64) Value=0.3814	Center(48,65) Value=0.3220	Center(48,65) Value=0.2981	Center(50,64) Value=0.2823



		Diameter (pixels)							
		38	40	42	44	46	48	50	52
SAD		Center(76,20) Value=45351	Center(75,21) Value=50749	Center(74,22) Value=57019	Center(73,23) Value=64409	Center(72,24) Value=72616	Center(71,25) Value=81215	Center(70,26) Value=89703	Center(69,27) Value=96118
		Center(38,66) Value=0.3094	Center(47,75) Value=0.3101	Center(42,67) Value=0.2965	Center(43,67) Value=0.3210	Center(42,68) Value=0.3200	Center(39,69) Value=0.2793	Center(38,69) Value=0.2901	Center(38,69) Value=0.2363



		Diameter (pixels)						
		36	38	40	42	44	46	48
SAD		Center(19,19) Value=21123	Center(20,20) Value=25649	Center(21,21) Value=29702	Center(22,22) Value=34059	Center(23,23) Value=39117	Center(24,24) Value=45764	Center(25,25) Value=52775
		Center(67,66) Value=0.41279	Center(66,64) Value=0.40192	Center(61,64) Value=0.3624	Center(65,62) Value=0.3114	Center(49,61) Value=0.29606	Center(60,61) Value=0.29257	Center(60,63) Value=0.28151



		Diameter (pixels)							
		38	40	42	44	46	48	50	52
SAD		Center(22,76) Value=34403	Center(24,75) Value=39519	Center(23,74) Value=44143	Center(27,73) Value=48773	Center(27,72) Value=53736	Center(27,71) Value=58980	Center(29,66) Value=64267	Center(29,67) Value=69490
		Center(62,66) Value=0.37923	Center(62,66) Value=0.32862	Center(69,67) Value=0.30003	Center(60,65) Value=0.28727	Center(38,60) Value=0.2464	Center(68,47) Value=0.2361	Center(65,63) Value=0.24266	Center(65,61) Value=0.2465



		Diameter (pixels)							
		37	39	41	43	45	47	49	51
SAD		Center(20,20) Value=23506	Center(21,21) Value=26147	Center(22,22) Value=34038	Center(23,23) Value=41391	Center(24,24) Value=49304	Center(25,25) Value=56605	Center(26,26) Value=64170	Center(27,27) Value=71755
		Center(64,46) Value=0.3651	Center(61,60) Value=0.3336	Center(34,40) Value=0.3469	Center(34,39) Value=0.3891	Center(60,79) Value=0.2865	Center(61,68) Value=0.2633	Center(78,79) Value=0.2523	Center(78,79) Value=0.2468



		Diameter (pixels)						
		34	36	38	40	42	44	46
SAD		Center(18,18) Value=21270	Center(19,19) Value=25726	Center(20,20) Value=29741	Center(21,21) Value=33858	Center(22,22) Value=38994	Center(23,23) Value=45197	Center(24,24) Value=52195
		Center(33,50) Value=0.3768	Center(47,26) Value=0.3391	Center(54,67) Value=0.4315	Center(54,66) Value=0.4506	Center(53,66) Value=0.3845	Center(17,80) Value=0.2852	Center(16,80) Value=0.2689


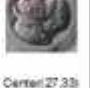
		Diameter (pixels)						
		36	38	40	42	44	46	48
SAD		Center(19,19) Value=15682	Center(20,20) Value=18544	Center(21,21) Value=21589	Center(22,22) Value=25577	Center(23,23) Value=30998	Center(24,24) Value=36713	Center(25,25) Value=43102
		Center(62,67) Value=0.4465	Center(63,66) Value=0.4097	Center(63,65) Value=0.3464	Center(64,63) Value=0.2961	Center(64,62) Value=0.3362	Center(63,61) Value=0.3591	Center(62,60) Value=0.3248

		Diameter (pixels)							
		38	40	42	44	46	48	50	52
SAD		Center(76,20) Value=43317	Center(21,75) Value=50091	Center(22,74) Value=56336	Center(23,73) Value=62677	Center(24,72) Value=69033	Center(25,71) Value=76635	Center(26,70) Value=85798	Center(27,61) Value=96332
		Center(24,37) Value=0.3161	Center(29,31) Value=0.3162	Center(29,33) Value=0.3364	Center(29,34) Value=0.3754	Center(29,35) Value=0.3894	Center(30,35) Value=0.3128	Center(74,75) Value=0.2062	Center(74,76) Value=0.200

		Diameter (pixels)							
		38	40	42	44	46	48	50	52
SAD		Center(76,20) Value=32875	Center(75,21) Value=39204	Center(74,22) Value=45638	Center(73,23) Value=53511	Center(72,24) Value=61248	Center(71,25) Value=68779	Center(70,26) Value=76801	Center(69,27) Value=84347
		Center(48,71) Value=0.2778	Center(46,21) Value=0.2696	Center(79,14) Value=0.2475	Center(79,13) Value=0.2437	Center(79,15) Value=0.2367	Center(78,15) Value=0.2185	Center(18,77) Value=0.2084	Center(18,78) Value=0.2112

		Diameter (pixels)							
		38	40	42	44	46	48	50	52
SAD		Center(70,20) Value=37305	Center(63,21) Value=42152	Center(64,22) Value=48654	Center(73,23) Value=55740	Center(65,24) Value=65410	Center(61,25) Value=73441	Center(59,26) Value=81217	Center(55,27) Value=90527
		Center(31,30) Value=0.3135	Center(31,30) Value=0.3910	Center(30,30) Value=0.3678	Center(28,37) Value=0.2904	Center(29,36) Value=0.3144	Center(30,36) Value=0.2877	Center(76,79) Value=0.2464	Center(77,80) Value=0.2290

		Diameter (pixels)						
		36	38	40	42	44	46	48
SAD		Center(77,19) Value=29707	Center(76,20) Value=34453	Center(75,21) Value=40297	Center(74,22) Value=46099	Center(73,23) Value=51752	Center(72,24) Value=59249	Center(71,25) Value=67591
		Center(41,27) Value=0.3450	Center(61,66) Value=0.3424	Center(30,56) Value=0.3243	Center(31,56) Value=0.3610	Center(31,57) Value=0.3579	Center(32,57) Value=0.2898	Center(63,66) Value=0.3093

		Diameter (pixels)						
		36	38	40	42	44	46	48
SAD		Center(77,19) Value=27651	Center(76,20) Value=31278	Center(75,21) Value=35938	Center(74,22) Value=42998	Center(73,23) Value=51274	Center(72,24) Value=59699	Center(71,25) Value=68390
		Center(27,33) Value=0.3478	Center(28,32) Value=0.3443	Center(31,80) Value=0.3195	Center(31,81) Value=0.3198	Center(35,81) Value=0.3089	Center(36,34) Value=0.3134	Center(36,32) Value=0.2651

		Diameter (pixels)							
		37	39	41	43	45	47	49	51
SAD		Center(20,29) Value=47401	Center(26,21) Value=55560	Center(22,24) Value=52110	Center(23,23) Value=57937	Center(24,24) Value=76137	Center(25,25) Value=53288	Center(26,26) Value=59936	Center(27,27) Value=99358
		Center(26,34) Value=0.3405	Center(49,37) Value=0.3536	Center(49,38) Value=0.3594	Center(49,39) Value=0.3766	Center(48,40) Value=0.3320	Center(47,41) Value=0.2800	Center(46,78) Value=0.2485	Center(46,78) Value=0.2317

		Diameter (pixels)						
		36	38	40	42	44	46	48
SAD		Center(19,77) Value=39486	Center(76,20) Value=45713	Center(75,21) Value=52746	Center(22,74) Value=58992	Center(23,73) Value=67695	Center(24,70) Value=74931	Center(25,71) Value=82744
		Center(52,25) Value=0.4021	Center(53,26) Value=0.4040	Center(58,27) Value=0.3885	Center(59,28) Value=0.3457	Center(59,29) Value=0.3260	Center(59,30) Value=0.2918	Center(43,46) Value=0.2340

		Diameter (pixels)							
		37	39	41	43	45	47	49	51
SAD		Center(20,77) Value=37375	Center(21,76) Value=44321	Center(22,75) Value=50753	Center(23,74) Value=56612	Center(24,73) Value=63257	Center(25,72) Value=70136	Center(26,71) Value=77063	Center(27,70) Value=84550
		Center(28,40) Value=0.3324	Center(22,40) Value=0.3670	Center(22,41) Value=0.3814	Center(24,42) Value=0.3550	Center(26,52) Value=0.3328	Center(26,28) Value=0.3710	Center(29,28) Value=0.4138	Center(26,29) Value=0.3202

		Diameter (pixels)						
		36	38	40	42	44	46	48
SAD		Center(19,77) Value=71025	Center(33,32) Value=80056	Center(34,32) Value=87549	Center(35,32) Value=97147	Center(36,33) Value=100426	Center(24,26) Value=119053	Center(25,25) Value=128467
		Center(30,31) Value=0.2880	Center(32,31) Value=0.2840	Center(41,40) Value=0.3124	Center(41,41) Value=0.3037	Center(41,42) Value=0.3629	Center(41,43) Value=0.3086	Center(43,70) Value=0.2722

		Diameter (pixels)							
		38	40	42	44	46	48	50	52
SAD		Center(20,76) Value=43756	Center(21,75) Value=49844	Center(22,74) Value=56685	Center(23,73) Value=64545	Center(24,72) Value=71584	Center(25,71) Value=79717	Center(26,70) Value=88536	Center(27,69) Value=97554
		Center(66,40) Value=0.4674	Center(66,47) Value=0.4017	Center(67,46) Value=0.4440	Center(66,45) Value=0.4120	Center(66,46) Value=0.3824	Center(33,64) Value=0.3941	Center(32,63) Value=0.3731	Center(31,62) Value=0.3361

		Diameter (pixels)							
		37	39	41	43	45	47	49	51
SAD		Center(20,77) Value=56257	Center(21,76) Value=63571	Center(23,29) Value=70536	Center(23,29) Value=78538	Center(24,27) Value=86023	Center(25,72) Value=96326	Center(26,71) Value=106270	Center(70,65) Value=117557
		Center(27,54) Value=0.3406	Center(26,55) Value=0.3380	Center(24,54) Value=0.3299	Center(24,53) Value=0.3244	Center(31,33) Value=0.3361	Center(30,33) Value=0.3112	Center(33,37) Value=0.3200	Center(32,37) Value=0.3423

		Diameter (pixels)							
		37	39	41	43	45	47	49	
SAD									
		Center(20,76) Value=50658	Center(21,76) Value=56206	Center(22,75) Value=62721	Center(23,74) Value=70194	Center(24,73) Value=78633	Center(25,72) Value=88574	Center(26,51) Value=98027	Center(27,51) Value=107480
NCC									
		Center(38,26) Value=0.2994	Center(37,26) Value=0.3701	Center(38,26) Value=0.3140	Center(32,56) Value=0.2094	Center(62,56) Value=0.2882	Center(76,75) Value=0.2608	Center(77,75) Value=0.2755	Center(77,75) Value=0.2755

		Diameter (pixels)							
		38	40	42	44	46	48	50	52
SAD									
		Center(20,76) Value=47294	Center(21,75) Value=54183	Center(22,74) Value=63392	Center(23,73) Value=74363	Center(24,72) Value=85066	Center(25,71) Value=95393	Center(26,70) Value=104593	Center(27,69) Value=112788
NCC									
		Center(46,70) Value=0.3921	Center(46,69) Value=0.3542	Center(71,51) Value=0.3295	Center(46,69) Value=0.3232	Center(44,69) Value=0.3320	Center(56,48) Value=0.2895	Center(55,47) Value=0.3177	Center(66,47) Value=0.3333

APPENDIX D

This Appendix contains the results of the proposed technique in Chapter 6. These results are the results of applying the correlation technique and getting the values all the maximum correlation cooeffient. The two techniques used were the SAD and the NCC.

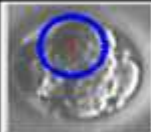
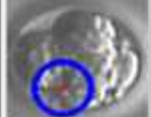
Image	X-center	Y-Center	Radius	Value
	33	44	22	0.354921
	71	38	19	0.329482

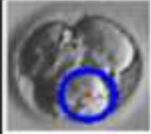
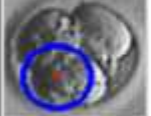
Image	X-center	Y-Center	Radius	Value
	70	55	18	0.442541
	66	36	23	0.330885

Image	X-center	Y-Center	Radius	Value
	34	33	22	0.413863
	57	71	22	0.402032
	73	38	19	0.346072
	13	74	26	0.227973
	79	115	26	0.222523

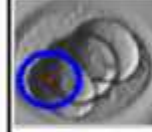
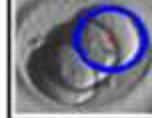

Image	X-center	Y-Center	Radius	Value
	62	24	20	0.390889
	42	66	23	0.377606
	53	46	26	0.330337




Image	X-center	Y-Center	Radius	Value
	64	60	19	0.39798
	56	64	23	0.381392
	48	66	24	0.322032

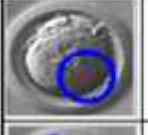
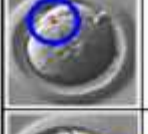

Image	X-center	Y-Center	Radius	Value
	64	61	20	0.394139
	28	35	18	0.355851
	50	70	19	0.334177

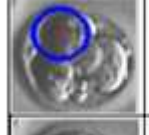
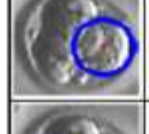
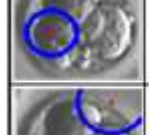
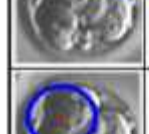
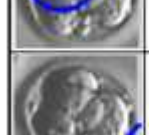

Image	X-center	Y-Center	Radius	Value
	30	38	21	0.429876
	56	70	23	0.375475
	57	29	19	0.364933
	13	74	26	0.227973
	39	36	26	0.227331
	79	115	26	0.222523

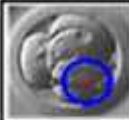

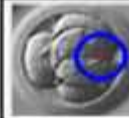


Image	X-center	Y-Center	Radius	Value
	66	62	18	0.328361
	38	25	18	0.314159
	45	70	19	0.302979
	115	84	24	0.228833
	86	115	24	0.227721

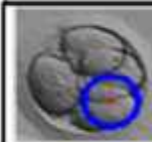
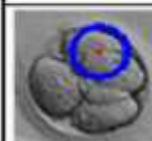
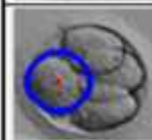
Image	X-center	Y-Center	Radius	Value
	67	65	18	0.412786
	30	57	18	0.409033
	53	30	21	0.3062


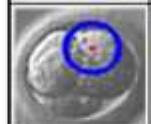
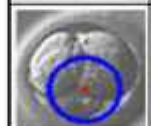

Image	X-center	Y-Center	Radius	Value
	64	65	19	0.379231
	32	58	20	0.315956
	65	51	26	0.246596
	48	26	23	0.234233



Image	X-center	Y-Center	Radius	Value
	52	67	18	0.446514
	68	42	21	0.288909


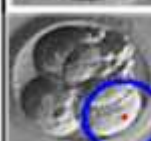
Image	X-center	Y-Center	Radius	Value
	29	35	23	0.389448
	74	75	25	0.268223



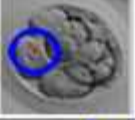

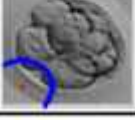
Image	X-center	Y-Center	Radius	Value
	54	66	20	0.450606
	33	50	17	0.376793
	46	26	17	0.370397
	17	80	22	0.285191
	82	15	22	0.278385


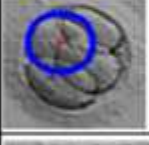

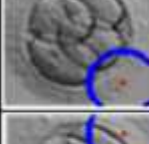
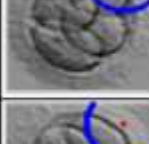
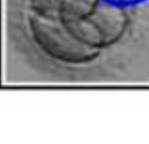
Image	X-center	Y-Center	Radius	Value
	64	46	18.5	0.362094
	34	39	21.5	0.359093
	51	59	20.5	0.33573
	80	79	22.5	0.286547
	15	77	23.5	0.251179
	15	77	24.5	0.239728

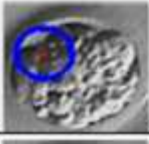
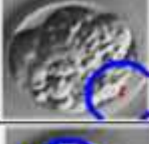
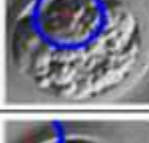
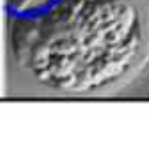
Image	X-center	Y-Center	Radius	Value
	38	27	18.5	0.342804
	79	79	22.5	0.283308
	33	42	22.5	0.271569
	15	15	22.5	0.270573

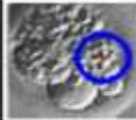
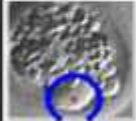


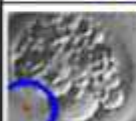
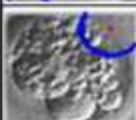

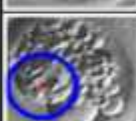
Image	X-center	Y-Center	Radius	Value
	48	71	19	0.277643
	81	52	19	0.269937
	46	21	20	0.269638
	81	83	19	0.266343
	79	14	21	0.24751
	12	78	22	0.237794
	20	77	26	0.209204
	56	26	25	0.205043

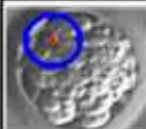

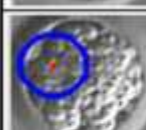
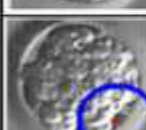
Image	X-center	Y-Center	Radius	Value
	25	32	18.5	0.313413
	55	28	21.5	0.274685
	37	29	22.5	0.25139
	75	74	25.5	0.228596

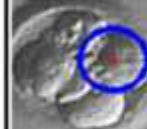
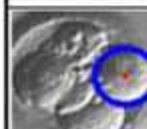

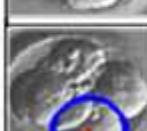
Image	X-center	Y-Center	Radius	Value
	43	67	22	0.321048
	47	75	20	0.310101
	34	24	24	0.266318
	74	53	24	0.264786



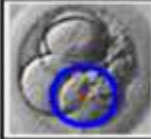
Image	X-center	Y-Center	Radius	Value
	59	28	24.5	0.413668
	22	41	20.5	0.361428
	69	50	21.5	0.33762

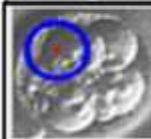
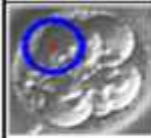
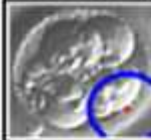
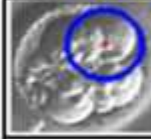
Image	X-center	Y-Center	Radius	Value
	31	30	20	0.391007
	31	30	19	0.313522
	76	79	25	0.246473
	33	63	25	0.242337



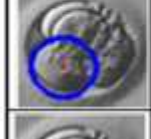
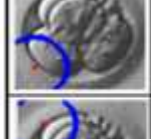

Image	X-center	Y-Center	Radius	Value
	58	26	19	0.404093
	43	49	24	0.234051
	65	34	24	0.229974
	77	15	24	0.228643
	19	19	24	0.22493

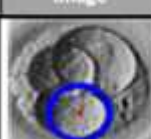
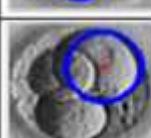
Image	X-center	Y-Center	Radius	Value
	68	47	20	0.461771
	32	63	25	0.373118



Image	X-center	Y-Center	Radius	Value
	62	37	25.5	0.342327
	27	54	18.5	0.340659






Image	X-center	Y-Center	Radius	Value
	59	28	24.5	0.413668
	49	38	20.5	0.393411
	26	34	18.5	0.340917
	16	78	24.5	0.249522
	16	78	25.5	0.231705



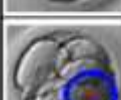


Image	X-center	Y-Center	Radius	Value
	31	56	21	0.361078
	41	27	18	0.345081
	61	66	19	0.342483
	53	65	24	0.309341
	43	49	24	0.234051



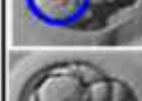
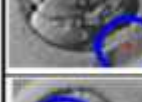


Image	X-center	Y-Center	Radius	Value
	27	33	18	0.34789
	60	31	19	0.339727
	81	81	21	0.319831
	39	34	23	0.312405
	31	42	25	0.311495
	44	63	24	0.280774

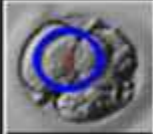

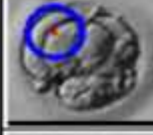

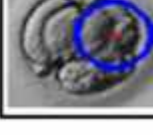
Image	X-center	Y-Center	Radius	Value
	41	41	21	0.363719
	58	29	25.5	0.320203
	30	31	18	0.288015
	68	48	18	0.285521
	43	70	24	0.272268

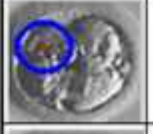
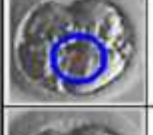
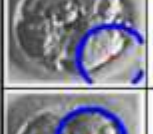
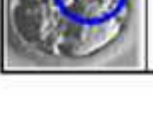

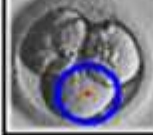
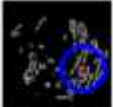
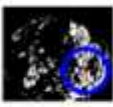
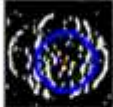
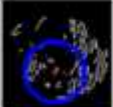
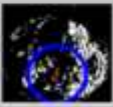
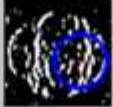
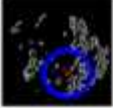
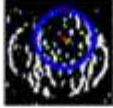
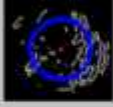

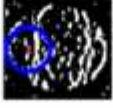
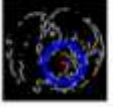
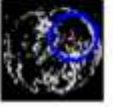

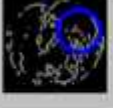
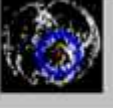

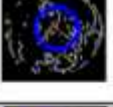
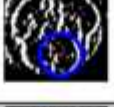
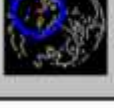

Image	X-center	Y-Center	Radius	Value
	37	26	19.5	0.370175
	61	50	18.5	0.292335
	77	75	24.5	0.275545
	37	62	24.5	0.268962

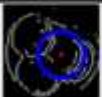
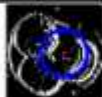

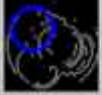
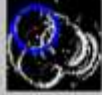

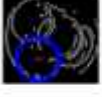
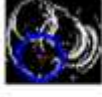

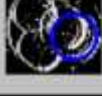

Image	X-center	Y-Center	Radius	Value
	49	70	19	0.392182
	72	52	20	0.342856

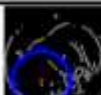
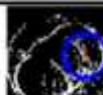

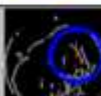
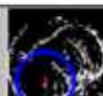

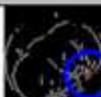
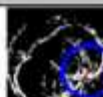

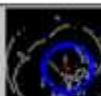
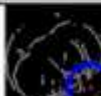
APPENDIX E

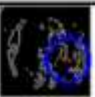
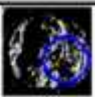

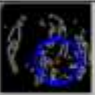
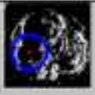

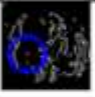





This Appendix contains the results of the proposed technique in Chapter 7. These results are the results of applying the template matching using the binary template. The technique worked on binary image that were produced by extracting their edges using either Sobel, new algorithm or the convolution mask approach without using the median filter.




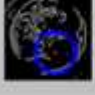













Sobel edge detection		New algorithm edge detection		Convolution edge detection	
Image	Results	Image	Results	Image	Results
	x_centre=60 y_centre=71 radius=19 value=21.1%		x_centre=58 y_centre=72 radius=19 value=51.6%		x_centre=55 y_centre=53 radius=25 value=45.1%
	x_centre=63 y_centre=46 radius=26 value=17.4%		x_centre=62 y_centre=48 radius=25 value=38.8%		x_centre=56 y_centre=67 radius=23 value=44.9%
	x_centre=67 y_centre=57 radius=20 value=16.8%				x_centre=37 y_centre=52 radius=25 value=44.5%
	x_centre=50 y_centre=50 radius=26 value=16.3%				x_centre=68 y_centre=49 radius=22 value=42.9%
					x_centre=52 y_centre=22 radius=19 value=42.2%


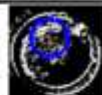



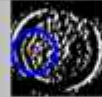












Sobel edge detection		New algorithm edge detection		Convolution edge detection	
Image	Results	Image	Results	Image	Results
	x_centre=61 y_centre=56 radius=18 value=25.4%		x_centre=37 y_centre=67 radius=21 value=45.5%		x_centre=38 y_centre=69 radius=19 value=63.3%
	x_centre=39 y_centre=70 radius=19 value=21.6%		x_centre=60 y_centre=55 radius=18 value=45.5%		x_centre=39 y_centre=32 radius=22 value=51.4%
	x_centre=47 y_centre=51 radius=19 value=20%				x_centre=71 y_centre=52 radius=19 value=47.2%
	x_centre=37 y_centre=32 radius=22 value=16.1%				x_centre=55 y_centre=41 radius=24 value=43.8%

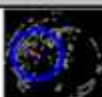
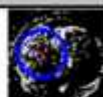

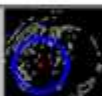


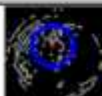

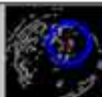




Sobel edge detection		New algorithm edge detection		Convolution edge detection	
Image	Results	Image	Results	Image	Results
	x_centre=51 y_centre=58 radius=23 value=26.8%		x_centre=60 y_centre=57 radius=23 value=55.2%		x_centre=35 y_centre=31 radius=22 value=68.1%
	x_centre=33 y_centre=29 radius=21 value=26.7%		x_centre=33 y_centre=29 radius=22 value=48.3%		x_centre=70 y_centre=36 radius=22 value=55.7%
	x_centre=71 y_centre=36 radius=21 value=21.8%		x_centre=69 y_centre=36 radius=22 value=44.2%		x_centre=61 y_centre=57 radius=22 value=55.7%
			x_centre=68 y_centre=68 radius=22 value=44.2%		x_centre=67 y_centre=68 radius=23 value=55.2%

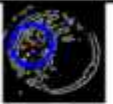
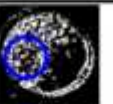



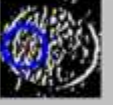
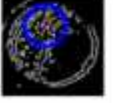
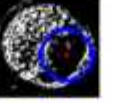

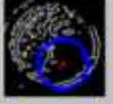

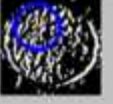
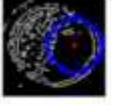
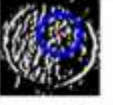


Sobel edge detection		New algorithm edge detection		Convolution edge detection	
Image	Results	Image	Results	Image	Results
	x_centre=65 y_centre=33 radius=25 value=19.8%		x_centre=44 y_centre=69 radius=19 value=42.5%		x_centre=53 y_centre=44 radius=26 value=49.7%
	x_centre=42 y_centre=64 radius=23 value=18.1%		x_centre=64 y_centre=33 radius=25 value=39.4%		x_centre=64 y_centre=29 radius=21 value=47.9%
	x_centre=62 y_centre=74 radius=20 value=17.1%		x_centre=57 y_centre=72 radius=23 value=32.5%		x_centre=39 y_centre=60 radius=24 value=41%
	x_centre=54 y_centre=55 radius=21 value=14.5%				
	x_centre=73 y_centre=75 radius=20 value=14.1%				

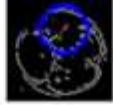
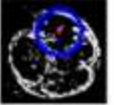
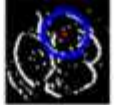
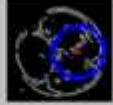
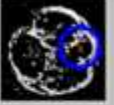
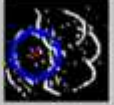
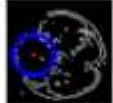
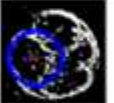
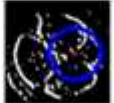
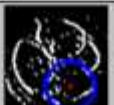
Sobel edge detection		New algorithm edge detection		Convolution edge detection	
Image	Results	Image	Results	Image	Results
	x_centre=57 y_centre=72 radius=23 value=22.4%		x_centre=57 y_centre=68 radius=24 value=48%		x_centre=61 y_centre=68 radius=22 value=48.7%
	x_centre=62 y_centre=61 radius=23 value=19.4%		x_centre=55 y_centre=28 radius=19 value=35.1%		x_centre=55 y_centre=35 radius=22 value=47.1%
	x_centre=57 y_centre=28 radius=19 value=19.4%				x_centre=70 y_centre=28 radius=22 value=45.1%
	x_centre=37 y_centre=71 radius=19 value=17.2%				x_centre=32 y_centre=41 radius=21 value=44.2%
					x_centre=33 y_centre=28 radius=24 value=40.1%
					x_centre=48 y_centre=53 radius=29 value=38.3%




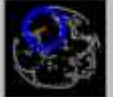

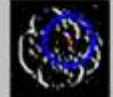
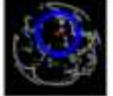
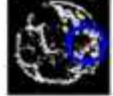
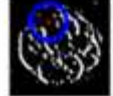
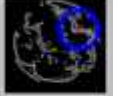


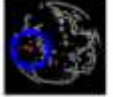

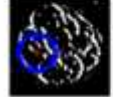
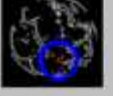
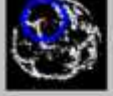
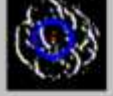
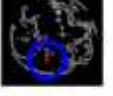
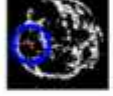

Sobel edge detection		New algorithm edge detection		Convolution edge detection	
Image	Results	Image	Results	Image	Results
	x_centre=56 y_centre=27 radius=18 value=27.9%		x_centre=66 y_centre=55 radius=22 value=57%		x_centre=34 y_centre=28 radius=18 value=52.3%
	x_centre=66 y_centre=56 radius=22 value=27%		x_centre=41 y_centre=27 radius=19 value=56.6%		x_centre=41 y_centre=51 radius=18 value=48.4%
	x_centre=38 y_centre=50 radius=19 value=26.1%		x_centre=56 y_centre=27 radius=18 value=56.2%		x_centre=47 y_centre=25 radius=19 value=48.3%
	x_centre=42 y_centre=27 radius=20 value=25.4%		x_centre=38 y_centre=48 radius=18 value=52.5%		x_centre=59 y_centre=30 radius=20 value=47.2%
	x_centre=27 y_centre=46 radius=21 value=22.9%		x_centre=27 y_centre=47 radius=21 value=43.2%		x_centre=49 y_centre=73 radius=19 value=44.4%
	x_centre=56 y_centre=27 radius=20 value=22.4%				x_centre=66 y_centre=63 radius=19 value=42.2%

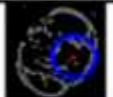
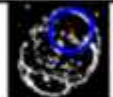
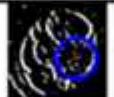

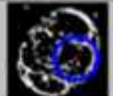
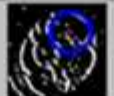
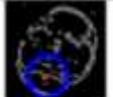
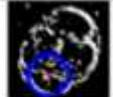
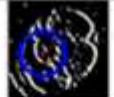
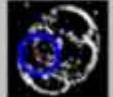

Sobel edge detection		New algorithm edge detection		Convolution edge detection	
Image	Results	Image	Results	Image	Results
	x_centre=50 y_centre=33 radius=20 value=23.7%		x_centre=33 y_centre=40 radius=18 value=49.4%		x_centre=37 y_centre=27 radius=21 value=48.1%
	x_centre=31 y_centre=62 radius=16 value=22.7%		x_centre=30 y_centre=61 radius=16 value=46.2%		x_centre=52 y_centre=24 radius=21 value=44.6%
	x_centre=27 y_centre=34 radius=18 value=20.7%		x_centre=50 y_centre=33 radius=21 value=47.1%		x_centre=56 y_centre=37 radius=23 value=43.1%
	x_centre=51 y_centre=67 radius=24 value=17.6%		x_centre=45 y_centre=70 radius=20 value=37.7%		x_centre=43 y_centre=72 radius=19 value=42.7%
	x_centre=66 y_centre=50 radius=24 value=16.3%		x_centre=63 y_centre=54 radius=23 value=33.7%		x_centre=38 y_centre=43 radius=19 value=42.2%
					x_centre=65 y_centre=65 radius=21 value=40.2%
					x_centre=31 y_centre=54 radius=18 value=40.2%
					x_centre=65 y_centre=65 radius=22 value=38.1%

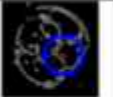
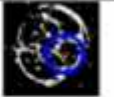




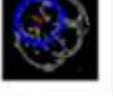





Sobel edge detection		New algorithm edge detection		Convolution edge detection	
Image	Results	Image	Results	Image	Results
	x_centre=43 y_centre=32 radius=22 value=22.7%		x_centre=42 y_centre=32 radius=22 value=50%		x_centre=43 y_centre=21 radius=19 value=54.4%
	x_centre=54 y_centre=35 radius=25 value=20%		x_centre=54 y_centre=36 radius=26 value=38.7%		x_centre=50 y_centre=38 radius=19 value=47.2%
	x_centre=38 y_centre=45 radius=18 value=18%				x_centre=51 y_centre=75 radius=22 value=46.1%
	x_centre=36 y_centre=61 radius=19 value=16.3%				x_centre=37 y_centre=63 radius=19 value=45.5%
					x_centre=54 y_centre=26 radius=20 value=44.1%
					x_centre=62 y_centre=70 radius=20 value=43.3%
					x_centre=39 y_centre=36 radius=25 value=40.7%

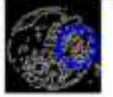


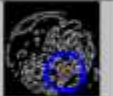


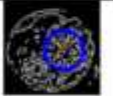


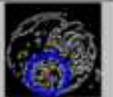


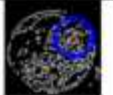


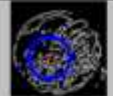


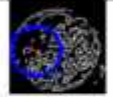
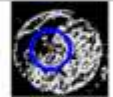


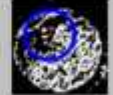


Sobel edge detection		New algorithm edge detection		Convolution edge detection	
Image	Results	Image	Results	Image	Results
	x_centre=41 y_centre=27 radius=19 value=30%		x_centre=50 y_centre=27 radius=19 value=60.6%		x_centre=58 y_centre=67 radius=23 value=52.7%
	x_centre=52 y_centre=28 radius=19 value=28%		x_centre=34 y_centre=33 radius=19 value=54.4%		x_centre=48 y_centre=24 radius=19 value=49.7%
	x_centre=30 y_centre=41 radius=19 value=26.3%		x_centre=56 y_centre=65 radius=24 value=43.2%		x_centre=50 y_centre=36 radius=23 value=48%
	x_centre=65 y_centre=56 radius=23 value=22.9%		x_centre=36 y_centre=44 radius=26 value=39.8%		x_centre=32 y_centre=35 radius=21 value=46.8%
	x_centre=48 y_centre=67 radius=25 value=21.3%				x_centre=38 y_centre=67 radius=19 value=43.8%
					x_centre=66 y_centre=56 radius=22 value=42%
					x_centre=46 y_centre=71 radius=21 value=41.4%


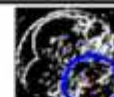
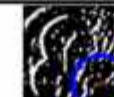
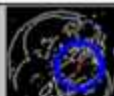
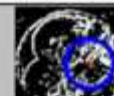

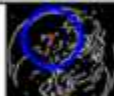
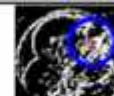


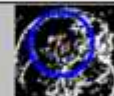

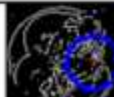
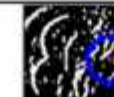
Sobel edge detection		New algorithm edge detection		Convolution edge detection	
Image	Results	Image	Results	Image	Results
	x_centre=31 y_centre=52 radius=21 value=28.9%		x_centre=31 y_centre=53 radius=20 value=59%		x_centre=33 y_centre=54 radius=20 value=41.1%
	x_centre=51 y_centre=65 radius=22 value=20%		x_centre=47 y_centre=72 radius=18 value=41.7%		x_centre=53 y_centre=29 radius=21 value=40.1%
	x_centre=51 y_centre=25 radius=18 value=18.3%		x_centre=54 y_centre=32 radius=24 value=36%		x_centre=49 y_centre=63 radius=23 value=38.9%
					x_centre=73 y_centre=60 radius=22 value=31.4%

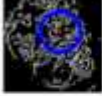


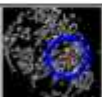

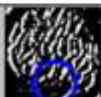
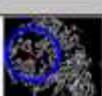


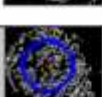



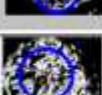
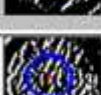
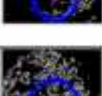
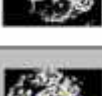
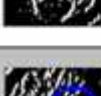




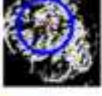



Sobel edge detection		New algorithm edge detection		Convolution edge detection	
Image	Results	Image	Results	Image	Results
	x_centre=63 y_centre=64 radius=22 value=21%		x_centre=39 y_centre=61 radius=20 value=41.9%		x_centre=65 y_centre=65 radius=20 value=44.6%
	x_centre=29 y_centre=38 radius=18 value=20.7%		x_centre=69 y_centre=63 radius=17 value=40.7%		x_centre=40 y_centre=58 radius=23 value=38%
	x_centre=37 y_centre=50 radius=19 value=20.5%		x_centre=48 y_centre=74 radius=17 value=40.7%		x_centre=26 y_centre=37 radius=17 value=36.8%
	x_centre=36 y_centre=70 radius=18 value=20.1%		x_centre=41 y_centre=63 radius=20 value=38.5%		x_centre=70 y_centre=48 radius=21 value=34.8%
	x_centre=63 y_centre=25 radius=17 value=19.4%		x_centre=63 y_centre=63 radius=23 value=38.3%		x_centre=66 y_centre=26 radius=17 value=33.7%
	x_centre=70 y_centre=64 radius=17 value=19.1%		x_centre=29 y_centre=38 radius=19 value=36.9%		x_centre=47 y_centre=44 radius=17 value=29.6%
	x_centre=71 y_centre=43 radius=17 value=17.1%		x_centre=63 y_centre=23 radius=17 value=36.6%		
			x_centre=64 y_centre=29 radius=17 value=34.3%		




Sobel edge detection		New algorithm edge detection		Convolution edge detection	
Image	Results	Image	Results	Image	Results
	x_centre=63 y_centre=65 radius=20 value=24.8%		x_centre=28 y_centre=60 radius=20 value=47.3%		x_centre=64 y_centre=65 radius=19 value=43%
	x_centre=28 y_centre=59 radius=22 value=22.9%		x_centre=54 y_centre=65 radius=20 value=46.7%		x_centre=28 y_centre=60 radius=19 value=37.2%
	x_centre=72 y_centre=40 radius=22 value=18.8%		x_centre=71 y_centre=38 radius=19 value=40%		x_centre=61 y_centre=33 radius=21 value=36.7%
			x_centre=62 y_centre=30 radius=18 value=35.5%		x_centre=67 y_centre=40 radius=22 value=34%

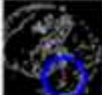


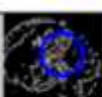


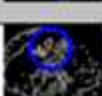


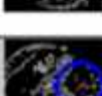


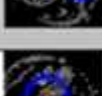

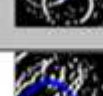
Sobel edge detection		New algorithm edge detection		Convolution edge detection	
Image	Results	Image	Results	Image	Results
	x_centre=64 y_centre=61 radius=18.5 value=26.4%		x_centre=64 y_centre=61 radius=18.5 value=48.5%		x_centre=36 y_centre=37 radius=21.5 value=43.2%
	x_centre=27 y_centre=61 radius=18.5 value=23.8%		x_centre=29 y_centre=59 radius=20.5 value=46%		x_centre=62 y_centre=58 radius=20.5 value=40.4%
	x_centre=37 y_centre=37 radius=22.5 value=23.4%		x_centre=67 y_centre=44 radius=18.5 value=41.5%		x_centre=68 y_centre=41 radius=24.5 value=37.5%
	x_centre=66 y_centre=44 radius=19.5 value=19.9%		x_centre=36 y_centre=38 radius=21.5 value=40.2%		x_centre=35 y_centre=66 radius=24.5 value=32.8%

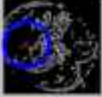

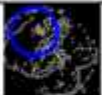
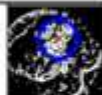
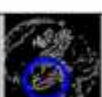

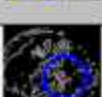
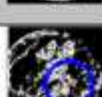

Sobel edge detection		New algorithm edge detection		Convolution edge detection	
Image	Results	Image	Results	Image	Results
	x_centre=50 y_centre=72 radius=18.5 value=35.4%		x_centre=56 y_centre=65 radius=18.5 value=70.3%		x_centre=40 y_centre=68 radius=19.5 value=49.1%
	x_centre=70 y_centre=61 radius=18.5 value=33.1%		x_centre=69 y_centre=60 radius=19.5 value=66.5%		x_centre=63 y_centre=45 radius=24.5 value=45.8%
	x_centre=51 y_centre=60 radius=19.5 value=32.5%		x_centre=71 y_centre=41 radius=18.5 value=65.5%		x_centre=60 y_centre=70 radius=18.5 value=46.5%
	x_centre=72 y_centre=43 radius=19.5 value=30.8%		x_centre=57 y_centre=64 radius=18.5 value=62.7%		x_centre=52 y_centre=28 radius=24.5 value=46.4%
	x_centre=38 y_centre=69 radius=18.5 value=29.3%		x_centre=41 y_centre=66 radius=20.5 value=61.1%		x_centre=38 y_centre=45 radius=21.5 value=46.2%
	x_centre=57 y_centre=39 radius=20.5 value=27.1%		x_centre=60 y_centre=39 radius=23.5 value=54.5%		x_centre=72 y_centre=43 radius=18.5 value=40.9%
	x_centre=53 y_centre=27 radius=24.5 value=26.2%		x_centre=49 y_centre=39 radius=19.5 value=54.2%		x_centre=67 y_centre=32 radius=18.5 value=40.4%
	x_centre=38 y_centre=40 radius=25.5 value=24.3%		x_centre=36 y_centre=38 radius=24.5 value=52.2%		x_centre=55 y_centre=68 radius=20.5 value=40.1%
					x_centre=37 y_centre=34 radius=20.5 value=36.7%

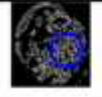





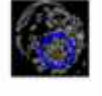



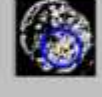




Sobel edge detection		New algorithm edge detection		Convolution edge detection	
Image	Results	Image	Results	Image	Results
	x_centre=66 y_centre=64 radius=23 value=30.7%		x_centre=66 y_centre=64 radius=23 value=69%		x_centre=65 y_centre=65 radius=23 value=57.3%
	x_centre=50 y_centre=61 radius=19 value=29.1%		x_centre=48 y_centre=62 radius=20 value=58%		x_centre=32 y_centre=38 radius=23 value=51.8%
	x_centre=30 y_centre=39 radius=24 value=25.9%		x_centre=31 y_centre=64 radius=19 value=48.8%		x_centre=62 y_centre=27 radius=20 value=47.8%
	x_centre=31 y_centre=64 radius=19 value=25%		x_centre=33 y_centre=40 radius=26 value=48.7%		x_centre=44 y_centre=59 radius=25 value=42.1%
	x_centre=51 y_centre=73 radius=22 value=23.6%				x_centre=46 y_centre=72 radius=19 value=37.7%

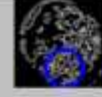


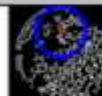





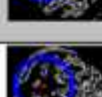
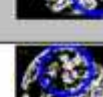

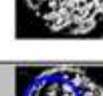



Sobel edge detection		New algorithm edge detection		Convolution edge detection	
Image	Results	Image	Results	Image	Results
	x_centre=39 y_centre=55 radius=19 value=32.7%		x_centre=47 y_centre=62 radius=19 value=56.9%		x_centre=48 y_centre=30 radius=25 value=50.4%
	x_centre=60 y_centre=63 radius=19 value=31.3%		x_centre=36 y_centre=53 radius=19 value=64.7%		x_centre=73 y_centre=49 radius=20 value=48.3%
	x_centre=36 y_centre=28 radius=25 value=30.6%		x_centre=48 y_centre=49 radius=24 value=62.6%		x_centre=33 y_centre=31 radius=25 value=46.8%
	x_centre=39 y_centre=42 radius=24 value=29.6%		x_centre=72 y_centre=50 radius=20 value=61.7%		x_centre=41 y_centre=58 radius=20 value=46.9%
	x_centre=72 y_centre=50 radius=20 value=28.8%		x_centre=37 y_centre=42 radius=25 value=60.3%		x_centre=39 y_centre=44 radius=21 value=43.7%
	x_centre=54 y_centre=50 radius=24 value=27.9%		x_centre=59 y_centre=62 radius=19 value=59.1%		x_centre=44 y_centre=67 radius=24 value=42.1%
	x_centre=47 y_centre=27 radius=22 value=27.2%		x_centre=37 y_centre=42 radius=26 value=59.1%		x_centre=66 y_centre=66 radius=20 value=41.7%
	x_centre=27 y_centre=59 radius=20 value=27%		x_centre=36 y_centre=30 radius=25 value=57.5%		x_centre=58 y_centre=43 radius=19 value=41.1%
			x_centre=47 y_centre=29 radius=25 value=56.9%		x_centre=58 y_centre=78 radius=20 value=39.8%

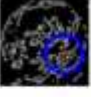


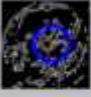


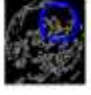


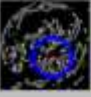


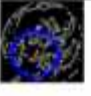
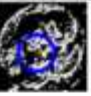

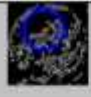





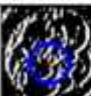

					x_centre=20 y_centre=54 radius=19 value=39.1%
					x_centre=22 y_centre=37 radius=21 value=38%
					x_centre=67 y_centre=66 radius=21 value=36.9%

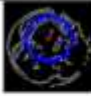









Sobel edge detection		New algorithm edge detection		Convolution edge detection	
Image	Results	Image	Results	Image	Results
	x_centre=75 y_centre=58 radius=19 Value=27. %		x_centre=74 y_centre=68 radius=19 value=52.2%		x_centre=46 y_centre=71 radius=23 value=50.9%
	x_centre=39 y_centre=56 radius=20 value=24.8%		x_centre=46 y_centre=72 radius=22 value=50.2%		x_centre=73 y_centre=62 radius=24 value=49.5%
	x_centre=25 y_centre=46 radius=19 value=24.7%		x_centre=22 y_centre=45 radius=19 value=50%		x_centre=48 y_centre=22 radius=22 value=49%
	x_centre=45 y_centre=72 radius=22 value=23.1%		x_centre=51 y_centre=34 radius=24 value=49.3%		x_centre=24 y_centre=45 radius=20 value=45.9%
	x_centre=44 y_centre=42 radius=19 value=23%		x_centre=46 y_centre=59 radius=19 value=46.3%		x_centre=53 y_centre=33 radius=24 value=44.7

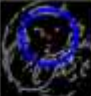
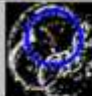




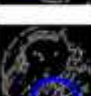


	x_centre=47 y_centre=23 radius=22 value=22.9%		x_centre=48 y_centre=21 radius=22 value=45.6%		
	x_centre=29 y_centre=30 radius=23 value=21.7%		x_centre=33 y_centre=60 radius=19 value=45%		
	x_centre=66 y_centre=41 radius=20 value=21.1%		x_centre=33 y_centre=27 radius=26 value=43.3%		
	x_centre=53 y_centre=61 radius=21 value=19.5%		x_centre=67 y_centre=60 radius=23 value=40.8%		
			x_centre=61 y_centre=46 radius=20 value=39.0%		

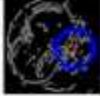
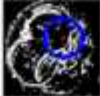
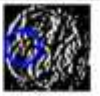
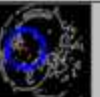
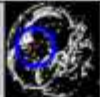

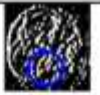




Sobel edge detection		New algorithm edge detection		Convolution edge detection	
Image	Results	Image	Results	Image	Results
	x_centre=54 y_centre=68 radius=18.5 value=34.1%		x_centre=65 y_centre=67 radius=18.5 value=67.1%		x_centre=48 y_centre=70 radius=20.5 value=47%
	x_centre=34 y_centre=64 radius=19.5 value=31.7%		x_centre=72 y_centre=69 radius=18.5 value=61.9%		x_centre=49 y_centre=34 radius=25.5 value=45.1%
	x_centre=64 y_centre=67 radius=19.5 value=31.4%		x_centre=34 y_centre=64 radius=19.5 value=60.3%		x_centre=70 y_centre=66 radius=20.5 value=44.4%
	x_centre=42 y_centre=49 radius=22.5 value=29%		x_centre=61 y_centre=65 radius=22.5 value=67.1%		x_centre=37 y_centre=34 radius=23.5 value=44.1%
	x_centre=53 y_centre=54 radius=25.5 value=28.3%		x_centre=41 y_centre=49 radius=22.5 value=65.9%		x_centre=33 y_centre=67 radius=19.5 value=42.9%

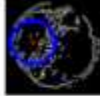
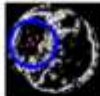

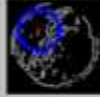


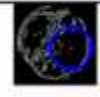



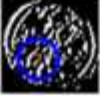

	x_centre=75 y_centre=62 radius=19.5 value=27.2%		x_centre=62 y_centre=44 radius=20.5 value=52.9%		x_centre=69 y_centre=74 radius=22.5 value=42.8%
	x_centre=24 y_centre=33 radius=22.5 value=28.1%		x_centre=49 y_centre=33 radius=25.5 value=51.6%		x_centre=56 y_centre=68 radius=25.5 value=42.5%
	x_centre=50 y_centre=33 radius=25.5 value=25.6%		x_centre=69 y_centre=72 radius=21.5 value=49.2%		x_centre=38 y_centre=50 radius=20.5 value=40.4%
	x_centre=37 y_centre=34 radius=25.5 value=23.7%		x_centre=23 y_centre=46 radius=22.5 value=48.4%		x_centre=69 y_centre=38 radius=18.5 value=40.1%
			x_centre=36 y_centre=3 radius=25.5 value=47.8%		x_centre=69 y_centre=74 radius=23.5 value=39.4%
					x_centre=24 y_centre=37 radius=18.5 value=39.2%
					x_centre=19 y_centre=20 radius=18.5 value=37.5%

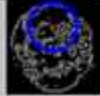



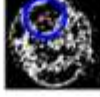
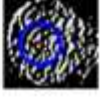
Sobel edge detection		New algorithm edge detection		Convolution edge detection	
Image	Results	Image	Results	Image	Results
	x_centre=61 y_centre=69 radius=20 value=30.2%		x_centre=58 y_centre=66 radius=24 value=62.6%		x_centre=27 y_centre=64 radius=22 value=51.9%
	x_centre=47 y_centre=64 radius=19 value=29.1%		x_centre=27 y_centre=64 radius=21 value=59.1%		x_centre=32 y_centre=42 radius=23 value=51.3%
	x_centre=27 y_centre=64 radius=21 value=27.6%		x_centre=49 y_centre=54 radius=20 value=57.2%		x_centre=70 y_centre=36 radius=24 value=50%
	x_centre=61 y_centre=66 radius=20 value=27.2%		x_centre=66 y_centre=39 radius=26 value=56.6%		x_centre=58 y_centre=68 radius=22 value=49.5%
	x_centre=63 y_centre=40 radius=26 value=27.1%		x_centre=54 y_centre=42 radius=19 value=56.6%		x_centre=54 y_centre=29 radius=24 value=48.2%
	x_centre=32 y_centre=43 radius=23 value=23.9%		x_centre=60 y_centre=54 radius=21 value=54.4%		x_centre=70 y_centre=36 radius=23 value=48.1%
			x_centre=49 y_centre=30 radius=21 value=52.8%		x_centre=36 y_centre=30 radius=21 value=44%
			x_centre=24 y_centre=42 radius=21 value=49.7%		x_centre=56 y_centre=47 radius=19 value=43.6%
					x_centre=76 y_centre=71 radius=19 value=39.7%

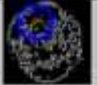
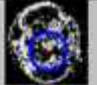







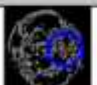









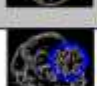


Sobel edge detection		New algorithm edge detection		Convolution edge detection	
Image	Results	Image	Results	Image	Results
	x_centre=40 y_centre=47 radius=23 value=29.3%		x_centre=40 y_centre=47 radius=23 value=55.5%		x_centre=43 y_centre=23 radius=19 value=59.7%
			x_centre=30 y_centre=36 radius=18 value=52.6%		x_centre=59 y_centre=24 radius=18 value=58.6%
			x_centre=60 y_centre=26 radius=18 value=46.1%		x_centre=39 y_centre=42 radius=21 value=53.1%
					x_centre=53 y_centre=58 radius=21 value=47.9%
					x_centre=38 y_centre=57 radius=20 value=45.4%
					x_centre=60 y_centre=47 radius=24 value=40.6%

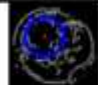









Sobel edge detection		New algorithm edge detection		Convolution edge detection	
Image	Results	Image	Results	Image	Results
	x_centre=36 y_centre=47 radius=25.5 value=27.5%		x_centre=36 y_centre=46 radius=25.5 value=57.8%		x_centre=60 y_centre=28 radius=24.5 value=55.3%
	x_centre=61 y_centre=31 radius=25.4 value=25.4%		x_centre=61 y_centre=30 radius=24.5 value=52.8%		x_centre=49 y_centre=56 radius=22.5 value=50.3%
	x_centre=73 y_centre=54 radius=21.5 value=23.7%		x_centre=72 y_centre=53 radius=21.5 value=51.2%		x_centre=21 y_centre=39 radius=19.5 value=49.1%

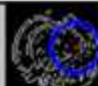





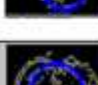


	x_centre=51 y_centre=70 radius=18.5 value=19.1%		x_centre=38 y_centre=59 radius=18.5 value=37.2%		x_centre=47 y_centre=21 radius=18.5 value=47.9%
	x_centre=45 y_centre=31 radius=18.5 value=18.3%		x_centre=44 y_centre=31 radius=18.5 value=36.5%		x_centre=36 y_centre=41 radius=25.5 value=47.8%
					x_centre=71 y_centre=45 radius=18.5 value=45.6%
					x_centre=36 y_centre=59 radius=22.5 value=42.6%
					x_centre=34 y_centre=23 radius=18.5 value=42.1%
					x_centre=64 y_centre=79 radius=18.5 value=40.1%
					x_centre=66 y_centre=42 radius=21.5 value=38.5%

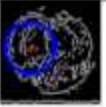





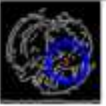


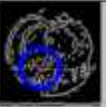
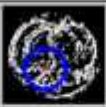

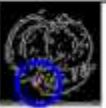

Sobel edge detection		New algorithm edge detection		Convolution edge detection	
Image	Results	Image	Results	Image	Results
	x_centre=44 y_centre=27 radius=21 value=26%		x_centre=42 y_centre=27 radius=22 value=57.2%		x_centre=36 y_centre=29 radius=23 value=49.5%
	x_centre=32 y_centre=32 radius=20 value=24.3%		x_centre=30 y_centre=31 radius=19 value=54.4%		x_centre=47 y_centre=34 radius=23 value=42.8%
	x_centre=53 y_centre=66 radius=24 value=20.3%				x_centre=32 y_centre=53 radius=20 value=41.7%
	x_centre=70 y_centre=41 radius=18 value=20.1%				x_centre=88 y_centre=65 radius=18 value=41.7%
					x_centre=62 y_centre=36 radius=19 value=39.1%
					x_centre=53 y_centre=69 radius=18 value=39%





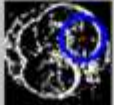

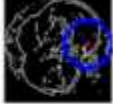
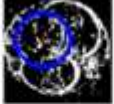

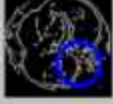
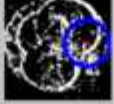

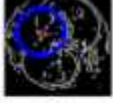
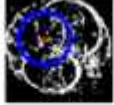
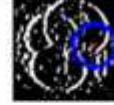
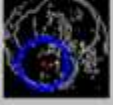
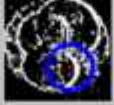
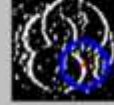
Sobel edge detection		New algorithm edge detection		Convolution edge detection	
Image	Results	Image	Results	Image	Results
	x_centre=29 y_centre=46 radius=23.5 value=31.3%		x_centre=59 y_centre=37 radius=19.5 value=59.8%		x_centre=55 y_centre=65 radius=18.5 value=51.4%
	x_centre=50 y_centre=43 radius=24.5 value=28%		x_centre=25 y_centre=39 radius=19.5 value=59.2%		x_centre=51 y_centre=37 radius=20.5 value=50.2%

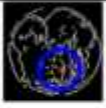

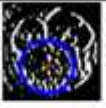
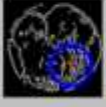
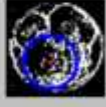

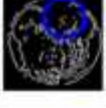
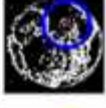


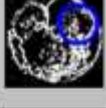

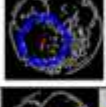
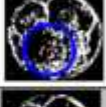
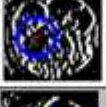
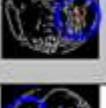



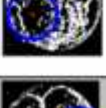
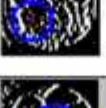



	x_centre=27 y_centre=35 radius=18.5 value=27.9%		x_centre=58 y_centre=49 radius=20.5 value=62.1%		x_centre=28 y_centre=38 radius=22.5 value=47.9%
	x_centre=71 y_centre=49 radius=24.5 value=27.5%		x_centre=45 y_centre=37 radius=19.5 value=60%		x_centre=73 y_centre=42 radius=19.5 value=46.9%
	x_centre=61 y_centre=36 radius=20.5 value=27.3%		x_centre=69 y_centre=48 radius=25.5 value=60%		x_centre=58 y_centre=49 radius=20.5 value=46.2%
	x_centre=48 y_centre=67 radius=18.5 value=26.5%		x_centre=38 y_centre=67 radius=18.5 value=49.7%		x_centre=38 y_centre=63 radius=18.5 value=45.3%
	x_centre=60 y_centre=68 radius=18.5 value=24.7%		x_centre=49 y_centre=62 radius=18.5 value=49.1%		x_centre=60 y_centre=25 radius=18.5 value=43.8%
	x_centre=42 y_centre=31 radius=25.5 value=23.5%				x_centre=35 y_centre=51 radius=19.5 value=42.6%
	x_centre=56 y_centre=56 radius=21.5 value=23.2%				x_centre=68 y_centre=49 radius=19.5 value=41.5%
	x_centre=36 y_centre=67 radius=18.5 value=22.6%				x_centre=53 y_centre=77 radius=19.5 value=40.4%
					x_centre=38 y_centre=26 radius=19.5 value=39.8%

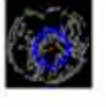
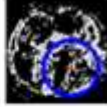

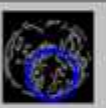
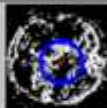

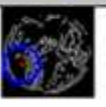
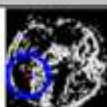

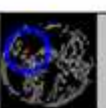
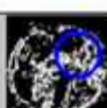

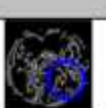
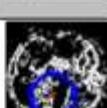

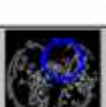



Sobel edge detection		New algorithm edge detection		Convolution edge detection	
Image	Results	Image	Results	Image	Results
	x_centre=37 y_centre=38 radius=20 value=28%		x_centre=36 y_centre=37 radius=20 value=55.8%		x_centre=38 y_centre=30 radius=25 value=48.9%
	x_centre=42 y_centre=69 radius=21 value=23.1%				x_centre=32 y_centre=42 radius=25 value=45.3%
	x_centre=34 y_centre=49 radius=24 value=21.6%				x_centre=44 y_centre=68 radius=18 value=43.7%
					x_centre=61 y_centre=31 radius=20 value=42.7%
					x_centre=31 y_centre=61 radius=18 value=37.5%
					x_centre=63 y_centre=48 radius=19 value=36.6%

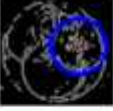
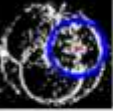

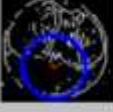
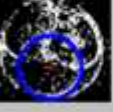
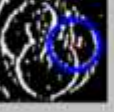
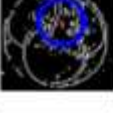
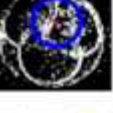

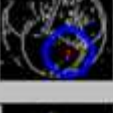


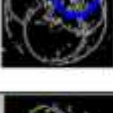


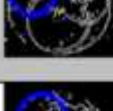

Sobel edge detection		New algorithm edge detection		Convolution edge detection	
Image	Results	Image	Results	Image	Results
	x_centre=42 y_centre=66 radius=23 value=28.2%		x_centre=42 y_centre=66 radius=23 value=69.8%		x_centre=41 y_centre=39 radius=20 value=62.9%
	x_centre=70 y_centre=55 radius=18 value=25.1%		x_centre=46 y_centre=30 radius=23 value=62.5%		x_centre=59 y_centre=54 radius=22 value=50%
	x_centre=43 y_centre=48 radius=24 value=24.8%		x_centre=41 y_centre=47 radius=24 value=50.4%		x_centre=38 y_centre=63 radius=21 value=48.9%

	x_centre=45 y_centre=30 radius=23 value=24.3%		x_centre=33 y_centre=31 radius=18 value=49.1%		x_centre=38 y_centre=26 radius=19 value=47.5%
	x_centre=31 y_centre=32 radius=18 value=23.3%		x_centre=70 y_centre=55 radius=18 value=46.1%		x_centre=51 y_centre=26 radius=19 value=45.5%
	x_centre=57 y_centre=64 radius=18 value=21.3%		x_centre=55 y_centre=62 radius=21 value=40.8%		x_centre=67 y_centre=42 radius=18 value=45.2%
	x_centre=61 y_centre=39 radius=18 value=20.7%		x_centre=59 y_centre=40 radius=19 value=40.8%		x_centre=53 y_centre=41 radius=22 value=44.4%
	x_centre=76 y_centre=38 radius=20 value=19.5%				x_centre=54 y_centre=73 radius=20 value=44.1%

Sobel edge detection		New algorithm edge detection		Convolution edge detection	
Image	Results	Image	Results	Image	Results
	x_centre=33 y_centre=63 radius=25 value=25.7%		x_centre=69 y_centre=48 radius=19 value=56%		x_centre=38 y_centre=35 radius=23 value=52.7%
	x_centre=68 y_centre=48 radius=20 value=25.4%		x_centre=34 y_centre=70 radius=19 value=55%		x_centre=65 y_centre=41 radius=25 value=48.3%
	x_centre=44 y_centre=75 radius=21 value=24.7%		x_centre=39 y_centre=35 radius=24 value=52.1%		x_centre=33 y_centre=62 radius=25 value=42.6%
	x_centre=66 y_centre=66 radius=19 value=24.4%		x_centre=45 y_centre=74 radius=20 value=51%		x_centre=28 y_centre=48 radius=21 value=41.9%
	x_centre=38 y_centre=33 radius=21 value=24.2%		x_centre=39 y_centre=35 radius=23 value=50.4%		x_centre=46 y_centre=73 radius=19 value=41.1%
	x_centre=65 y_centre=37 radius=22 value=20.2%		x_centre=66 y_centre=59 radius=20 value=47%		x_centre=63 y_centre=65 radius=20 value=40.3%

Sobel edge detection		New algorithm edge detection		Convolution edge detection	
Image	Results	Image	Results	Image	Results
	x_centre=65 y_centre=54 radius=19.5 value=26.9%		x_centre=65 y_centre=63 radius=18.5 value=60.4%		x_centre=63 y_centre=43 radius=25.5 value=54.6%
	x_centre=65 y_centre=65 radius=19.5 value=26.1%		x_centre=62 y_centre=43 radius=25.5 value=57.4%		x_centre=29 y_centre=65 radius=24.5 value=45.7%
	x_centre=25 y_centre=59 radius=19.5 value=25.8%		x_centre=29 y_centre=60 radius=22.5 value=53.7%		x_centre=36 y_centre=28 radius=19.5 value=44.9%
	x_centre=35 y_centre=72 radius=18.5 value=25%		x_centre=34 y_centre=71 radius=18.5 value=52.9%		x_centre=50 y_centre=32 radius=18.5 value=40.4%
	x_centre=58 y_centre=38 radius=22.5 value=23.9%		x_centre=62 y_centre=43 radius=24.5 value=50.6%		x_centre=63 y_centre=64 radius=21.5 value=44.5%
	x_centre=54 y_centre=75 radius=20.5 value=23.6%		x_centre=54 y_centre=65 radius=28.5 value=50.2%		x_centre=41 y_centre=74 radius=18.5 value=39.5%
	x_centre=34 y_centre=26 radius=18.5 value=21.8%		x_centre=56 y_centre=29 radius=23.5 value=49.5%		x_centre=62 y_centre=30 radius=18.5 value=38.6%
	x_centre=71 y_centre=42 radius=18.5 value=21.8%		x_centre=47 y_centre=78 radius=22.5 value=49.4%		x_centre=49 y_centre=52 radius=18.5 value=33.4%

Sobel edge detection		New algorithm edge detection		Convolution edge detection	
Image	Results	Image	Results	Image	Results
	x_centre=54 y_centre=51 radius=18.5 value=30.8%		x_centre=64 y_centre=58 radius=24.5 value=64.6%		x_centre=40 y_centre=30 radius=21.5 value=53%
	x_centre=66 y_centre=52 radius=25.5 value=30.5%		x_centre=52 y_centre=50 radius=18.5 value=54%		x_centre=68 y_centre=23 radius=18.5 value=52.6%
	x_centre=61 y_centre=21 radius=18.5 value=26.1%		x_centre=60 y_centre=21 radius=18.5 value=50.2%		x_centre=64 y_centre=60 radius=22.5 value=49.3%
	x_centre=36 y_centre=28 radius=20.5 value=24.7%		x_centre=36 y_centre=64 radius=19.5 value=50%		x_centre=36 y_centre=58 radius=24.5 value=48.6%
	x_centre=63 y_centre=67 radius=19.5 value=23.8%		x_centre=67 y_centre=43 radius=19.5 value=49.1%		x_centre=51 y_centre=65 radius=18.5 value=42.4%
	x_centre=31 y_centre=58 radius=19.5 value=23%		x_centre=36 y_centre=29 radius=20.5 value=48.6%		
			x_centre=60 y_centre=62 radius=18.5 value=48.5%		
			x_centre=61 y_centre=69 radius=18.5 value=48.2%		

Sobel edge detection		New algorithm edge detection		Convolution edge detection	
Image	Results	Image	Results	Image	Results
	x_centre=46 y_centre=68 radius=23 value=30.7%		x_centre=45 y_centre=66 radius=23 value=64.9%		x_centre=67 y_centre=45 radius=26 value=64.3%
	x_centre=66 y_centre=45 radius=26 value=30.2%		x_centre=66 y_centre=45 radius=26 value=62.8%		x_centre=47 y_centre=67 radius=21 value=56.2%
	x_centre=38 y_centre=51 radius=19 value=23.3%		x_centre=38 y_centre=50 radius=20 value=48.3%		x_centre=41 y_centre=27 radius=21 value=52%
	x_centre=72 y_centre=58 radius=19 value=20.8%		x_centre=33 y_centre=62 radius=19 value=45.2%		x_centre=29 y_centre=34 radius=19 value=46.3%
	x_centre=33 y_centre=63 radius=19 value=20.8%		x_centre=28 y_centre=33 radius=19 value=43%		x_centre=35 y_centre=47 radius=19 value=41.3%
	x_centre=41 y_centre=24 radius=19 value=20.5%				
	x_centre=29 y_centre=32 radius=19 value=20.5%				

APPENDIX F

The results of the approach discussed in Chapter 8 are shown in this Appendix. This approach used the template matching on the binary images but the median filter was applied to the image before detecting its edges. This Appendix will show the results when using the Sobel edge detector.

202






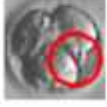
Image after edge detection	Image	Radius	x-centre	y-centre	Result (%)
		19	38	69	17.5
		18	60	56	15.9
		18	70	53	15.3
		18	60	77	14.7
		23	60	67	10.5


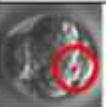


Image after edge detection	Image	Radius	x-centre	y-centre	Result (%)
		19	60	71	17.7
		26	61	49	13.6
		26	41	47	12.4






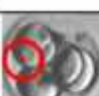
Image after edge detection	Image	Radius	x-centre	y-centre	Result (%)
		22	33	30	21.4
		23	51	58	21.1
		21	71	35	19.5
		22	58	69	16.9
		18	47	21	14.2


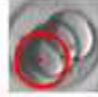
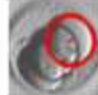

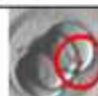
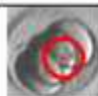
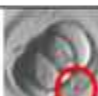
Image after edge detection	Image	Radius	x-centre	y-centre	Result (%)
		26	64	34	17.4
		24	42	63	15.2
		26	53	44	14.7
		24	54	73	12.8
		19	54	57	11.6
		19	79	71	11.3



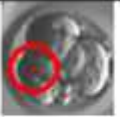

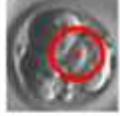
Image after edge detection	Image	Radius	x-centre	y-centre	Result (%)
		23	59	68	18.6
		19	57	28	16.5
		18	38	69	14.0
		21	48	62	13.0





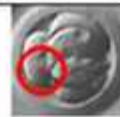

Image after edge detection	Image	Radius	x-centre	y-centre	Result (%)
		22	66	56	22.4
		19	43	26	21.9
		18	37	49	21.0
		19	57	26	19.4
		18	21	23	17.4


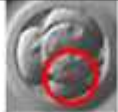

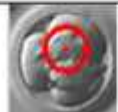




Image after edge detection	Image	Radius	x-centre	y-centre	Result (%)
		22	66	56	22.4
		19	43	26	21.9
		18	37	49	21.0
		19	57	26	19.4
		18	21	23	17.4
		18	25	49	17.4
		18	25	37	17.1

Image after edge detection	Image	Radius	x-centre	y-centre	Result (%)
		19	33	41	17.4
		20	40	23	15.1
		19	31	51	15.1
		21	55	35	14.0
		22	64	65	13.50
		18	52	19	13.3
		23	69	53	12.8
		21	52	71	12.5


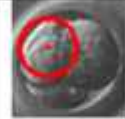
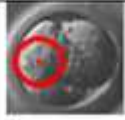
Image after edge detection	Image	Radius	x-centre	y-centre	Result (%)
		23	40	32	16.7
		19	52	27	13.6





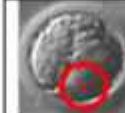


Image after edge detection	Image	Radius	x-centre	y-centre	Result (%)
		20	60	28	20.2
		18	30	39	16.3
		23	49	65	16.4
		18	71	53	16.3
		24	59	64	14.8
		24	39	28	14.4


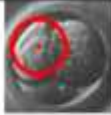

Image after edge detection	Image	Radius	x-centre	y-centre	Result (%)
		23	40	32	15.7
		19	52	27	13.6


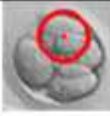



Image after edge detection	Image	Radius	x-centre	y-centre	Result (%)
		21	32	53	24.4
		16	47	69	15.3
		23	68	61	15.2
		16	51	25	14.0








Image after edge detection	Image	Radius	x-centre	y-centre	Result (%)
		20	50	28	20.2
		18	30	39	18.3
		23	49	65	16.4
		18	71	53	16.3
		24	59	64	14.8
		24	39	28	14.4


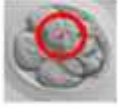

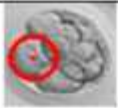



Image after edge detection	Image	Radius	x-centre	y-centre	Result (%)
		19	37	50	16.6
		17	70	64	16.2
		19	62	27	15.2
		21	56	65	14.8
		19	29	39	13.6
		21	36	66	12.5





Image after edge detection	Image	Radius	x-centre	y-centre	Result (%)
		21	27	60	18.0
		23	57	63	16.4
		18	74	41	13.0


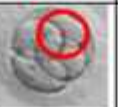
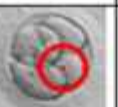


Image after edge detection	Image	Radius	x-centre	y-centre	Result (%)
		20	30	69	19.2
		19	54	60	17.7
		21	36	38	16.4
		26	68	42	15.1












Image after edge detection	Image	Radius	x-centre	y-centre	Result (%)
		19	83	55	26.1
		18	57	65	26.0
		19	73	56	24.4
		18	38	68	23.9
		19	72	41	22.6
		18	52	48	21.5
		25	40	48	20.4
		25	53	29	18.9
		22	56	75	18.8



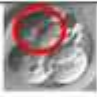


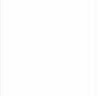

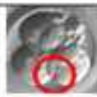


Image after edge detection	Image	Radius	x-centre	y-centre	Result (%)
		23	86	65	25.2
		24	30	39	21.6
		19	60	61	18.8
		21	62	74	18.7
		21	29	51	16.9
		19	76	51	16.3
		19	32	64	16.3
		19	60	26	16




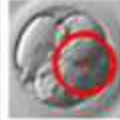


Image after edge detection	Image	Radius	x-centre	y-centre	Result (%)
		21	44	24	21.8
		18	30	31	20.4
		24	52	64	17.4
		18	72	41	16.5
		19	31	64	15.5













Image after edge detection	Image	Radius	x-centre	y-centre	Result (%)
		21	43	53	28.1
		19	50	63	24.7
		19	43	41	23.6
		20	73	49	23.6
		22	47	27	23.4
		21	38	64	21.8
		23	30	31	20.6
		22	62	64	20.5
		19	53	41	20.2
		19	74	68	20



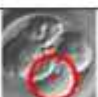
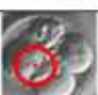
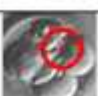





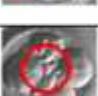
Image after edge detection	Image	Radius	x-centre	y-centre	Result (%)
		19	25	45	20
		23	71	63	19.7
		19	57	34	18.0
		19	38	69	17.7
		24	45	69	17.2
		21	27	28	16.6
		19	60	46	16.1
		22	47	23	15.9
		24	45	44	15.0



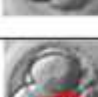
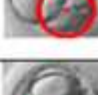






Image after edge detection	Image	Radius	x-centre	y-centre	Result (%)
		23	33	45	21.3
		23	72	54	20.5
		24	62	31	19.5
		18	30	10	13.7
		18	45	31	13.7
		19	46	53	13.3
		18	56	75	13.0
		20	34	55	12.9










Image after edge detection	Image	Radius	x-centre	y-centre	Result (%)
		19	51	68	25.2
		19	73	59	25
		20	40	70	21.9
		23	24	46	21.7
		19	63	70	21.5
		26	37	53	20.9
		23	55	33	19.6
		24	52	53	15.9


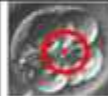


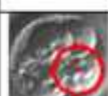

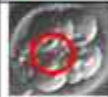




Image after edge detection	Image	Radius	x-centre	y-centre	Result (%)
		20	50	54	24.3
		21	61	55	22.6
		21	27	64	21.8
		23	58	67	21.5
		26	65	39	20.5
		19	53	42	20.2
		21	37	25	18.2
		22	44	64	17.8
		23	32	42	16.9







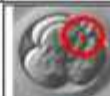

Image after edge detection	Image	Radius	x-centre	y-centre	Result (%)
		18	29	35	21.5
		24	39	49	19.3
		18	45	20	16.9
		18	60	26	16.9
		18	33	65	16.9
		18	26	50	16.8











Image after edge detection	Image	Radius	x-centre	y-centre	Result (%)
		21	58	37	21.6
		20	25	39	21.1
		23	71	51	20.1
		18	41	68	18.9
		20	46	38	18.4
		20	58	50	17.9
		24	35	32	16.8
		18	38	48	16.5
		18	59	68	15.6

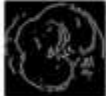




Image after edge detection	Image	Radius	x-centre	y-centre	Result (%)
		21	44	75	20.3
		22	38	33	20.0
		20	33	71	19.7
		26	62	42	19.5





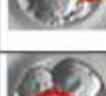




Image after edge detection	Image	Radius	x-centre	y-centre	Result (%)
		20	26	59	21.6
		18	66	64	20.7
		18	46	78	20.1
		24	65	44	18.3
		18	32	71	18.0
		18	63	75	17.1
		23	56	29	16.2
		18	73	74	16.2











Image after edge detection	Image	Radius	x-centre	y-centre	Result (%)
		21	58	37	21.6
		20	25	39	21.1
		23	71	51	20.1
		18	41	68	18.9
		20	46	38	18.4
		20	58	50	17.9
		24	36	32	16.8
		18	38	48	16.5
		18	59	68	15.6






Image after edge detection	Image	Radius	x-centre	y-centre	Result (%)
		20	35	39	20.3
		20	42	70	18.1
		17	71	52	15.6
		22	62	37	13.7










Image after edge detection	Image	Radius	x-centre	y-centre	Result (%)
		23	42	67	23.6
		21	43	27	21.0
		21	42	41	19.0
		18	70	55	18.9
		18	77	38	17.4
		21	55	29	16.1
		19	30	33	16.1
		20	62	66	15.5







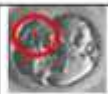


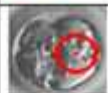












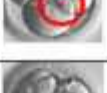
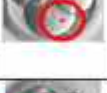

Image after edge detection	Image	Radius	x-centre	y-centre	Result (%)
		26	66	52	22.8
		23	62	63	21.0
		19	63	20	18.3
		19	63	61	18.3
		21	36	28	17.8
		26	37	67	17.3
		22	63	24	16
		19	51	66	15.9
		19	40	82	15.9
		21	32	38	14.8
					

Image after edge detection	Image	Radius	x-centre	y-centre	Result (%)
		26	66	45	25.6
		23	45	67	24.4
		19	28	34	16.5
		19	32	62	16.5
		20	42	66	16.0
		19	56	74	15.9
		20	57	57	14.3
		20	73	57	14.3
		20	50	22	14.0
					
					

APPENDIX G

The results of the approach discussed in Chapter 8 are shown in this Appendix. This approach used the template matching on the binary images but the median filter was applied to the image before detecting its edges. This Appendix will show the results when using the new algorithm and convolution mask edge detectors.










Image	New algorithm edge detection		Image	Convolution edge detection	
	Image	Results		Image	Results
		x_centre=59 y_centre=73 radius=19 value=53.6%			x_centre=37 y_centre=52 radius=25 value=43%
		x_centre=63 y_centre=48 radius=25 value=44%			x_centre=61 y_centre=57 radius=20 value=41.4%
		x_centre=39 y_centre=49 radius=25 value=41.5%			x_centre=62 y_centre=22 radius=19 value=35.5%
		x_centre=50 y_centre=51 radius=28 value=36.9%			













Image	New algorithm edge detection		Image	Convolution edge detection	
	Image	Results		Image	Results
		x_centre=37 y_centre=67 radius=21 value=49.7%			x_centre=38 y_centre=69 radius=19 value=51.9%
		x_centre=60 y_centre=55 radius=18 value=48.8%			x_centre=40 y_centre=32 radius=23 value=49.7%
		x_centre=50 y_centre=76 radius=18 value=45.2%			x_centre=70 y_centre=52 radius=19 value=45.2%
		x_centre=44 y_centre=52 radius=19 value=38.8%			x_centre=65 y_centre=41 radius=24 value=38.4%
		x_centre=69 y_centre=36 radius=19 value=38.3%			
		x_centre=41 y_centre=30 radius=23 value=35%			











Image	New algorithm edge detection		Image	Convolution edge detection	
	Image	Results		Image	Results
		x_centre=34 y_centre=29 radius=22 value=62.5%			x_centre=35 y_centre=31 radius=22 value=66.1%
		x_centre=51 y_centre=58 radius=24 value=59.3%			x_centre=70 y_centre=35 radius=21 value=55.9%
		x_centre=70 y_centre=35 radius=22 value=56.5%			x_centre=57 y_centre=68 radius=23 value=52.9%
		x_centre=55 y_centre=73 radius=18 value=50.2%			x_centre=51 y_centre=56 radius=23 value=52.7%














Image	New algorithm edge detection		Image	Convolution edge detection	
	Image	Results		Image	Results
		x_centre=64 y_centre=33 radius=26 value=48.9%			x_centre=53 y_centre=46 radius=26 value=48.3%
		x_centre=39 y_centre=60 radius=24 value=44.9%			x_centre=64 y_centre=29 radius=21 value=46%
		x_centre=62 y_centre=44 radius=26 value=41.9%			x_centre=44 y_centre=23 value=38.7%
		x_centre=54 y_centre=57 radius=19 value=41.6%			x_centre=56 y_centre=71 radius=21 value=34%
		x_centre=67 y_centre=73 radius=23 value=40.5%			
		x_centre=77 y_centre=72 radius=20 value=36.2%			
		x_centre=65 y_centre=50 radius=19 value=34.1%			














Image	New algorithm edge detection		Image	Convolution edge detection	
	Image	Results		Image	Results
		x_centre=56 y_centre=68 radius=24 value=55.3%			x_centre=69 y_centre=29 radius=23 value=47%
		x_centre=67 y_centre=28 radius=19 value=47%			x_centre=61 y_centre=56 radius=22 value=46.8%
		x_centre=37 y_centre=71 radius=20 value=46.6%			x_centre=56 y_centre=35 radius=22 value=44.4%
		x_centre=49 y_centre=55 radius=18 value=39.6%			x_centre=33 y_centre=41 radius=21 value=43.4%
		x_centre=70 y_centre=59 radius=18 value=39.6%			x_centre=48 y_centre=53 radius=19 value=37.2%
					x_centre=33 y_centre=28 radius=24 value=35.8%


















Image	New algorithm edge detection		Image	Convolution edge detection	
	Image	Results		Image	Results
		x_centre=43 y_centre=27 radius=20 value=62.5%			x_centre=36 y_centre=27 radius=19 value=46.6%
		x_centre=56 y_centre=27 radius=19 value=59%			x_centre=49 y_centre=34 radius=21 value=44.7%
		x_centre=66 y_centre=56 radius=22 value=56.2%			x_centre=42 y_centre=52 radius=19 value=42.7%
		x_centre=40 y_centre=48 radius=19 value=55.5%			x_centre=59 y_centre=30 radius=20 value=42.2%
		x_centre=24 y_centre=22 radius=19 value=53.6%			x_centre=67 y_centre=58 radius=22 value=39.1%
		x_centre=31 y_centre=35 radius=21 value=46.6%			x_centre=54 y_centre=65 radius=26 value=38.5%
		x_centre=28 y_centre=47 radius=21 value=44.2%			x_centre=31 y_centre=36 radius=23 value=37.1%
					x_centre=31 y_centre=67 radius=22 value=31.1%

















Image	New algorithm edge detection		Image	Convolution edge detection	
	Image	Results		Image	Result
		x_centre=35 y_centre=42 radius=20 value=49.1%			x_centre=44 y_centre=23 radius=21 value=45.3%
		x_centre=42 y_centre=24 radius=21 value=44.2%			x_centre=30 y_centre=31 radius=19 value=37.5%
		x_centre=54 y_centre=34 radius=20 value=44.1%			x_centre=57 y_centre=37 radius=23 value=36.6%
		x_centre=45 y_centre=70 radius=20 value=40.6%			x_centre=38 y_centre=43 radius=19 value=35.6%
		x_centre=23 y_centre=29 radius=19 value=37.7%			x_centre=55 y_centre=72 radius=19 value=35.6%
		x_centre=63 y_centre=66 radius=21 value=37.7%			x_centre=42 y_centre=71 radius=19 value=35.5%
		x_centre=68 y_centre=49 radius=23 value=36%			x_centre=63 y_centre=61 radius=25 value=34.2%















Image	New algorithm edge detection		Image	Convolution edge detection	
	Image	Results		Image	Results
		x_centre=37 y_centre=27 radius=19 value=45.2%			x_centre=36 y_centre=27 radius=21 value=51%
		x_centre=52 y_centre=32 radius=23 value=38%			x_centre=52 y_centre=76 radius=22 value=43.2%
		x_centre=17 y_centre=36 radius=19 value=36.9%			x_centre=60 y_centre=30 radius=26 value=42.5%
		x_centre=26 y_centre=20 radius=19 value=36.6%			x_centre=50 y_centre=19 radius=19 value=42.5%
		x_centre=38 y_centre=21 radius=19 value=35.2%			x_centre=37 y_centre=63 radius=19 value=38.6%
					x_centre=38 y_centre=40 radius=26 value=35.2%
					x_centre=56 y_centre=42 radius=26 value=33.1%















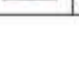
Image	New algorithm edge detection		Image	Convolution edge detection	
	Image	Results		Image	Results
		x_centre=48 y_centre=29 radius=20 value=56.6%			x_centre=59 y_centre=67 radius=23 value=45.3%
		x_centre=32 y_centre=33 radius=19 value=52.2%			x_centre=49 y_centre=36 radius=23 value=45.6%
		x_centre=61 y_centre=67 radius=26 value=46.2%			x_centre=48 y_centre=23 radius=19 value=44.4%
		x_centre=21 y_centre=35 radius=19 value=45.6%			x_centre=37 y_centre=34 radius=24 value=40.6%
		x_centre=65 y_centre=66 radius=22 value=42.9%			x_centre=47 y_centre=71 radius=22 value=35.6%
					x_centre=59 y_centre=29 radius=19 value=38%
					x_centre=38 y_centre=56 radius=19 value=35.9%
					x_centre=50 y_centre=61 radius=20 value=32.1%











Image	New algorithm edge detection		Image	Convolution edge detection	
	Image	Results		Image	Results
		x_centre=31 y_centre=53 radius=21 value=60.9%			x_centre=54 y_centre=27 radius=19 value=39.6%
		x_centre=49 y_centre=75 radius=17 value=45.6%			x_centre=33 y_centre=54 radius=21 value=35.4%
		x_centre=67 y_centre=63 radius=23 value=41.8%			x_centre=47 y_centre=69 radius=19 value=34.3%
		x_centre=53 y_centre=30 radius=23 value=40.1%			x_centre=73 y_centre=60 radius=23 value=28.5%














Image	New algorithm edge detection		Image	Convolution edge detection	
	Image	Results		Image	Results
		x_centre=54 y_centre=69 radius=18 value=45.8%			x_centre=55 y_centre=65 radius=20 value=40.3%
		x_centre=41 y_centre=56 radius=24 value=43.2%			x_centre=26 y_centre=37 radius=17 value=33.4%
		x_centre=34 y_centre=43 radius=23 value=41.2%			x_centre=35 y_centre=49 radius=17 value=33.1%
		x_centre=65 y_centre=47 radius=21 value=39%			x_centre=70 y_centre=48 radius=21 value=32.8%
		x_centre=51 y_centre=25 radius=18 value=39%			x_centre=55 y_centre=26 radius=17 value=29.9%
		x_centre=39 y_centre=69 radius=19 value=35.8%			











Image	New algorithm edge detection		Image	Convolution edge detection	
	Image	Results		Image	Results
		x_centre=27 y_centre=60 radius=20 value=50.2%			x_centre=53 y_centre=64 radius=20 value=37.3%
		x_centre=58 y_centre=63 radius=22 value=49%			x_centre=51 y_centre=33 radius=21 value=33.2%
		x_centre=53 y_centre=29 radius=17 value=35.9%			x_centre=70 y_centre=37 radius=19 value=31.9%
		x_centre=72 y_centre=38 radius=18 value=34.3%			x_centre=28 y_centre=60 radius=20 value=29.4%











Image	New algorithm edge detection		Image	Convolution edge detection	
	Image	Results		Image	Results
		x_centre=27 y_centre=59 radius=19 value=61.6%			x_centre=36 y_centre=37 radius=22 value=43.9%
		x_centre=38 y_centre=38 radius=22 value=60.2%			x_centre=61 y_centre=67 radius=21 value=36.4%
		x_centre=66 y_centre=60 radius=19 value=48.3%			x_centre=67 y_centre=39 radius=24 value=34.2%
		x_centre=67 y_centre=44 radius=19 value=40.2%			x_centre=30 y_centre=60 radius=19 value=31.9%
















Image	detection		Image	detection	
	Image	Results		Image	Results
		x_centre=66 y_centre=66 radius=23 value=69%			x_centre=66 y_centre=66 radius=23 value=65.5%
		x_centre=30 y_centre=38 radius=23 value=61.9%			x_centre=32 y_centre=38 radius=23 value=61.1%
		x_centre=60 y_centre=61 radius=19 value=63.6%			x_centre=62 y_centre=27 radius=20 value=43%
		x_centre=31 y_centre=64 radius=19 value=60%			x_centre=44 y_centre=69 radius=26 value=34.5%
		x_centre=76 y_centre=62 radius=19 value=49.7%			x_centre=46 y_centre=72 radius=19 value=31.9%
		x_centre=64 y_centre=76 radius=19 value=48%			
		x_centre=29 y_centre=61 radius=20 value=47.6%			
		x_centre=60 y_centre=26 radius=19 value=45%			






















Image	New algorithm edge detection		Image	Convolution edge detection	
	Image	Results		Image	Results
		x_centre=42 y_centre=51 radius=20 value=69.7%			x_centre=42 y_centre=51 radius=20 value=43.7%
		x_centre=72 y_centre=50 radius=20 value=64.4%			x_centre=47 y_centre=46 radius=20 value=44.6%
		x_centre=64 y_centre=49 radius=19 value=63.9%			x_centre=71 y_centre=49 radius=21 value=44.1%
		x_centre=47 y_centre=27 radius=20 value=60.3%			x_centre=31 y_centre=21 radius=25 value=42.6%
		x_centre=39 y_centre=41 radius=24 value=60.2%			x_centre=42 y_centre=22 radius=26 value=39.4%
		x_centre=67 y_centre=69 radius=19 value=61.6%			x_centre=36 y_centre=60 radius=25 value=36.2%
		x_centre=30 y_centre=70 radius=19 value=60.6%			x_centre=68 y_centre=70 radius=20 value=36.6%
		x_centre=42 y_centre=64 radius=20 value=67.7%			x_centre=68 y_centre=68 radius=22 value=54.7%
		x_centre=64 y_centre=42 radius=19 value=64.7%			x_centre=20 y_centre=64 radius=19 value=54.1%
					x_centre=18 y_centre=27 radius=21 value=52%


















Image	New algorithm edge detection		Image	Convolution edge detection	
	Image	Results		Image	Results
		x_centre=45 y_centre=71 radius=23 value=55.7%			x_centre=47 y_centre=74 radius=20 value=49.7%
		x_centre=71 y_centre=54 radius=23 value=54.1%			x_centre=73 y_centre=52 radius=24 value=47.5%
		x_centre=24 y_centre=45 radius=19 value=51.6%			x_centre=49 y_centre=21 radius=22 value=44.4%
		x_centre=50 y_centre=40 radius=19 value=50.8%			x_centre=24 y_centre=45 radius=20 value=41.4%
		x_centre=36 y_centre=58 radius=20 value=50.2%			x_centre=49 y_centre=34 radius=26 value=35.6%
		x_centre=32 y_centre=27 radius=25 value=49.7%			x_centre=38 y_centre=28 radius=26 value=32.7%
		x_centre=47 y_centre=29 radius=26 value=47.9%			
		x_centre=38 y_centre=46 radius=19 value=44.6%			
		x_centre=56 y_centre=59 radius=21 value=42.3%			




























Image	New algorithm edge detection		Image	Convolution edge detection	
	Image	Results		Image	Results
		x_centre=72 y_centre=59 radius=19 value=58.8%			x_centre=56 y_centre=66 radius=20 value=42.6%
		x_centre=52 y_centre=68 radius=19 value=54.2%			x_centre=71 y_centre=55 radius=21 value=41.7%
		x_centre=39 y_centre=70 radius=20 value=59.5%			x_centre=49 y_centre=34 radius=26 value=41.7%
		x_centre=75 y_centre=47 radius=19 value=59.5%			x_centre=36 y_centre=34 radius=24 value=40.9%
		x_centre=59 y_centre=52 radius=20 value=57%			x_centre=56 y_centre=74 radius=23 value=40.1%
		x_centre=37 y_centre=53 radius=26 value=52.9%			x_centre=59 y_centre=38 radius=19 value=36.3%
		x_centre=47 y_centre=44 radius=22 value=52.2%			x_centre=33 y_centre=65 radius=19 value=36%
		x_centre=71 y_centre=70 radius=25 value=52%			x_centre=53 y_centre=53 radius=21 value=35.6%
		x_centre=51 y_centre=32 radius=26 value=51.9%			x_centre=24 y_centre=36 radius=19 value=36.4%
		x_centre=24 y_centre=46 radius=23 value=49.1%			x_centre=39 y_centre=49 radius=21 value=34.8%
		x_centre=28 y_centre=35 radius=23 value=45.7%			x_centre=18 y_centre=21 radius=19 value=32.8%
					x_centre=79 y_centre=67 radius=22 value=32.7%













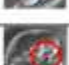




Image	New algorithm edge detection		Image	Convolution edge detection	
	Image	Results		Image	Results
		x_centre=49 y_centre=54 radius=20 value=57.1%			x_centre=27 y_centre=64 radius=22 value=48%
		x_centre=56 y_centre=65 radius=24 value=55.7%			x_centre=32 y_centre=42 radius=23 value=47.7%
		x_centre=29 y_centre=64 radius=21 value=51.9%			x_centre=58 y_centre=68 radius=22 value=47.1%
		x_centre=55 y_centre=41 radius=19 value=58.8%			x_centre=70 y_centre=35 radius=24 value=46.7%
		x_centre=23 y_centre=43 radius=24 value=53.1%			x_centre=54 y_centre=29 radius=24 value=43.8%
		x_centre=44 y_centre=65 radius=21 value=53.1%			x_centre=35 y_centre=30 radius=21 value=43.2%
		x_centre=36 y_centre=25 radius=20 value=51.8%			x_centre=69 y_centre=72 radius=25 value=41.5%
					x_centre=56 y_centre=47 radius=19 value=39.4%













Image	New algorithm edge detection		Image	Convolution edge detection	
	Image	Results		Image	Results
		x_centre=33 y_centre=34 radius=18 value=65.3%			x_centre=60 y_centre=24 radius=18 value=59.4%
		x_centre=44 y_centre=48 radius=22 value=58.8%			x_centre=43 y_centre=23 radius=20 value=56.7%
		x_centre=46 y_centre=20 radius=18 value=49.3%			x_centre=43 y_centre=49 radius=18 value=51.9%
		x_centre=64 y_centre=35 radius=24 value=48.4%			x_centre=32 y_centre=32 radius=20 value=46.6%
					x_centre=54 y_centre=58 radius=21 value=45.2%
					x_centre=49 y_centre=69 radius=24 value=37.8%




















Image	New algorithm edge detection		Image	Convolution edge detection	
	Image	Results		Image	Results
		x_centre=32 y_centre=47 radius=24 value=58.7%			x_centre=59 y_centre=27 radius=24 value=49.7%
		x_centre=72 y_centre=66 radius=23 value=56.6%			x_centre=36 y_centre=66 radius=18 value=46.7%
		x_centre=68 y_centre=23 radius=19 value=53.7%			x_centre=48 y_centre=53 radius=20 value=44.9%
		x_centre=46 y_centre=31 radius=18 value=40.8%			x_centre=21 y_centre=39 radius=20 value=44.3%
		x_centre=23 y_centre=30 radius=18 value=40.5%			x_centre=69 y_centre=45 radius=18 value=43.7%
		x_centre=66 y_centre=74 radius=18 value=40.5%			x_centre=44 y_centre=22 radius=20 value=43.5%
					x_centre=35 y_centre=36 radius=21 value=41.7%
					x_centre=35 y_centre=54 radius=18 value=36.6%
					x_centre=57 y_centre=77 radius=20 value=35.6%
					x_centre=70 y_centre=66 radius=19 value=33.7%
					x_centre=46 y_centre=41 radius=22 value=32.7%











Image	New algorithm edge detection		Image	Convolution edge detection	
	Image	Results		Image	Results
		x_centre=39 y_centre=31 radius=26 value=63.6%			x_centre=41 y_centre=30 radius=26 value=46.6%
		x_centre=54 y_centre=64 radius=25 value=52.7%			x_centre=30 y_centre=29 radius=19 value=44.1%
		x_centre=27 y_centre=37 radius=21 value=45.5%			x_centre=32 y_centre=53 radius=20 value=38.5%
					x_centre=65 y_centre=67 radius=24 value=35.3%
					x_centre=57 y_centre=29 radius=19 value=35.2%




















Image	New algorithm edge detection		Image	Convolution edge detection	
	Image	Results		Image	Results
		x_centre=59 y_centre=40 radius=23 value=64.2%			x_centre=51 y_centre=43 radius=26 value=49.3%
		x_centre=60 y_centre=36 radius=19 value=62.2%			x_centre=55 y_centre=36 radius=19 value=43.8%
		x_centre=58 y_centre=50 radius=20 value=55.8%			x_centre=44 y_centre=28 radius=23 value=43.1%
		x_centre=38 y_centre=57 radius=18 value=54.7%			x_centre=64 y_centre=40 radius=25 value=42.8%
		x_centre=70 y_centre=50 radius=24 value=54.1%			x_centre=29 y_centre=38 radius=22 value=42%
		x_centre=47 y_centre=37 radius=20 value=51.8%			x_centre=35 y_centre=51 radius=19 value=40%
		x_centre=34 y_centre=33 radius=24 value=49.1%			x_centre=38 y_centre=62 radius=19 value=39.4%
					x_centre=40 y_centre=82 radius=19 value=35.2%
					x_centre=82 y_centre=77 radius=20 value=34.4%
					x_centre=40 y_centre=40 radius=22 value=31.8%

















Image	New algorithm edge detection		Image	Convolution edge detection	
	Image	Results		Image	Results
		x_centre=42 y_centre=66 radius=23 value=65.3%			x_centre=41 y_centre=44 radius=22 value=50.2%
		x_centre=42 y_centre=33 radius=26 value=60.3%			x_centre=39 y_centre=62 radius=21 value=45.8%
		x_centre=42 y_centre=48 radius=24 value=58.9%			x_centre=63 y_centre=44 radius=20 value=46.2%
		x_centre=70 y_centre=64 radius=19 value=52.2%			x_centre=46 y_centre=27 radius=21 value=44.7%
		x_centre=58 y_centre=60 radius=27 value=48.1%			x_centre=52 y_centre=73 radius=20 value=41.7%
		x_centre=77 y_centre=38 radius=19 value=43.8%			x_centre=64 y_centre=58 radius=19 value=41.6%
		x_centre=76 y_centre=67 radius=19 value=40.2%			x_centre=45 y_centre=51 radius=22 value=39.1%












Image	New algorithm edge detection		Image	Convolution edge detection	
	Image	Results		Image	Results
		x_centre=36 y_centre=45 radius=26 value=56.6%			x_centre=36 y_centre=30 radius=24 value=44.5%
		x_centre=37 y_centre=32 radius=25 value=51%			x_centre=32 y_centre=41 radius=26 value=41.5%
		x_centre=50 y_centre=69 radius=21 value=48.8%			x_centre=38 y_centre=61 radius=19 value=40.8%
					x_centre=61 y_centre=31 radius=20 value=38.2%
					x_centre=54 y_centre=60 radius=19 value=33.3%
					x_centre=47 y_centre=79 radius=19 value=32.7%















Image	New algorithm edge detection		Image	Convolution edge detection	
	Image	Results		Image	Results
		x_centre=62 y_centre=43 radius=26 value=61.6%			x_centre=62 y_centre=43 radius=26 value=53.6%
		x_centre=26 y_centre=20 radius=20 value=56.9%			x_centre=28 y_centre=25 radius=25 value=43.6%
		x_centre=65 y_centre=64 radius=19 value=56.9%			x_centre=37 y_centre=28 radius=19 value=42.2%
		x_centre=46 y_centre=79 radius=19 value=52.6%			x_centre=65 y_centre=64 radius=20 value=37.4%
		x_centre=56 y_centre=32 radius=25 value=48.1%			x_centre=42 y_centre=78 radius=20 value=36.6%
		x_centre=54 y_centre=53 radius=25 value=46.6%			
		x_centre=34 y_centre=26 radius=19 value=44.4%			






























Image	New algorithm edge detection		Image	Convolution edge detection	
	Image	Results		Image	Results
		x_centre=43 y_centre=73 radius=22 value=57.2%			x_centre=39 y_centre=35 radius=23 value=51.8%
		x_centre=39 y_centre=33 radius=22 value=56%			x_centre=66 y_centre=41 radius=25 value=46.4%
		x_centre=68 y_centre=47 radius=19 value=56.8%			x_centre=29 y_centre=48 radius=21 value=38%
		x_centre=32 y_centre=62 radius=26 value=54%			x_centre=46 y_centre=73 radius=19 value=37.5%
		x_centre=66 y_centre=34 radius=19 value=50.5%			x_centre=33 y_centre=62 radius=25 value=36.7%
		x_centre=28 y_centre=50 radius=23 value=44.2%			x_centre=63 y_centre=66 radius=20 value=32.3%
		x_centre=63 y_centre=60 radius=19 value=43.8%			

Image	New algorithm edge detection		Image	Convolution edge detection	
	Image	Results		Image	Results
		x_centre=66 y_centre=59 radius=24 value=66.3%			x_centre=39 y_centre=21 radius=21 value=52%
		x_centre=37 y_centre=29 radius=21 value=55.4%			x_centre=58 y_centre=24 radius=19 value=50.8%
		x_centre=30 y_centre=58 radius=19 value=54.4%			x_centre=54 y_centre=60 radius=23 value=47.2%
		x_centre=69 y_centre=47 radius=22 value=51.6%			x_centre=37 y_centre=68 radius=26 value=46.2%
		x_centre=68 y_centre=22 radius=19 value=51.1%			
		x_centre=57 y_centre=44 radius=19 value=50%			
		x_centre=49 y_centre=67 radius=19 value=50%			
		x_centre=40 y_centre=63 radius=19 value=41.9%			

Image	New algorithm edge detection		Image	Convolution edge detection	
	Image	Results		Image	Results
		x_centre=45 y_centre=67 radius=23 value=66.2%			x_centre=67 y_centre=45 radius=26 value=62%
		x_centre=67 y_centre=44 radius=25 value=60.5%			x_centre=46 y_centre=66 radius=22 value=52.4%
		x_centre=39 y_centre=50 radius=20 value=51.3%			x_centre=41 y_centre=27 radius=21 value=48.6%
		x_centre=29 y_centre=33 radius=19 value=49.1%			x_centre=29 y_centre=34 radius=19 value=42.5%
		x_centre=43 y_centre=25 radius=19 value=43.3%			x_centre=35 y_centre=47 radius=19 value=34.7%
		x_centre=65 y_centre=68 radius=20 value=42.2%			
		x_centre=73 y_centre=57 radius=19 value=41.1%			

APPENDIX H

The results of the approach discussed in Chapter 8 are shown in this Appendix. This approach used the two templates on the binary images but the median filter was applied to the image before detecting its edges. The two factors BPS and IPS are used to substitute them in a 2 variable equation to measure the goodness of the detected cell. This Appendix will show the results when using the convolution mask edge detector.

Image	Radius	x-centre	y-centre	BPS	IPS	Measure of goodness
	25	37	52	0.43	0.11	0.71
	20	61	57	0.41	0.14	0.65
	23	55	48	0.39	0.21	0.66
	25	48	51	0.35	0.14	0.64
	20	72	49	0.35	0.16	0.63
	19	52	22	0.35	0.2	0.63

Image	Radius	x-centre	y-centre	BPS	IPS	Measure of goodness
	21	64	29	0.458333333	0.050185874	0.743845892
	25	51	45	0.400843882	0.067967275	0.695163821
	23	44	64	0.383027523	0.11102719	0.675040848

Image	Radius	x-centre	y-centre	BPS	IPS	Measure of goodness
	19	38	69	0.5	0.114486	0.770791802
	23	41	31	0.47	0.1805136	0.731037372
	19	70	52	0.43	0.1133178	0.718088136
	19	66	35	0.37	0.1308411	0.662838216
	19	27	61	0.31	0.125	0.617195503

Image	Radius	x-centre	y-centre	BPS	IPS	Measure of goodness
	22	35	31	0.657005	0.143216	0.870962348
	21	70	35	0.541667	0.118558	0.799138734
	22	51	57	0.514483	0.133166	0.776118221
	22	57	68	0.507246	0.124791	0.772302604
	19	57	1	0.336111	0.061916	0.641092175
	22	46	32	0.326087	0.19933	0.610347155

Image	Radius	x-centre	y-centre	BPS	IPS	Measure of goodness
	22	70	29	0.444444	0.1365159	0.720882899
	22	61	68	0.461353	0.2001675	0.71877422
	21	33	41	0.427083	0.0855019	0.714948995
	19	59	32	0.425	0.0957944	0.711911576
	19	48	53	0.358333	0.1869159	0.639752651
	19	50	72	0.358333	0.1904206	0.638907175
	24	33	28	0.336245	0.1618457	0.627027206

Image	Radius	x-centre	y-centre	BPS	IPS	Measure of goodness
	19	42	52	0.408333333	0.220794393	0.671111753
	22	67	58	0.367149758	0.163316583	0.652351511
	19	29	34	0.388888889	0.248831776	0.647022608
	19	49	72	0.347222222	0.099299065	0.64663122
	20	60	69	0.310160428	0.118448637	0.61268232

Image	Radius	x-centre	y-centre	BPS	IPS	Measure of goodness
	23	59	67	0.474770642	0.128398792	0.746505624
	24	48	69	0.377729258	0.14600551	0.664620894
	22	66	56	0.367149758	0.147403685	0.655585025
	20	44	49	0.35828877	0.238993711	0.625683081



Image	Radius	x-centre	y-centre	BPS	IPS	Measure of goodness
	22	52	75	0.379227	0.128978	0.668984
	19	51	37	0.391867	0.21729	0.658834
	19	65	69	0.355556	0.098131	0.65381
	21	55	26	0.377604	0.243494	0.639757
	21	31	55	0.359875	0.207249	0.635494






Image	Radius	x-centre	y-centre	BPS	IPS	Measure of goodness
	21	44	23	0.434896	0.1784387	0.703854894
	19	53	73	0.344444	0.0630841	0.548085471
	19	42	71	0.347222	0.1016355	0.546327715
	19	30	32	0.361111	0.1892523	0.641468334
	22	55	25	0.36715	0.2110553	0.640796236
	25	63	61	0.324895	0.0868471	0.629197658
	23	57	37	0.332569	0.1963746	0.616296122
	19	38	43	0.336111	0.2301402	0.610355953




Image	Radius	x-centre	y-centre	BPS	IPS	Measure of goodness
	19	56	28	0.38	0.06	0.67
	20	33	54	0.36	0.07	0.66
	23	49	63	0.34	0.09	0.64




Image	Radius	x-centre	y-centre	BPS	IPS	Measure of goodness
	21	36	37	0.416666667	0.106877323	0.703480758
	21	51	57	0.359375	0.132899628	0.651770546
	25	58	41	0.327004219	0.136563877	0.624019904

Image	Radius	x-centre	y-centre	BPS	IPS	Measure of goodness
	20	55	65	0.368884	0.1006289	0.664774477
	18	35	48	0.316568	0.0952381	0.621170592
	21	70	48	0.3125	0.0864312	0.618705054

Image	Radius	x-centre	y-centre	BPS	IPS	Measure of goodness
	19	53	65	0.363889	0.051402	0.665458
	21	51	33	0.322917	0.116171	0.623792
	19	70	38	0.302778	0.094626	0.609526










Image	Radius	x-centre	y-centre	BPS	IPS	Measure of goodness
	18	49	39	0.437869832	0.141534392	0.714607155
	19	40	68	0.452777778	0.234813084	0.701461443
	21	37	45	0.403645833	0.17936803	0.678540452
	24	53	27	0.390829694	0.164600551	0.671539929
	18	68	32	0.381656805	0.223544974	0.649001233
	18	57	50	0.375739645	0.207671958	0.648671643
	18	72	43	0.372781065	0.238095238	0.637568897
	20	38	33	0.339572193	0.167714885	0.628579246
	18	68	64	0.349112426	0.228835979	0.621250722





Image	Radius	x-centre	y-centre	BPS	IPS	Measure of goodness
	23	65	65	0.541284	0.1102719	0.800451055
	23	32	38	0.497706	0.0861027	0.771273282
	20	62	27	0.42246	0.0870031	0.710972207
	25	44	59	0.333333	0.183134	0.620033033







Image	Radius	x-centre	y-centre	BPS	IPS	Measure of goodness
	20	48	73	0.475935829	0.070210608	0.756104569
	24	73	52	0.467248908	0.134297521	0.739441912
	22	48	22	0.420289855	0.087102178	0.709176642
	20	34	45	0.403743316	0.205450734	0.671842032
	24	52	33	0.334061135	0.150137741	0.627497299
	22	35	37	0.338164251	0.19681742	0.620789232








Image	Radius	x-centre	y-centre	BPS	IPS	Measure of goodness
	25	48	30	0.48	0.23	0.72
	20	73	49	0.43	0.13	0.71
	18	58	44	0.42	0.21	0.68
	25	31	32	0.41	0.24	0.66
	21	38	45	0.35	0.23	0.62
	20	20	36	0.34	0.22	0.61
	18	37	70	0.34	0.25	0.61












Image	Radius	x-centre	y-centre	BPS	IPS	Measure of goodness
	23	36	34	0.401376	0.1812689	0.676238858
	19	56	66	0.413889	0.2219626	0.675168062
	24	53	34	0.395197	0.1742424	0.672907308
	20	71	55	0.393048	0.2190776	0.659425976
	22	69	74	0.376812	0.2001675	0.651530663
	18	24	37	0.372781	0.207672	0.646274312
	18	70	38	0.363905	0.2261905	0.6339542
	18	31	65	0.337278	0.1851852	0.622822408
	20	54	53	0.342246	0.2075472	0.621439943
	21	39	49	0.320313	0.1747212	0.611095157
	20	45	71	0.334225	0.2232704	0.610726178









Image	Radius	x-centre	y-centre	SPS	IPS	Measure of goodness
	22	27	64	0.67343	0.104154	0.75796648
	23	32	42	0.494126	0.10094	0.72188149
	18	59	72	0.449704	0.164021	0.71918967
	24	70	35	0.441043	0.190083	0.705704481
	24	54	29	0.423981	0.220386	0.683294753
	21	35	30	0.408854	0.203532	0.676462536
	25	70	72	0.405003	0.217747	0.689406722
	18	56	45	0.384615	0.240741	0.646194764

Image	Radius	x-centre	y-centre	SPS	IPS	Measure of goodness
	19	57	24	0.452777778	0.348831776	0.696721573
	21	53	58	0.419270513	0.236847584	0.674155486
	19	54	74	0.388666667	0.230140187	0.615034712
	22	67	90	0.347936087	0.186767189	0.63114933
	19	51	47	0.347222222	0.237549533	0.64732557
	19	21	43	0.338311111	0.22546729	0.611656789


Image	Radius	x-centre	y-centre	SPS	IPS	Measure of goodness
	20	50	37	0.422459881	0.20754717	0.686171006
	22	28	38	0.396115266	0.175879397	0.671285257
	20	58	49	0.395721925	0.244214801	0.653898831
	19	73	47	0.369444444	0.203273228	0.64471273
	19	15	51	0.380555556	0.248831776	0.640421534
	24	39	30	0.364628821	0.330716253	0.633229865
	19	40	82	0.343666667	0.183613215	0.629853479
	19	62	51	0.358313333	0.218817757	0.625930781
	25	58	72	0.353320675	0.241032096	0.620279573

Image	Radius	x-centre	y-centre	SPS	IPS	Measure of goodness
	24	59	27	0.471614	0.2348485	0.715867676
	19	27	39	0.425	0.174654	0.697032121
	19	47	53	0.416967	0.2254673	0.676363542
	19	45	22	0.413111	0.2254673	0.67191353
	23	70	51	0.389808	0.2311178	0.653358749
	25	38	41	0.368188	0.2076485	0.643514376
	20	44	65	0.371658	0.2473795	0.623807136
	19	55	78	0.348444	0.2184579	0.620346578




Image	Radius	x-centre	y-centre	SPS	IPS	Measure of goodness
	24	37	30	0.432114	0.1652893	0.704976837
	25	32	42	0.377637	0.1623663	0.681200175
	20	61	31	0.363636	0.1446541	0.615392446





Image	Radius	x-centre	y-centre	SPS	IPS	Measure of goodness
	18	30	29	0.433333	0.172897	0.703881
	25	42	29	0.42616	0.199497	0.681363
	20	32	54	0.352941	0.186583	0.635401
	24	55	67	0.340611	0.137052	0.635352

Image	Radius	x-centre	y-centre	SPS	IPS	Measure of goodness
	20	41	39	0.481183	0.219078	0.728286
	21	39	62	0.440104	0.244424	0.688509
	20	62	43	0.429766	0.249476	0.671067
	22	45	51	0.364754	0.236181	0.631698
	19	46	78	0.341607	0.239486	0.612383

Image	Radius	x-centre	y-centre	BPS	IPS	Measure of goodness
	23	39	35	0.504587156	0.121601208	0.770881403
	25	65	41	0.457805907	0.108873505	0.736513381
	21	29	48	0.3671875	0.096654275	0.663787169
	25	33	62	0.360759494	0.110761485	0.656458021
	19	47	74	0.361111111	0.147196262	0.650609442
	20	61	30	0.320855615	0.137316562	0.618725889




Image	Radius	x-centre	y-centre	BPS	IPS	Measure of goodness
	22	46	66	0.519323671	0.173366834	0.770199434
	25	67	45	0.493670886	0.076777848	0.769307892
	21	41	27	0.471354167	0.144981413	0.74045825
	19	29	34	0.413888889	0.136682243	0.696137368





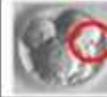




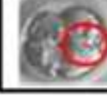
Image	Radius	x-centre	y-centre	BPS	IPS	Measure of goodness
	25	62	43	0.514768	0.1195721	0.778997349
	25	28	65	0.421941	0.1246067	0.704914251
	19	37	28	0.419444	0.1752336	0.692289136
	20	65	64	0.358289	0.2410901	0.62505367
	20	42	78	0.350267	0.2243187	0.623459583

Image	Radius	x-centre	y-centre	BPS	IPS	Measure of goodness
	21	39	31	0.505208	0.222119	0.745161
	19	58	24	0.483333	0.200935	0.735416
	22	64	60	0.454106	0.130653	0.729738
	19	35	64	0.447222	0.167056	0.716433
	22	53	68	0.381643	0.21608	0.651123

APPENDIX I

The results of the approach discussed in Chapter 8 are shown in this Appendix. This approach used the two templates on the binary images but the median filter was applied to the image before detecting its edges. The two factors BPS and IPS are used to substitute them in a 2 variable equation to measure the goodness of the detected cell. This Appendix will show the results when using the convolution mask edge detector.



Image	Radius	x-centre	y-centre	BPS	IPS	Measure of goodness
	25	63	48	0.34	0.14	0.63
	25	38	48	0.32	0.1	0.62




Image	Radius	x-centre	y-centre	BPS	IPS	Measure of goodness
	25	64	33	0.377	0.08	0.67
	24	39	60	0.34	0.11	0.64
	26	52	44	0.32	0.1	0.62

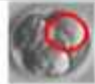

Image	Radius	x-centre	y-centre	BPS	IPS	Measure of goodness
	21	37	66	0.42	0.16	0.69
	19	69	51	0.4	0.18	0.67





Image	Radius	x-centre	y-centre	BPS	IPS	Measure of goodness
	22	66	55	0.45	0.13	0.72
	19	40	48	0.41	0.24	0.66
	22	28	52	0.34	0.22	0.62
	26	48	59	0.31	0.11	0.61




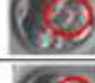
Image	Radius	x-centre	y-centre	BPS	IPS	Measure of goodness
	23	59	68	0.46	0.23	0.71
	19	57	28	0.36	0.1	0.66
	24	48	65	0.36	0.23	0.62
	19	36	70	0.34	0.23	0.61





Image	Radius	x-centre	y-centre	BPS	IPS	Measure of goodness
	23	50	57	0.5	0.17	0.75
	22	34	29	0.48	0.15	0.74
	22	70	34	0.44	0.1	0.72
	23	57	68	0.41	0.24	0.67





Image	Radius	x-centre	y-centre	BPS	IPS	Measure of goodness
	19	49	28	0.47	0.22	0.72
	23	47	64	0.36	0.09	0.66
	23	59	64	0.34	0.08	0.64
	22	65	53	0.31	0.13	0.61



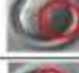

Image	Radius	x-centre	y-centre	BPS	IPS	Measure of goodness
	19	54	38	0.34	0.12	0.64
	20	35	41	0.36	0.24	0.62
	25	52	66	0.32	0.12	0.62
	19	31	52	0.34	0.21	0.62

Image	Radius	x-centre	y-centre	BPS	IPS	Measure of goodness
	21	39	35	0.36	0.18	0.64
	26	50	34	0.32	0.14	0.62






Image	Radius	x-centre	y-centre	BPS	IPS	Measure of goodness
	21	31	52	0.5	0.13	0.76
	21	42	67	0.37	0.17	0.65
	19	61	31	0.35	0.08	0.65
	18	71	64	0.32	0.1	0.62
	22	53	68	0.32	0.17	0.61





Image	Radius	x-centre	y-centre	BPS	IPS	Measure of goodness
	18	27	61	0.44	0.21	0.7
	19	54	60	0.41	0.17	0.69
	22	37	37	0.37	0.13	0.66
	18	67	45	0.34	0.14	0.63






Image	Radius	x-centre	y-centre	BPS	IPS	Measure of goodness
	21	41	52	0.36	0.13	0.65
	21	68	48	0.36	0.16	0.64
	20	56	66	0.36	0.19	0.64
	18	27	39	0.33	0.13	0.62
	18	51	25	0.32	0.16	0.61

Image	Radius	x-centre	y-centre	BPS	IPS	Measure of goodness
	20	27	60	0.45	0.12	0.72
	20	55	65	0.4	0.11	0.69
	21	47	30	0.31	0.11	0.61





Image	Radius	x-centre	y-centre	BPS	IPS	Measure of goodness
	24	36	38	0.43	0.22	0.68
	19	49	37	0.42	0.24	0.67
	24	53	26	0.39	0.21	0.66
	18	36	27	0.31	0.13	0.61





Image	Radius	x-centre	y-centre	BPS	IPS	Measure of goodness
	23	45	70	0.45	0.19	0.71
	23	71	53	0.44	0.21	0.7
	25	48	28	0.4	0.2	0.67
	22	31	23	0.36	0.15	0.65

Image	Radius	x-centre	y-centre	BPS	IPS	Measure of goodness
	19	77	48	0.38	0.24	0.64






Image	Radius	x-centre	y-centre	BPS	IPS	Measure of goodness
	23	65	64	0.59	0.2	0.81
	23	30	38	0.49	0.14	0.76
	20	28	50	0.4	0.22	0.66
	24	65	31	0.36	0.18	0.64
	18	50	60	0.37	0.25	0.63






Image	Radius	x-centre	y-centre	BPS	IPS	Measure of goodness
	25	49	31	0.41	0.19	0.68
	19	48	42	0.4	0.22	0.66
	22	23	46	0.39	0.24	0.65
	22	28	34	0.37	0.19	0.64
	21	37	48	0.34	0.23	0.61







Image	Radius	x-centre	y-centre	BPS	IPS	Measure of goodness
	20	26	65	0.47	0.24	0.71
	21	37	25	0.4	0.2	0.67
	21	24	42	0.39	0.21	0.66
	19	66	31	0.38	0.23	0.64
	24	49	24	0.37	0.23	0.63
	19	22	54	0.36	0.22	0.63

Image	Radius	x-centre	y-centre	BPS	IPS	Measure of goodness
	23	40	46	0.43	0.21	0.69
	23	64	36	0.36	0.11	0.66





Image	Radius	x-centre	y-centre	BPS	IPS	Measure of goodness
	19	25	38	0.5	0.19	0.75
	22	51	42	0.44	0.23	0.69
	23	71	50	0.41	0.2	0.68
	19	25	50	0.37	0.23	0.64




Image	Radius	x-centre	y-centre	BPS	IPS	Measure of goodness
	23	33	45	0.45	0.11	0.73
	22	72	54	0.46	0.22	0.71
	24	61	31	0.44	0.17	0.71






Image	Radius	x-centre	y-centre	BPS	IPS	Measure of goodness
	20	35	38	0.44	0.11	0.72
	19	61	33	0.38	0.14	0.66
	20	41	69	0.38	0.19	0.65
	20	52	65	0.32	0.14	0.61
	24	33	49	0.32	0.17	0.61






Image	Radius	x-centre	y-centre	BPS	IPS	Measure of goodness
	19	30	30	0.49	0.19	0.74
	22	42	27	0.48	0.21	0.72
	24	51	64	0.41	0.08	0.7
	22	34	61	0.37	0.18	0.65
	23	66	45	0.33	0.17	0.61





Image	Radius	x-centre	y-centre	BPS	IPS	Measure of goodness
	23	41	66	0.53	0.19	0.77
	24	41	48	0.46	0.23	0.71
	20	49	29	0.42	0.22	0.67
	22	52	64	0.36	0.23	0.63




Image	Radius	x-centre	y-centre	BPS	IPS	Measure of goodness
	25	66	43	0.49	0.12	0.75
	24	35	25	0.35	0.15	0.64
	22	67	63	0.34	0.23	0.61






Image	Radius	x-centre	y-centre	BPS	IPS	Measure of goodness
	22	38	33	0.45	0.13	0.72
	25	64	41	0.45	0.16	0.72
	21	43	74	0.45	0.23	0.7
	25	33	62	0.41	0.22	0.68
	23	28	49	0.34	0.17	0.62









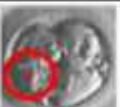
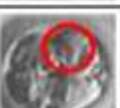
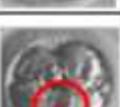

Image	Radius	x-centre	y-centre	BPS	IPS	Measure of goodness
	25	62	42	0.5	0.17	0.75
	20	26	59	0.46	0.14	0.73
	24	55	30	0.39	0.16	0.67
	24	37	64	0.37	0.24	0.64
	20	36	28	0.34	0.19	0.62

Image	Radius	x-centre	y-centre	BPS -	IPS -	Measure of goodness
	23	63	60	0.53	0.24	0.75
	21	36	28	0.44	0.23	0.69
	21	47	23	0.4	0.25	0.65
	20	61	24	0.39	0.24	0.65
	20	29	57	0.36	0.24	0.62
	21	69	49	0.35	0.23	0.62
	20	30	39	0.33	0.2	0.61

APPENDIX J

This Appendix shows the results of applying the test images to the enhanced “AND” technique using the new algorithm as an edge detector. Some of these results are discussed in Chapter 9.

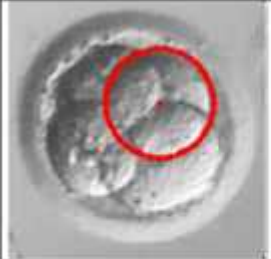



Image	Radius	x-centre	y-centre	BPS	IPS	Measure of goodness
	38	72	107	0.35	0.11	0.64
	37	101	61	0.30	0.15	0.60
	36	64	65	0.28	0.10	0.59
	42	106	108	0.27	0.14	0.57



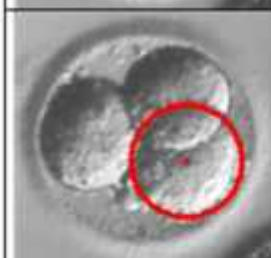

Image	Radius	x-centre	y-centre	BPS	IPS	Measure of goodness
	39	61	112	0.47	0.09	0.75
	36	91	51	0.37	0.07	0.67
	39	105	120	0.33	0.12	0.63
	32	124	104	0.26	0.15	0.56




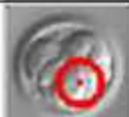
Image	Radius	x-centre	y-centre	BPS	IPS	Measure of goodness
	14	48	38	0.45	0.16	0.72
	16	24	42	0.45	0.24	0.69
	16	35	24	0.38	0.21	0.65
	14	50	48	0.35	0.24	0.62

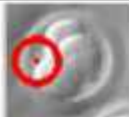
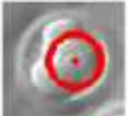


Image	Radius	x-centre	y-centre	BPS	IPS	Measure of goodness
	14	39	20	0.40	0.23	0.66
	17	39	47	0.35	0.09	0.65
	18	48	36	0.31	0.14	0.61
	14	21	30	0.37	0.30	0.61


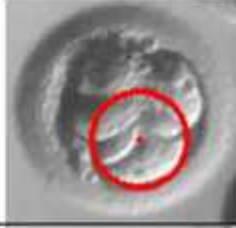


Image	Radius	x-centre	y-centre	BPS	IPS	Measure of goodness
	31	87	59	0.33	0.14	0.62
	33	96	87	0.32	0.17	0.61
	33	66	100	0.29	0.14	0.59
	32	67	62	0.26	0.08	0.58




Image	Radius	x-centre	y-centre	BPS	IPS	Measure of goodness
	26	46	48	0.42	0.14	0.70
	26	82	71	0.38	0.10	0.67
	21	38	81	0.26	0.08	0.57

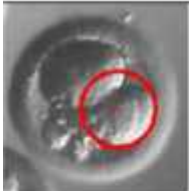

Image	Radius	x-centre	y-centre	BPS	IPS	Measure of goodness
	35	102	112	0.36	0.09	0.65
	34	69	86	0.23	0.06	0.55






Image	Radius	x-centre	y-centre	BPS	IPS	Measure of goodness
	16	26	31	0.47	0.17	0.73
	17	46	55	0.54	0.32	0.727
	16	49	31	0.44	0.21	0.70
	18	29	45	0.40	0.26	0.654
	18	52	42	0.41	0.29	0.64






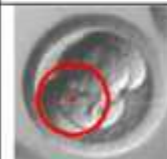
Image	Radius	x-centre	y-centre	BPS	IPS	Measure of goodness
	16	47	62	0.48	0.15	0.74
	16	40	35	0.44	0.18	0.71
	14	54	36	0.36	0.18	0.64
	18	57	58	0.36	0.22	0.63

Image	Radius	x-centre	y-centre	BPS	IPS	Measure of goodness
	26	92	76	0.23	0.11	0.54
	33	88	56	0.21	0.05	0.54